

Glasgow, May 16th, 2013

# Reconstructing paleostress magnitudes from calcite twins

Olivier LACOMBE



# Why to characterize stresses in the crust ?

The motivation arises :

from applied geological purposes, such as geological hazards, engineering activities and resource exploration;

and

from fundamental geological purposes, such as understanding the mechanical behaviour of geological materials and deciphering various tectonic mechanisms, from those related to plate motions at a large scale to those causing jointing and faulting or even microstructures at a smaller scale.

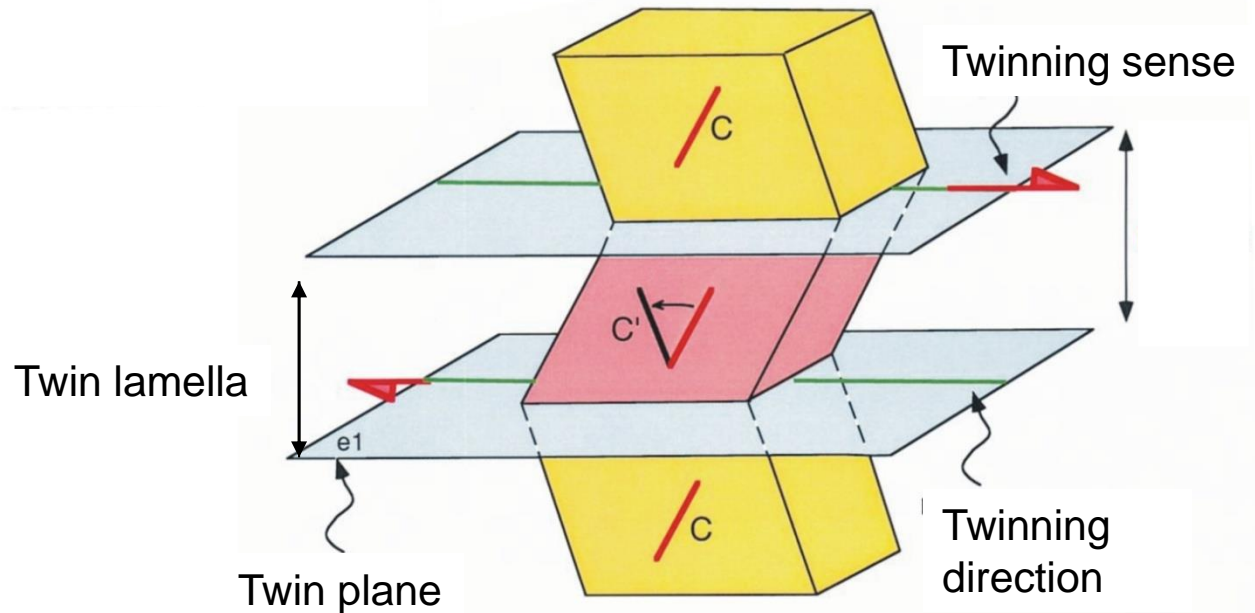
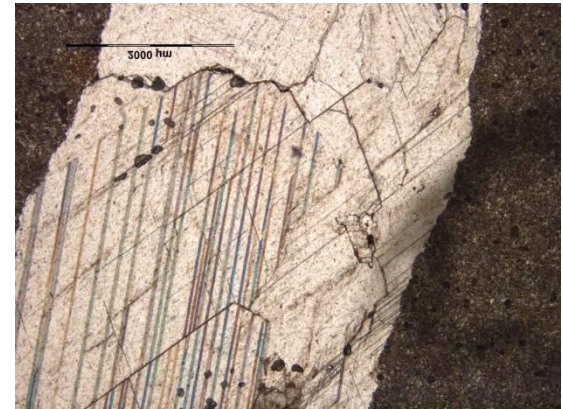
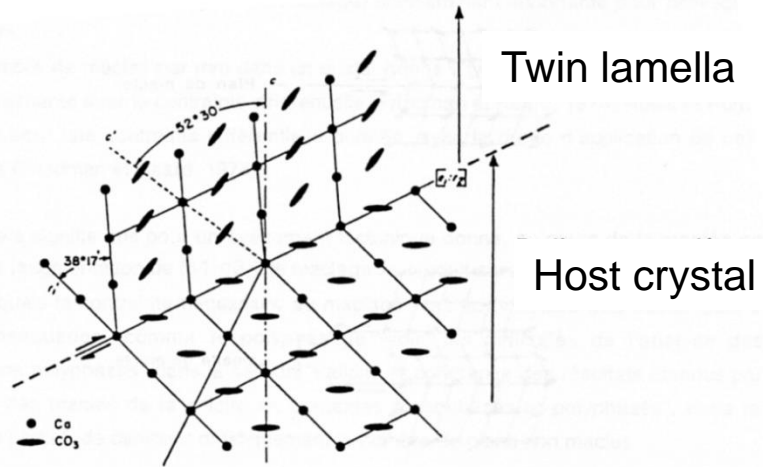
Despite an increasing number of in situ stress measurements, magnitudes of crustal stresses remain poorly constrained...

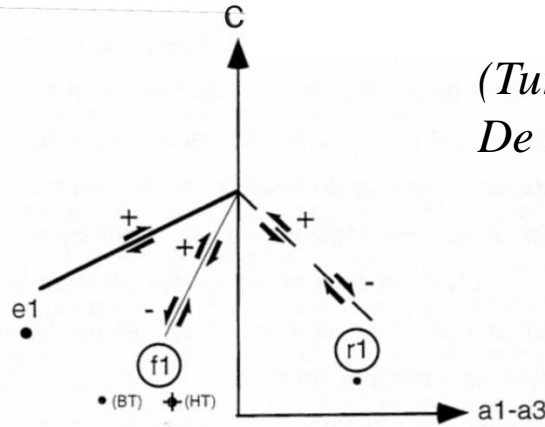
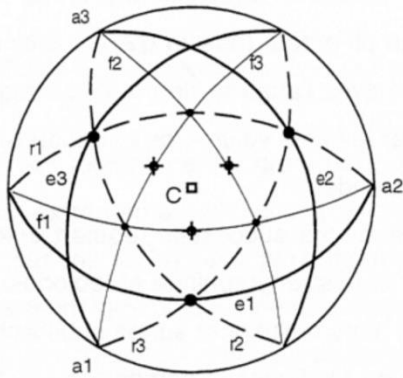
Twinning of minerals depends on the magnitude of the shear stress which has been applied to them.

One can make use of this property to evaluate the magnitudes of stresses which have been supported by a rock during its history.

An access to paleostress magnitudes in the upper crust : Calcite twinning paleopiezometry

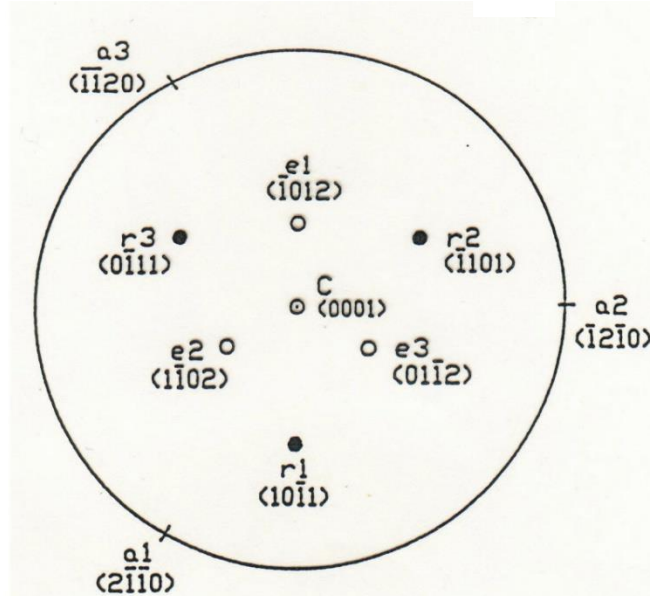
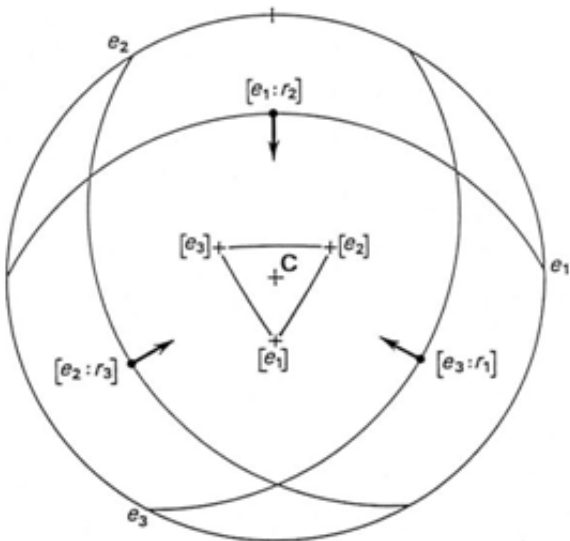
# Twinning ~ simple shearing in a particular sense and direction along e-planes {01-12}



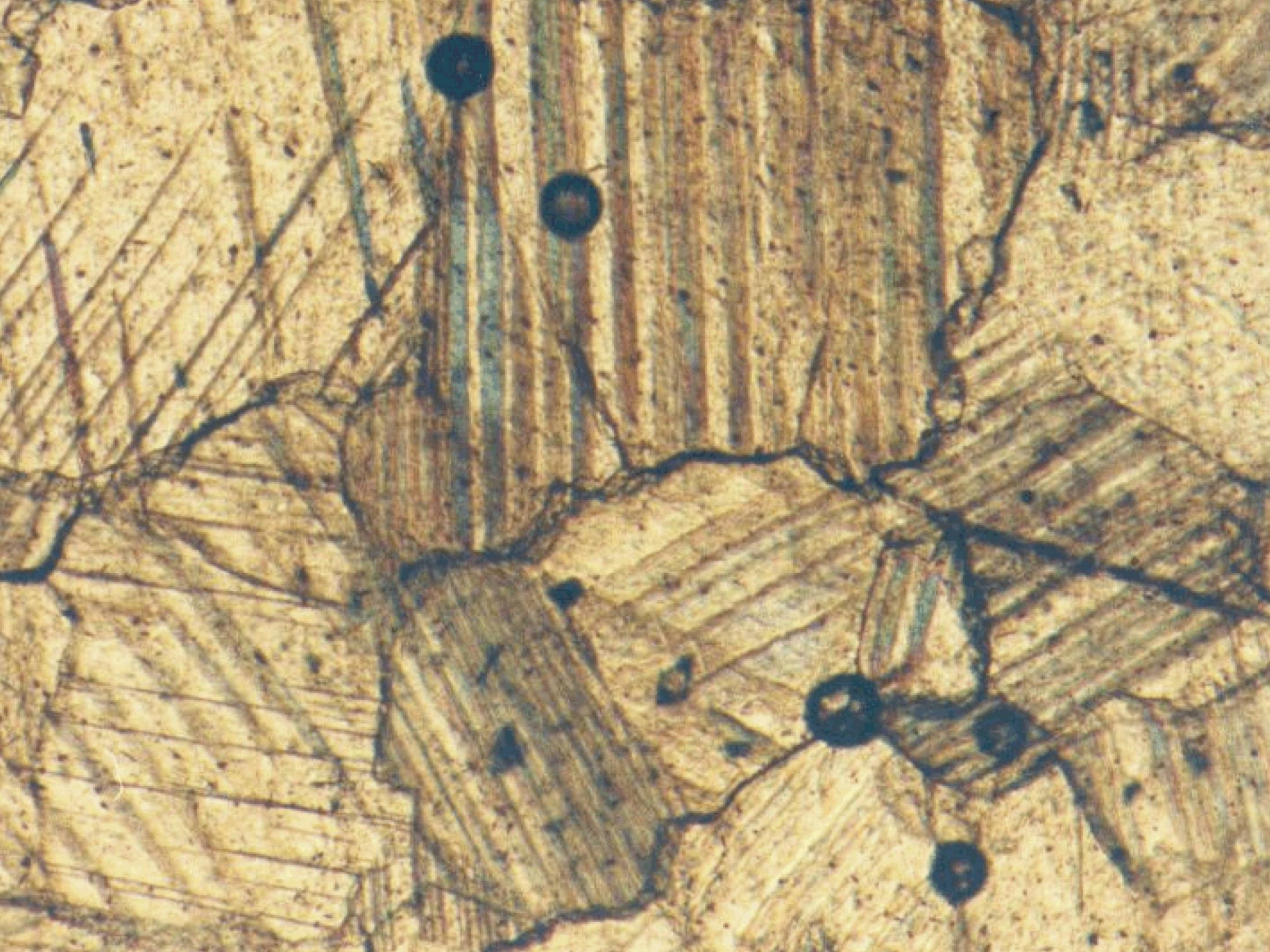


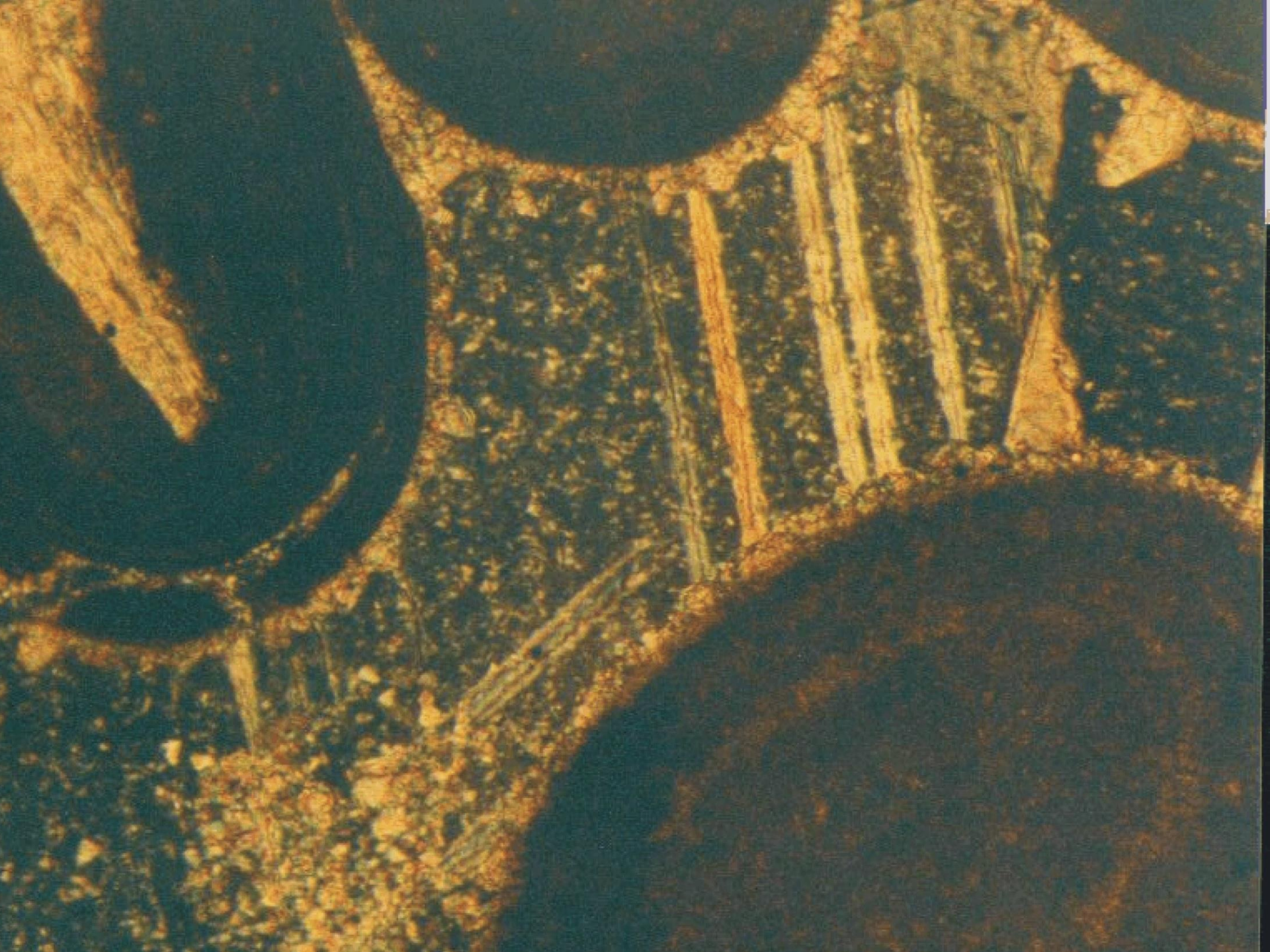
(Turner and Weiss, 1976;  
De Bresser et al., 1997)

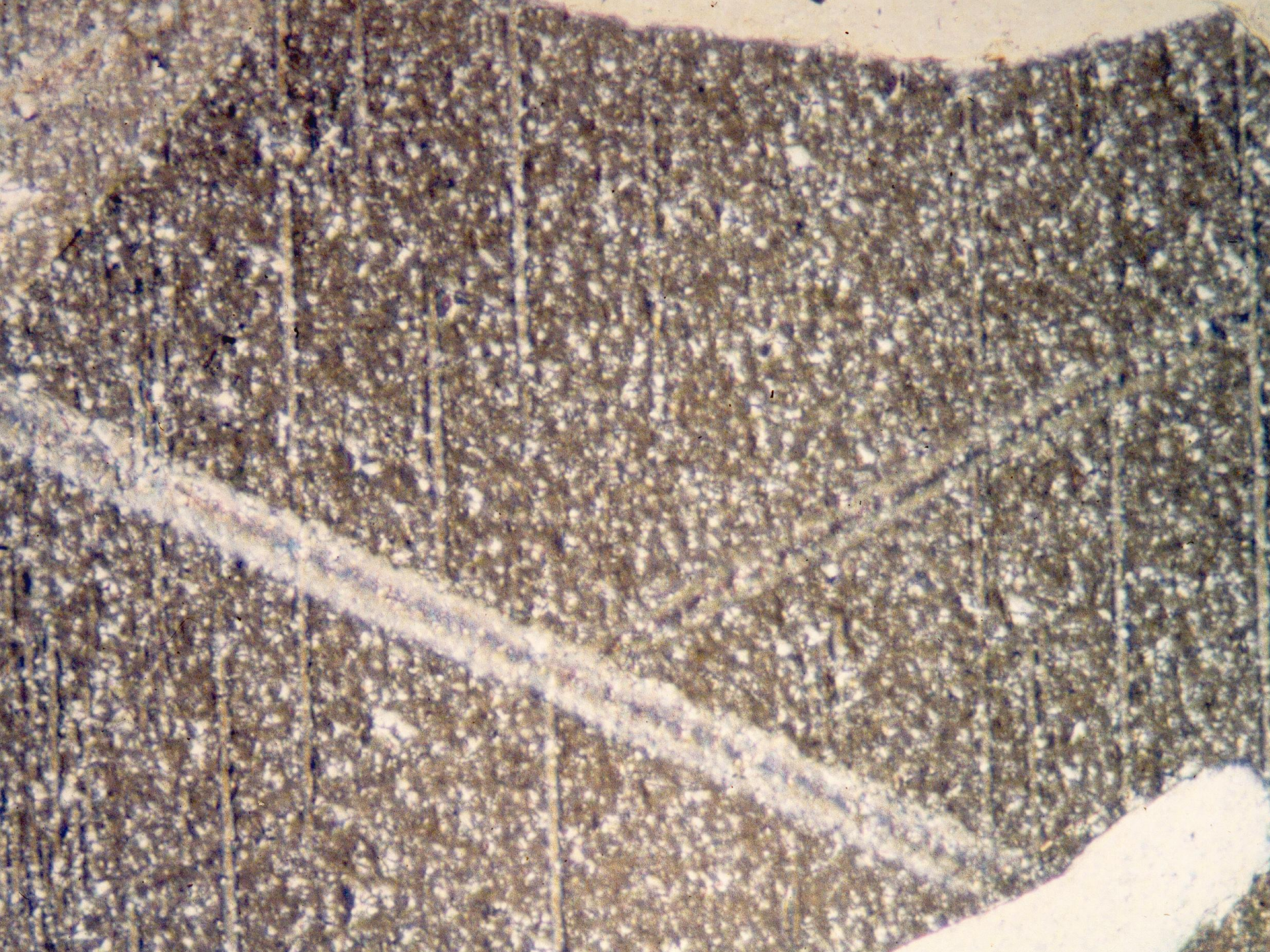
e-twinning and r, f-glide systems in calcite



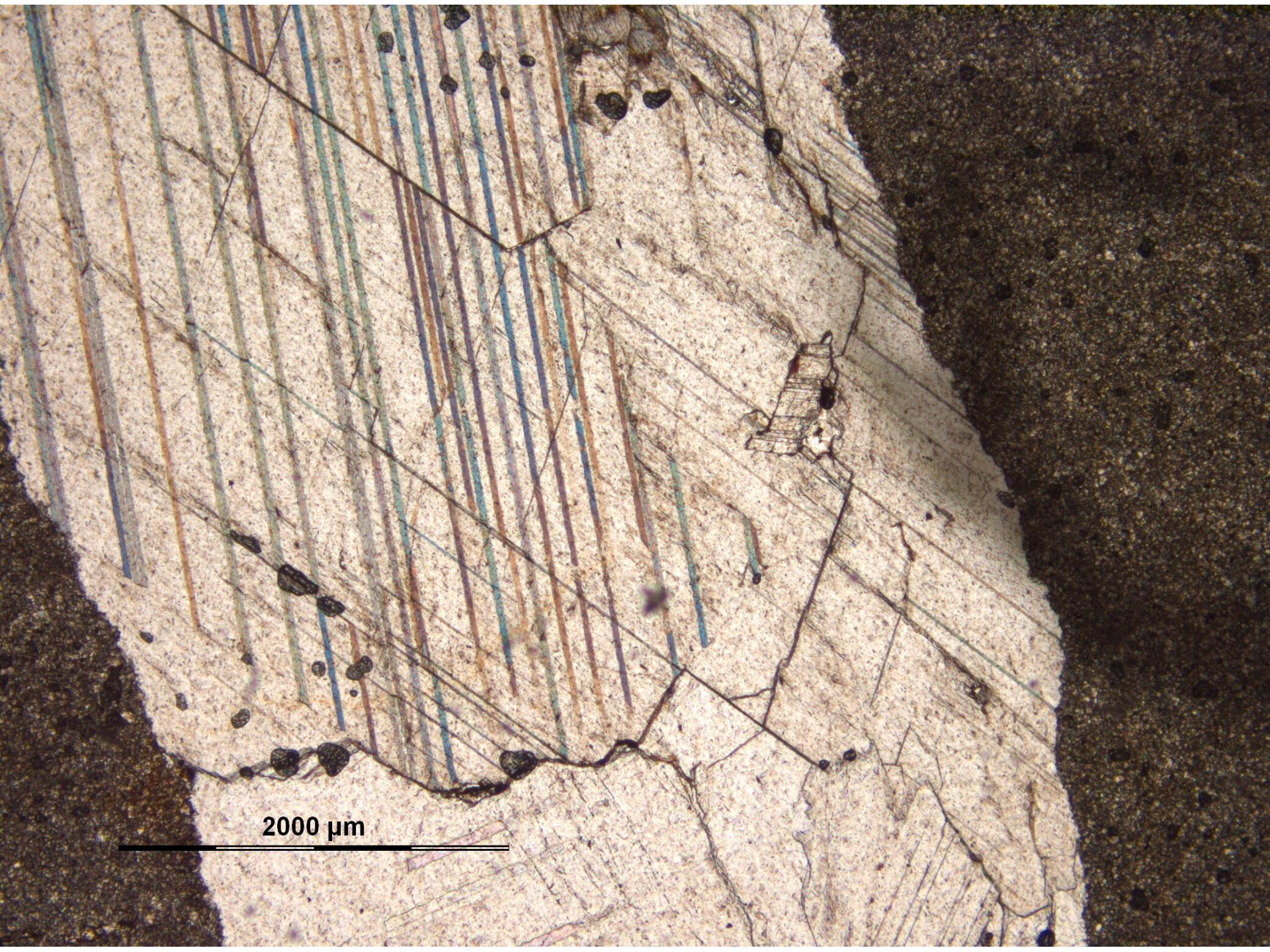
$C, e_i$	$= 26,5^\circ$
$e_i, e_j$	$= 44,5^\circ$
$e_i, r_i$	$= 71,5^\circ$
$e_i, r_j$	$= 37,5^\circ$
$r_i, r_j$	$= 75^\circ$
$C, r_i$	$= 44,5^\circ$



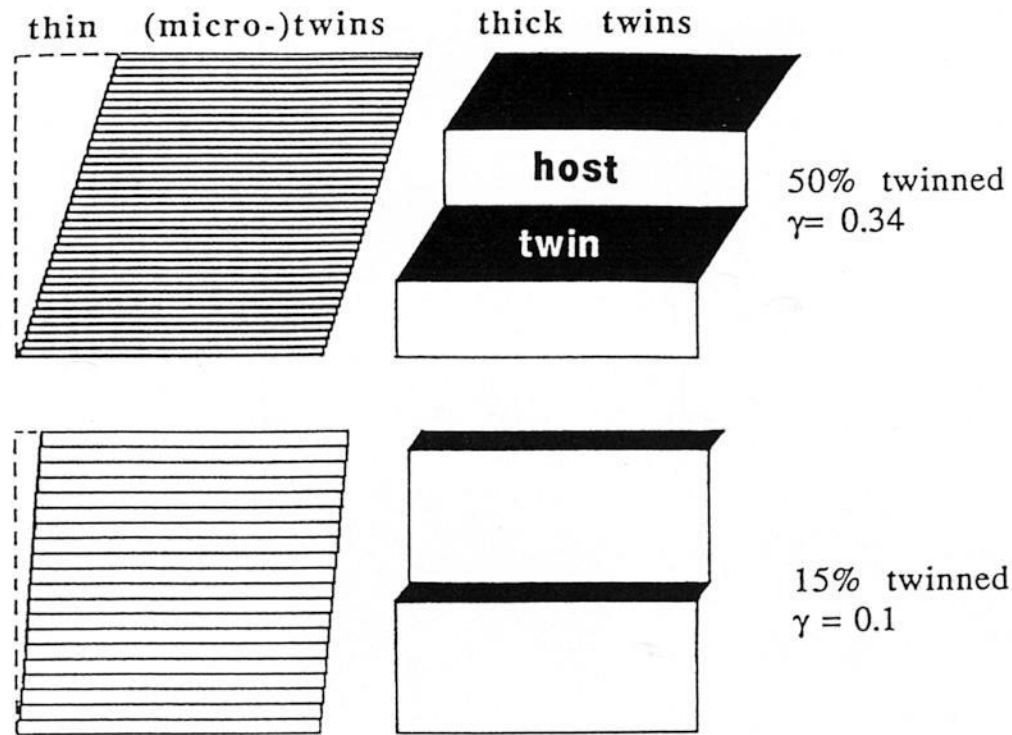








2000  $\mu\text{m}$



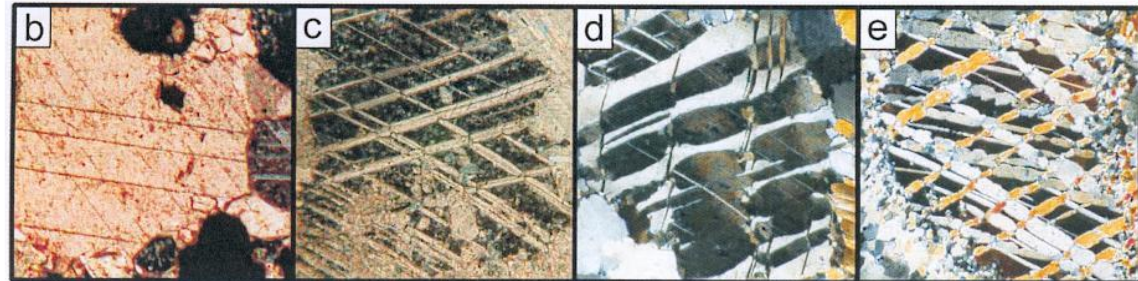
Schematic diagram illustrating the difference between thin and thick twins, twin density (number of twins per mm) and percentage volume fraction of twin lamellae. In both cases, exactly the same amount of shearing by 15% ( $\gamma=0.1$ ) and 50% ( $\gamma=0.34$ ) twinning respectively is distributed either relatively homogeneously into many thin twins or just a few thick ones - the latter case is leading to very inhomogeneous deformation and causes larger steps in the grain boundary.

(Burkhard, 1993)

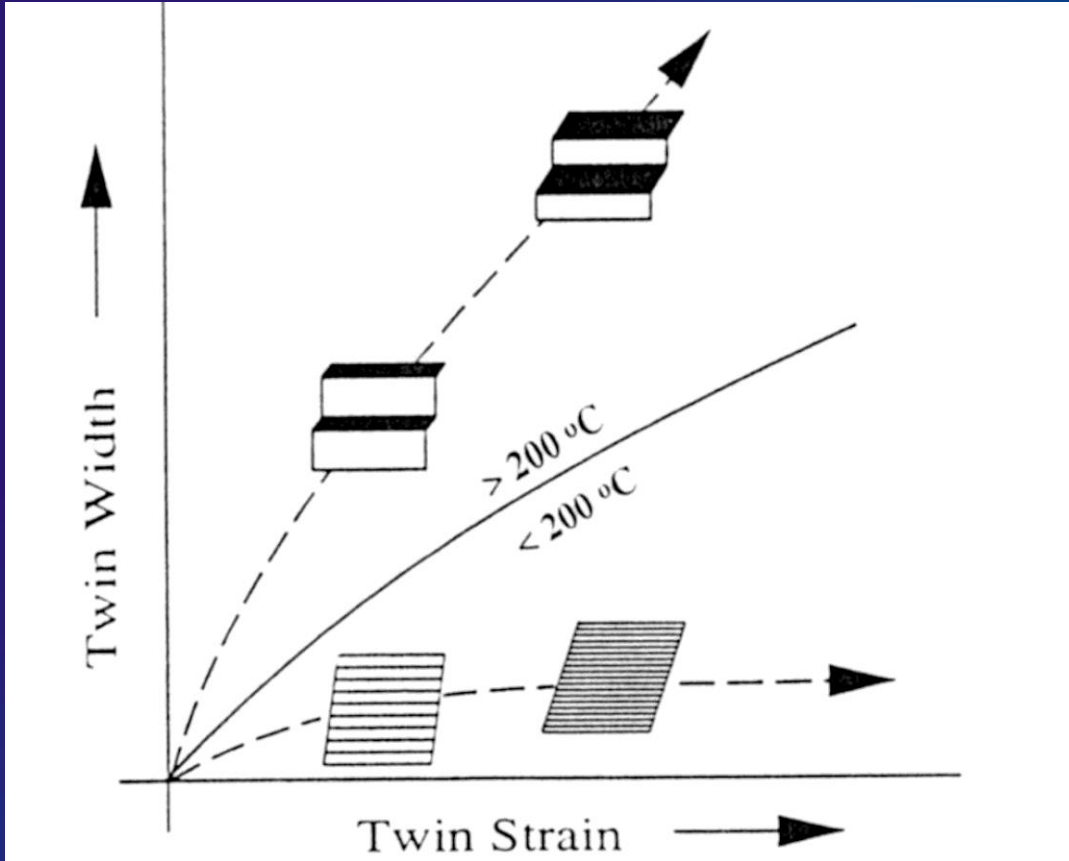
	type I	type II	type III	type IV
<b>Geometry</b>	-thin	-thick ( $\gg 1\mu\text{m}$ )	-curved twins	-thick, patchy
<b>Description</b>	-straight -rational	-straight -slightly lenseshaped -rational	-twins in twins -irrational -completely twinned	-sutured boundaries -trails of tiny grains -irrational
<b>Interpretations</b>	-little deformation -little cover -low temperature  -(post-metamorphic) -(late tectonic)	-considerable def. -completely twinned grains are possible  -syn- or post- metamorphic	-large deformation. -intracrystalline def. mechanisms e.g. (r- & f-glide) -syn-metamorphic deformation.	-large deformation -recrystallization (grain boundary migration) -pre- or syn- metamorphic
<b>Temperature</b>	< 200°C	150-300°C	> 200°C	>250°C



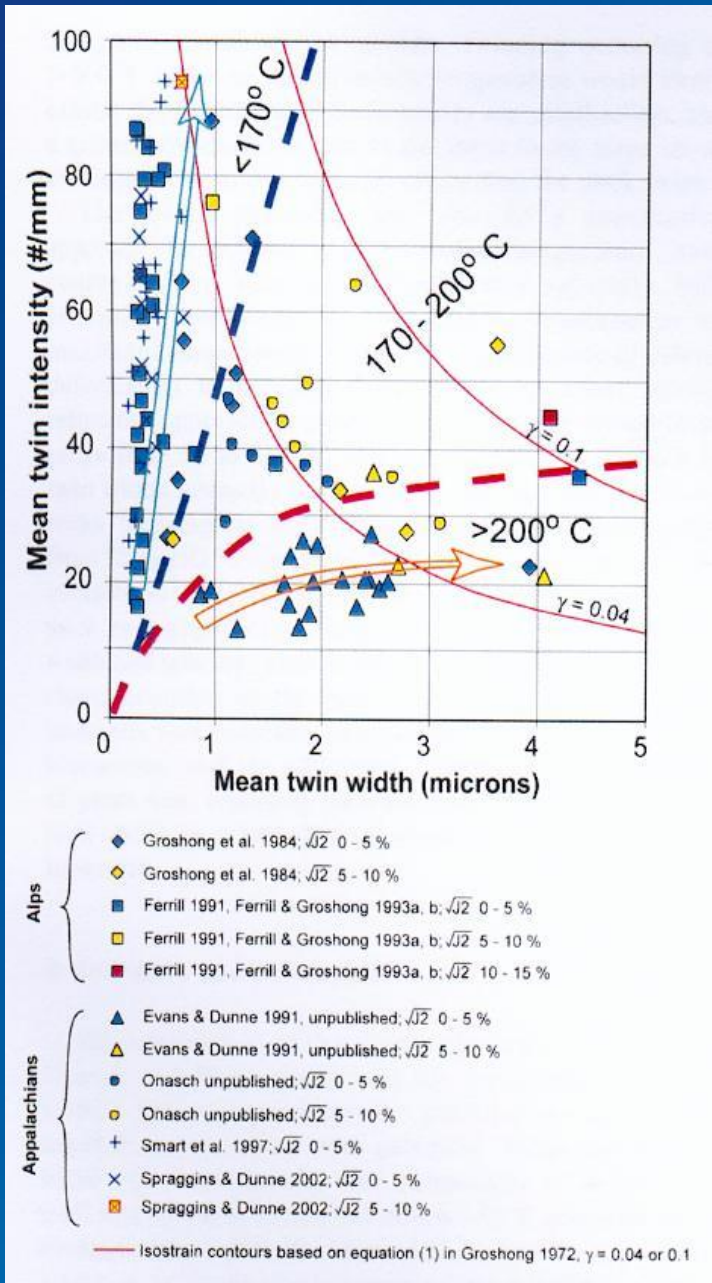
*Increasing temperature*



*(Burkhard, 1993;  
Ferrill et al., 2004)*



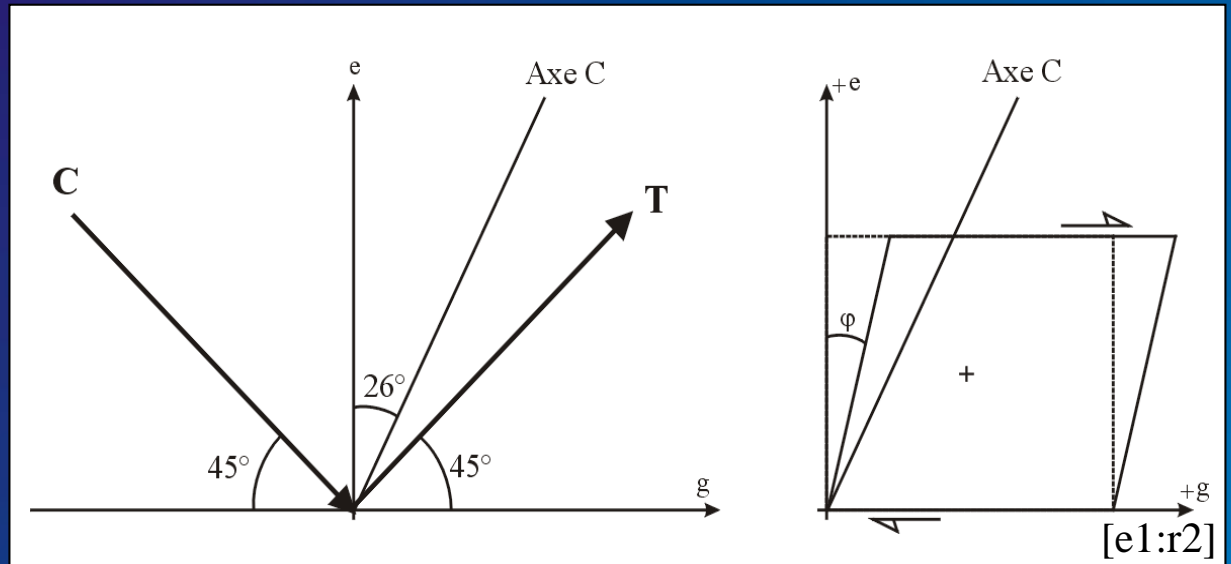
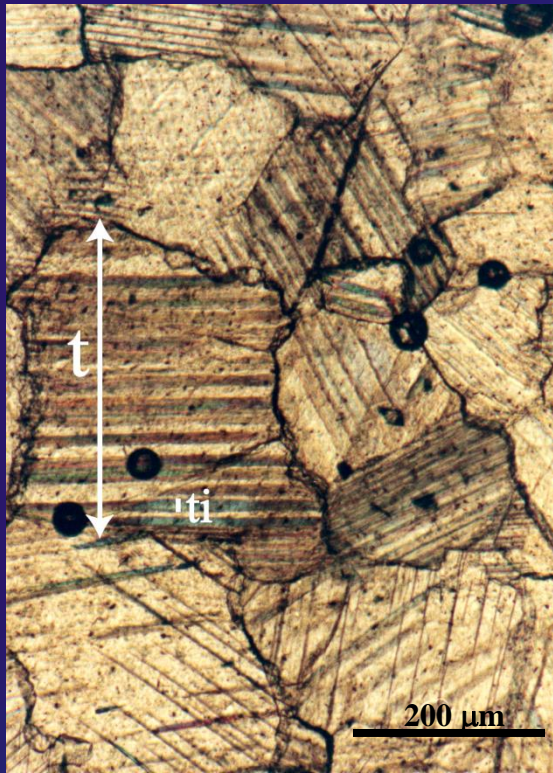
(Ferrill, 1998)



(Ferrill et al., 2004)

**Stress and strain analysis of calcite twinning :  
The 'historical' techniques**

# Groshong (1974, 1984) : determination of the strain tensor by twinning



$$\Gamma_{eg} = \frac{1}{2} \cdot \tan \varphi = \frac{0.347}{t} \cdot \sum_{i=1}^n t_i$$

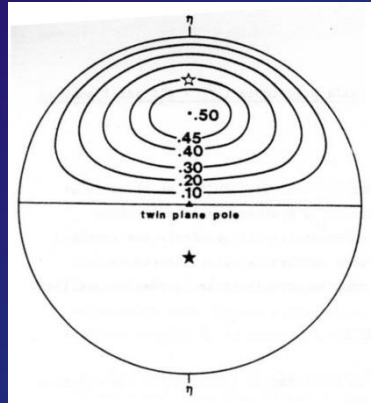
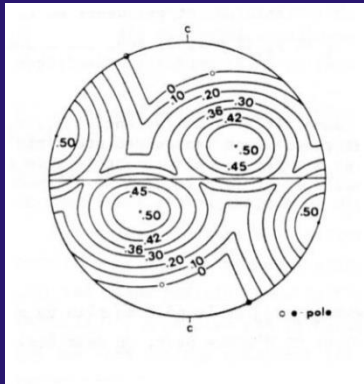
Deformation  
by shearing  
for a twin set

$\Gamma_{eg} = (lelg - neng) \epsilon_x + (memg - neng) \epsilon_y + (lemg + melg) \Gamma_{xy} + (men_g + nemg) \Gamma_{yz} + (nelg + leng) \Gamma_{zx}$ ,  
with  $\epsilon_x$ ,  $\epsilon_y$ ,  $\Gamma_{yz}$ ,  $\Gamma_{xy}$  and  $\Gamma_{zx}$  being the components of the strain tensor in (x,y,z) and  $le$ ,  $me$ ,  $ne$   
and  $lg$ ,  $mg$ ,  $ng$  the direction cosines of  $e$  and  $g$  in (x,y,z).  $\epsilon_z = -(\epsilon_x + \epsilon_y)$  assuming  $\Delta V = 0$

## Limitations :

- time consuming
- finite strain tensor by twinning only
- significance of finite strain tensor in case of polyphase tectonics ?

Jamison and Spang (1976) :  
determination of differential stress magnitudes

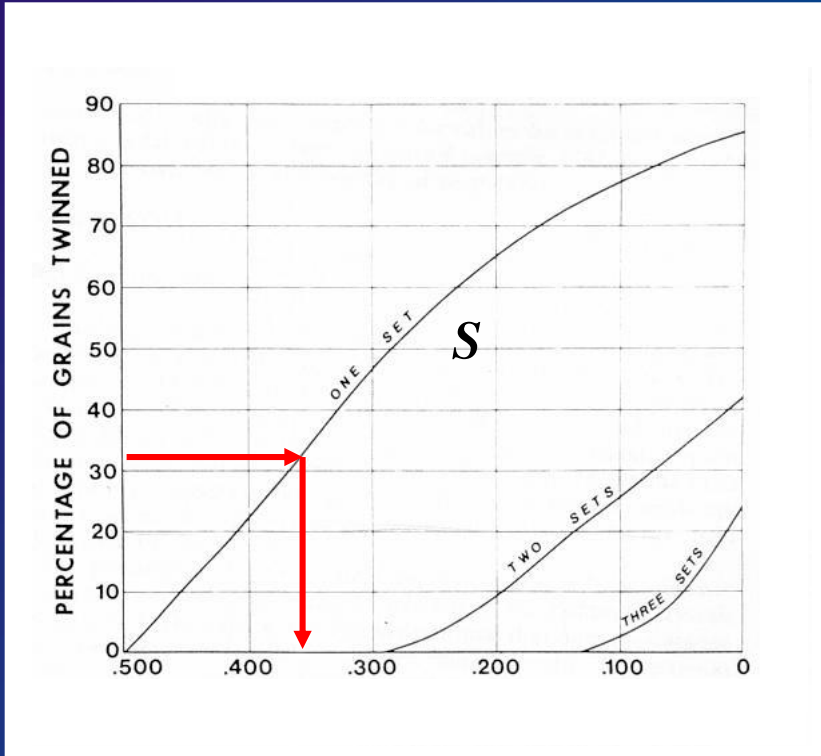


$$\tau_s = \Delta\sigma \cdot S$$



if  $\tau_c$  is known,  $\Delta\sigma$

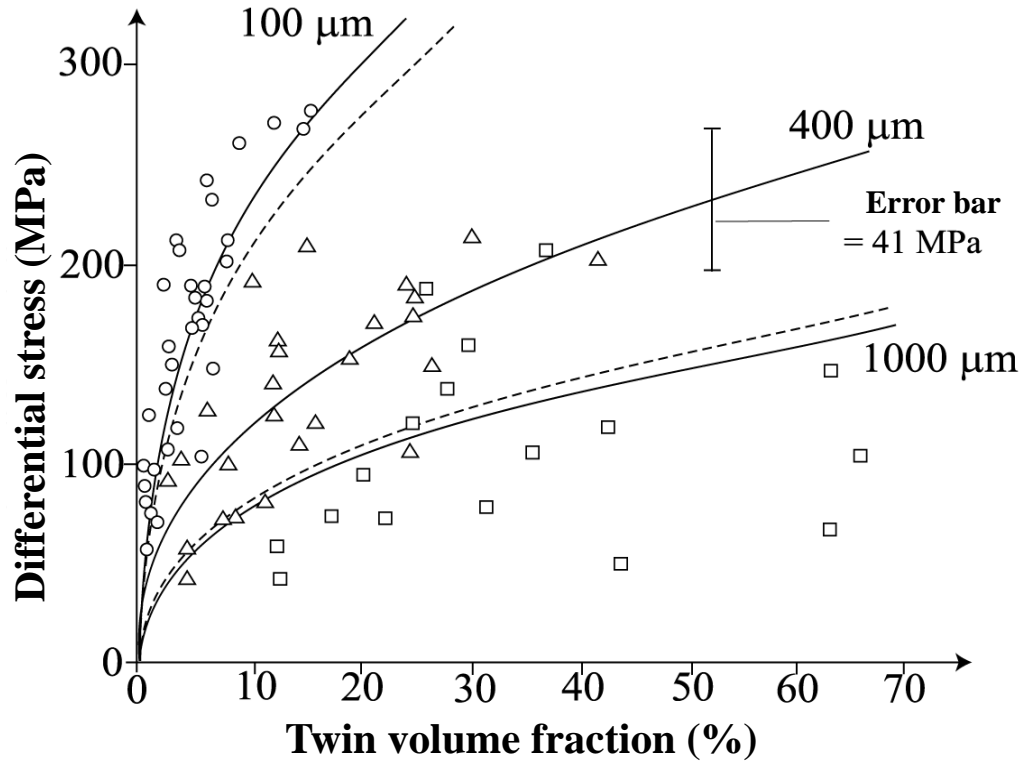
In a sample with no preferred crystallographic orientation, the percentages of grains twinned on 0, 1, 2 ou 3 twin planes are functions of the applied differential stress ( $\sigma_1 - \sigma_3$ ) value.  
Experimentally calibrated



Limitations :

- uniaxial stress
- critical resolved shear stress for twinning = constant  $\tau_c = 10$  MPa
- takes into account neither grain size nor mutual compatibility of twin systems
- significance of 'bulk' maximum differential stresses in case of polyphase tectonics ?

Rowe and Rutter (1990) : determination of differential stress magnitudes



*Twin volume fraction,*  
 $V$

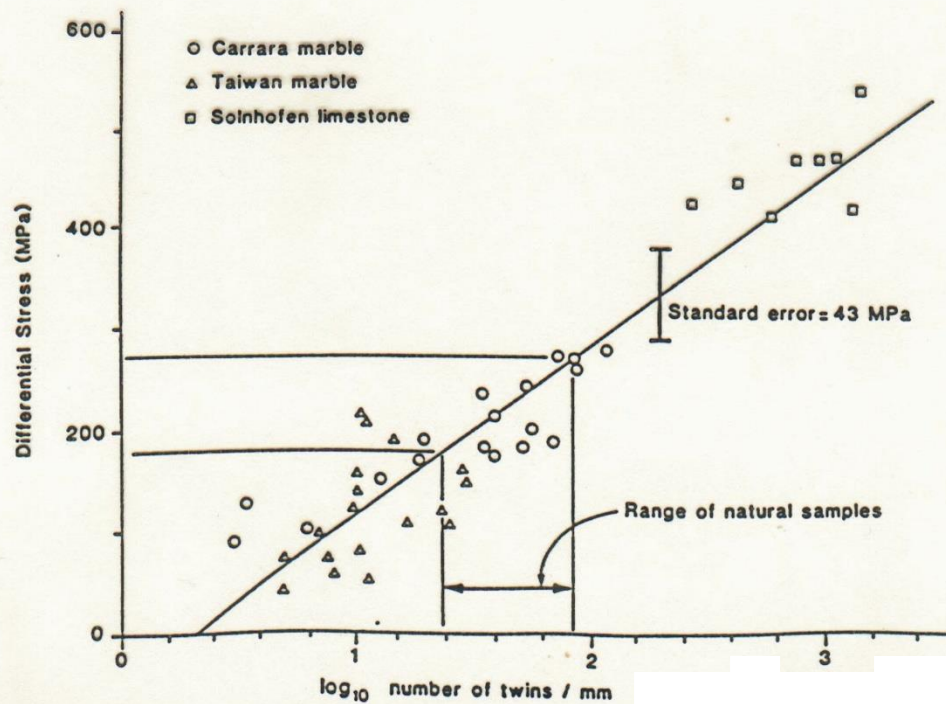
○ Grain size 100 μm  
△ Grain size 400 μm  
□ Grain size 1000 μm

$$\log \sigma = 2,72 + 0,40 \cdot (\log V - \log d)$$



Rowe and Rutter (1990) : determination of differential stress magnitudes

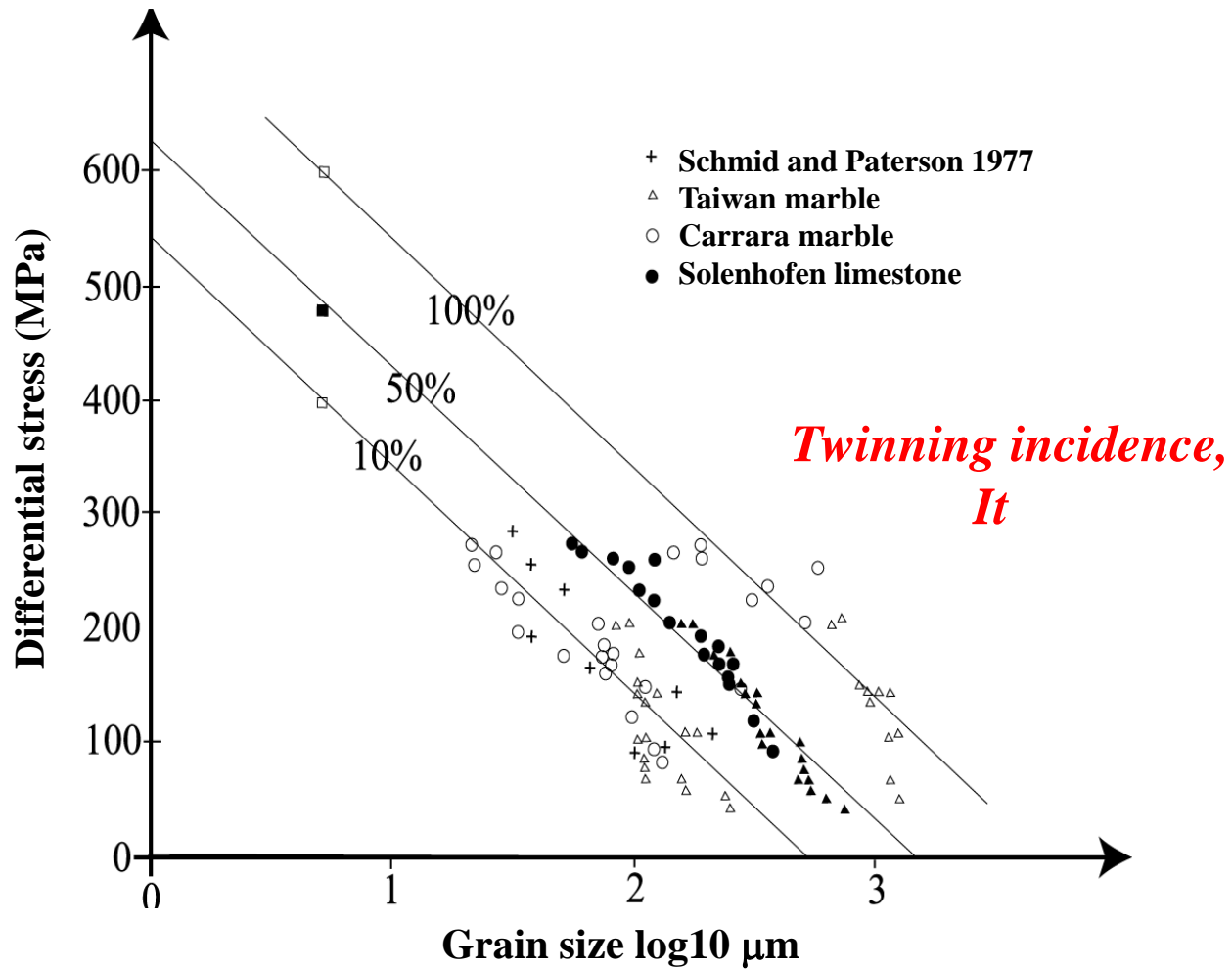
*Twin density,  $D$*



$$\sigma = -52,0 + 171,1 \cdot \log D$$

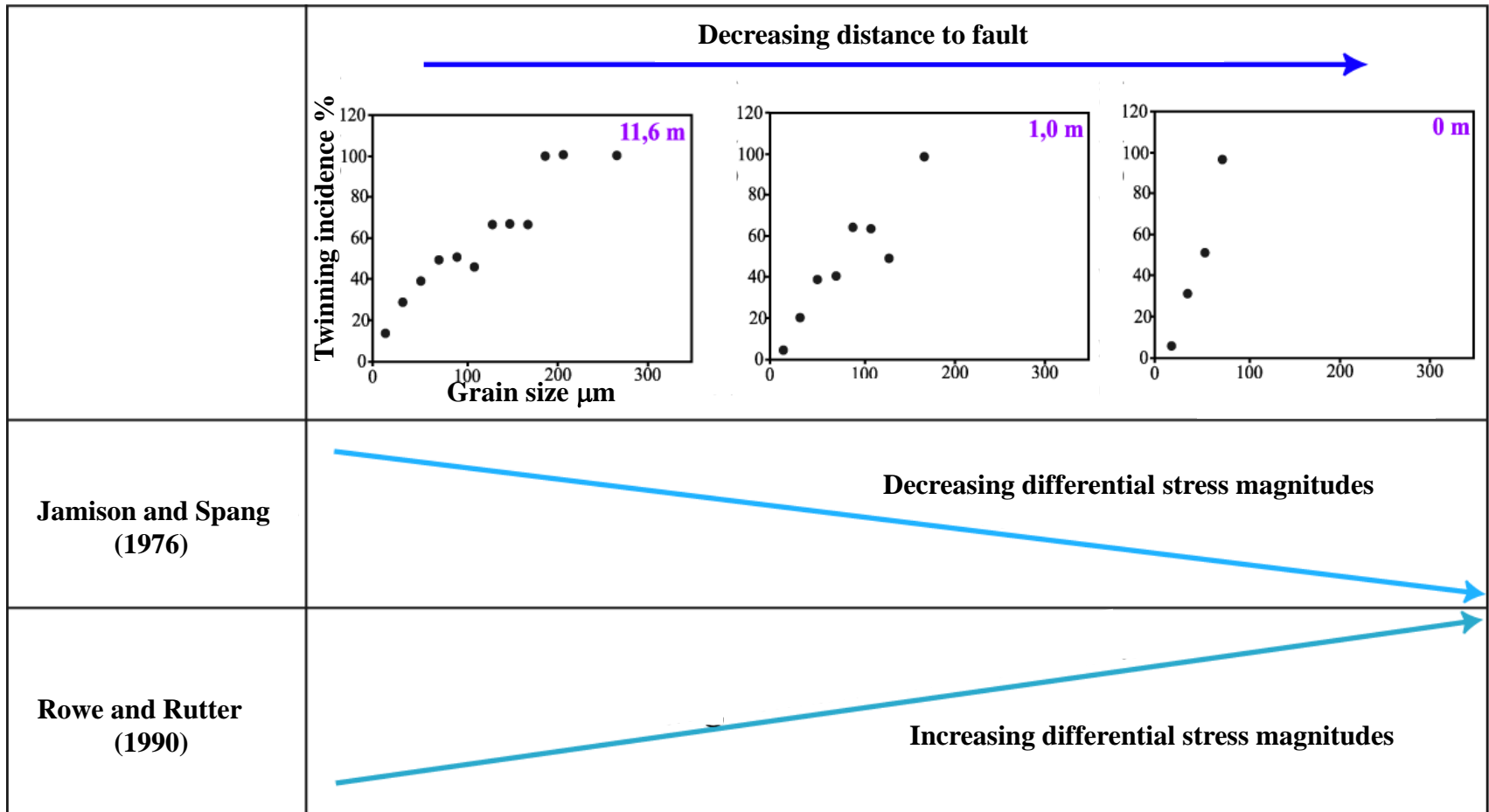
Independent on grain size

Rowe and Rutter (1990) : determination of differential stress magnitudes



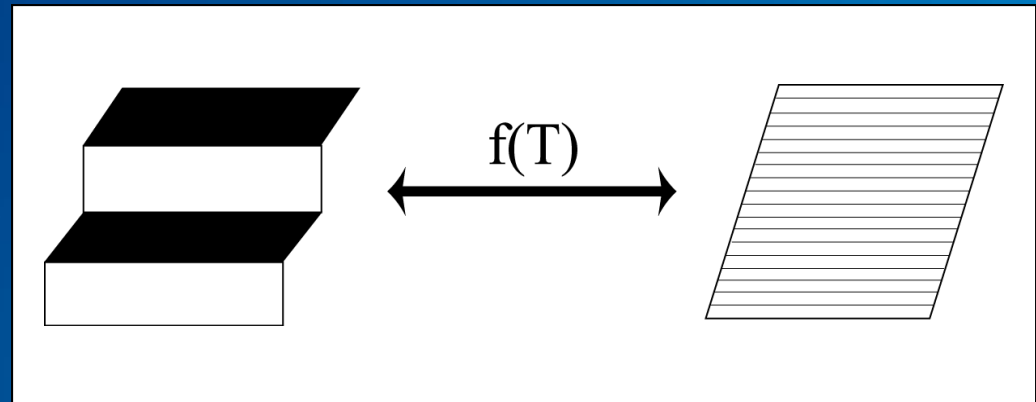
$$\sigma = 523 + 2,13 It - 204 \cdot \log d$$

# Influence of grain size distribution on estimates of differential stress magnitudes (after Newman, 1994)



# Influence of temperature on estimates of differential stress magnitudes (Ferrill, 1998)

	Référence			
Subalpine belt	Ferrill (1998)	Jamison et Spang (1976)	44 MPa	75 - 250 °C
		densité de macles de Rowe et Rutter (1990)	235 MPa	
Southern Pyrenees	Holl & Anastasio (1995)	Jamison et Spang (1976)	65 MPa	190 - 235 °C
		densité de macles de Rowe et Rutter (1990)	249 MPa	



⇒ Rowe and Rutter technique : well calibrated for temperature  $> 400^{\circ}\text{C}$ , BUT cannot be used at low  $T^{\circ}\text{C}$

To sum up :

- Turner's (1953) dynamic analysis : yields only  $\sigma_1$  and  $\sigma_3$  orientations
- Groshong's (1984) strain gauge technique : yields a twin strain tensor
- Jamison and Spang (1976) and Rowe and Rutter (1990) techniques :  
yield only 'bulk' maximum differential stress ( $\sigma_1 - \sigma_3$ )

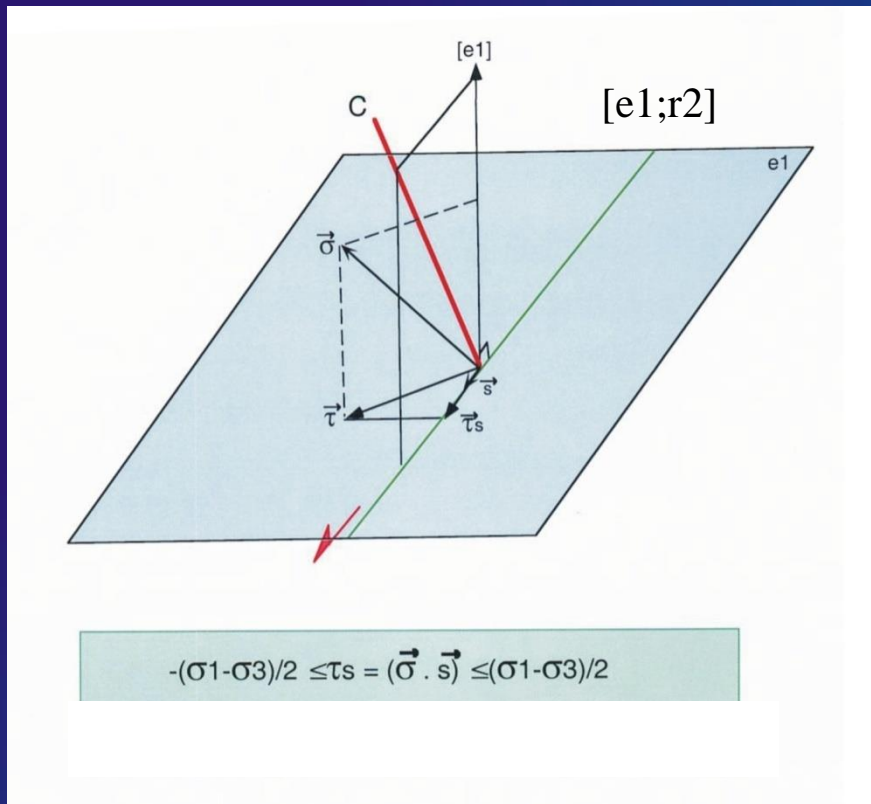
None of these techniques allows to relate differential stresses to principal stress orientations and stress regimes;

moreover,

they are commonly used separately without care of their specific limitations

**The Calcite Stress Inversion Technique**  
*(Etchecopar, 1984)*

« Etchecopar » (1984) technique : determination of the reduced stress tensor



The inversion process is very similar to that used for fault-slip data :  
 twin gliding along the twinning direction within the twin plane is geometrically comparable to slip along a slickenside lineation within a fault plane.

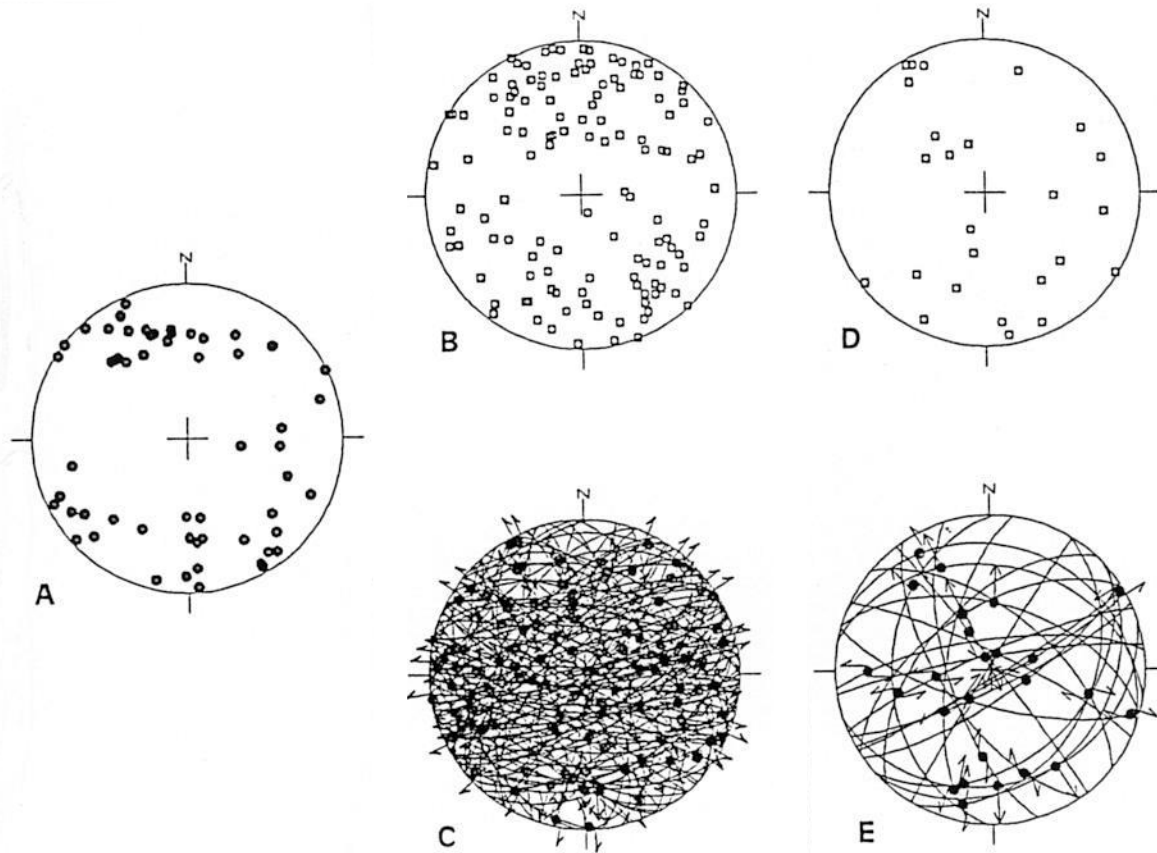
But the inversion process takes into account both twinned planes (resolved shear stress > CRSS)

**AND**

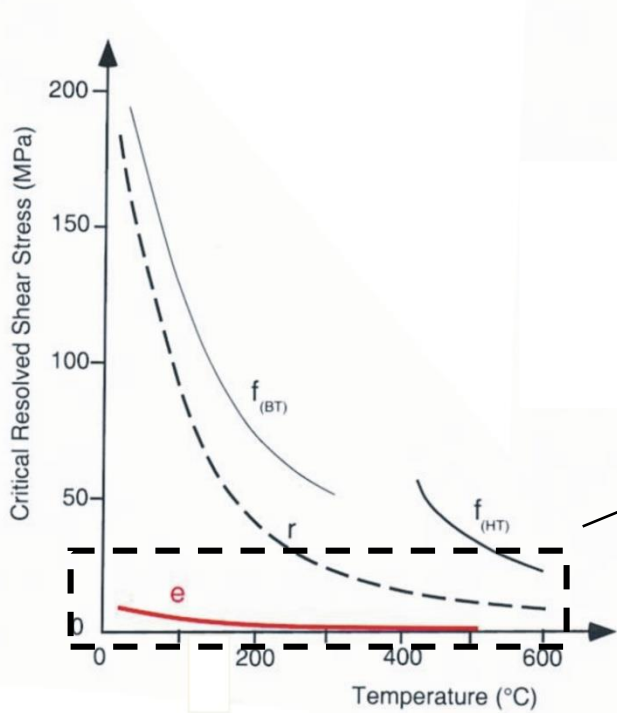
untwinned planes (resolved shear stress < CRSS),  
a major difference with inversion of fault-slip data

$$\begin{bmatrix} \sigma_1 \\ \sigma_2 \\ \sigma_3 \\ \Phi \end{bmatrix} \quad \Phi = \frac{(\sigma_2 - \sigma_3)}{(\sigma_1 - \sigma_3)}$$

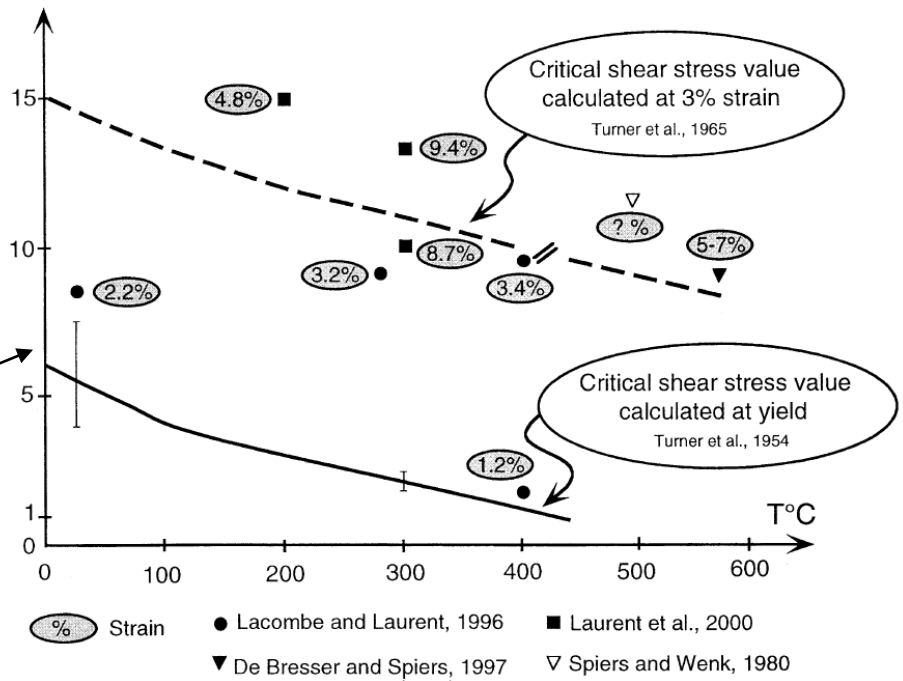
# The data...







Critical shear stress value for twinning (MPa)

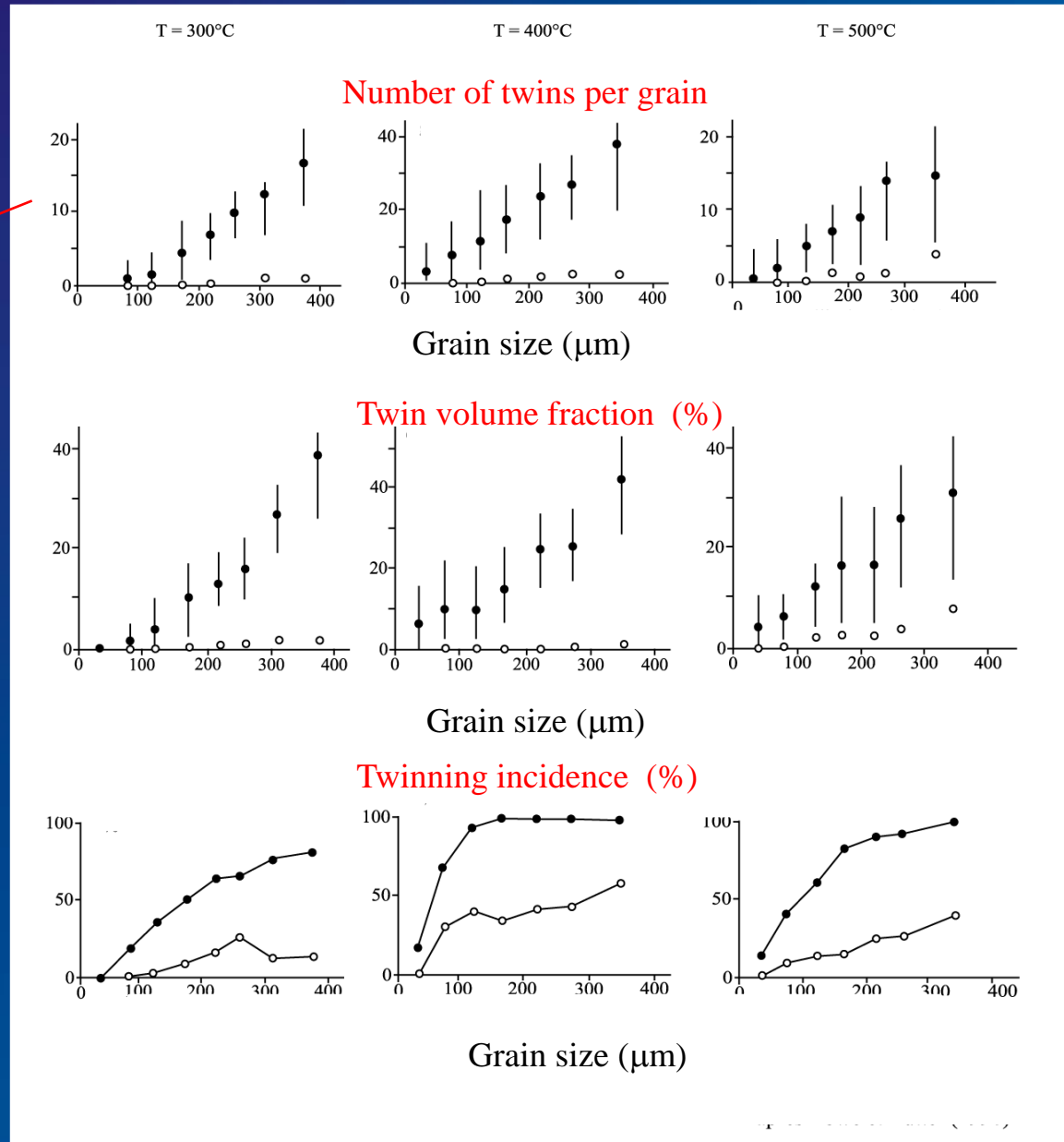


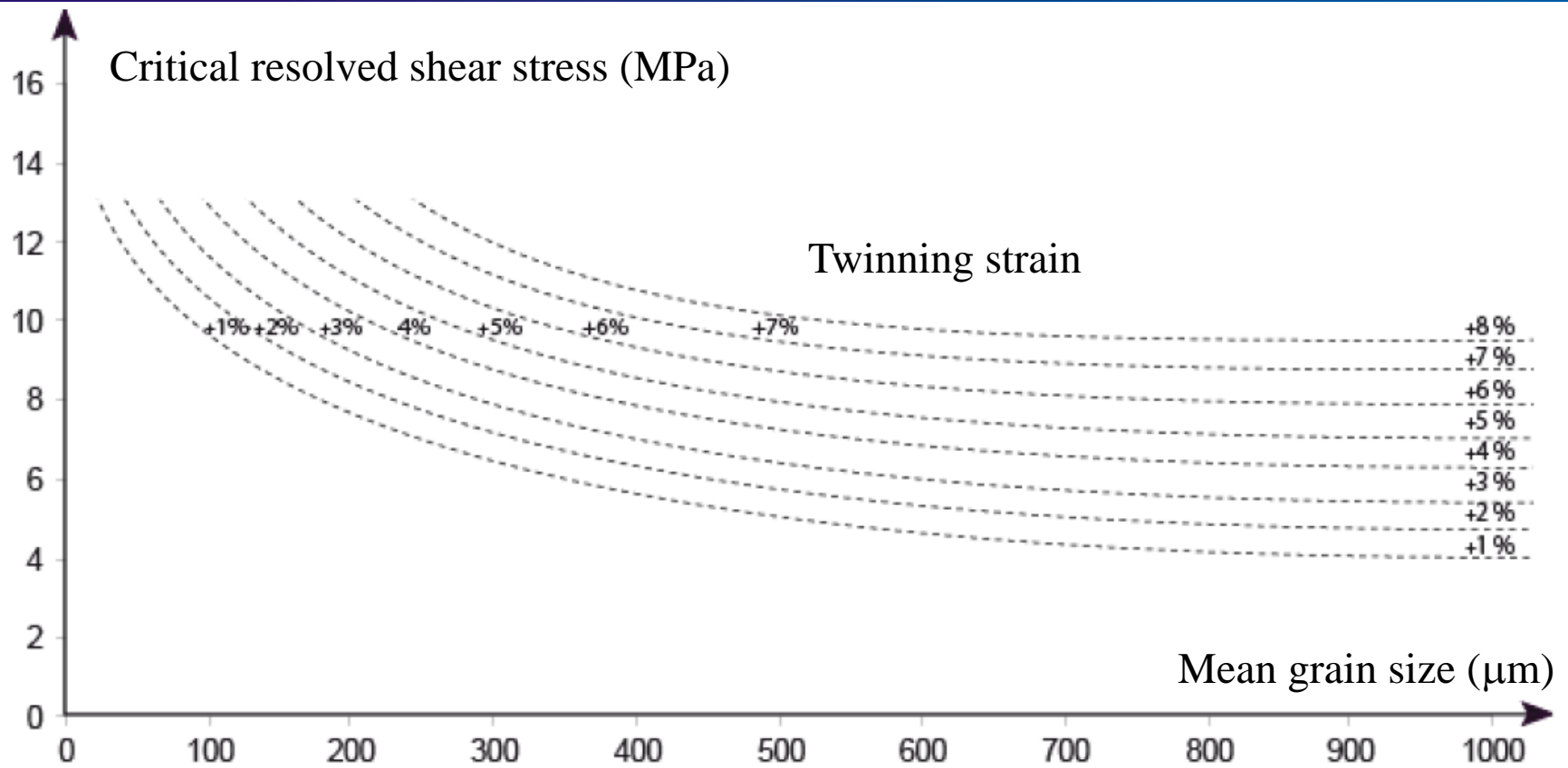
The Critical Resolved Shear Stress for twinning is ~ independent on T°C but depends on grain size and internal strain (hardening)

(Lacombe, 2001, 2010)

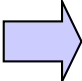
# Influence of grain size

(Rowe and Rutter, 1990)





(Amrouch, 2010)

Inversion of calcite twin data  **Reduced stress tensor  
(4 parameters)**

Orientation of principal stresses and stress ellipsoid shape ratio

$$\Phi = \frac{(\sigma_2 - \sigma_3)}{(\sigma_1 - \sigma_3)}$$



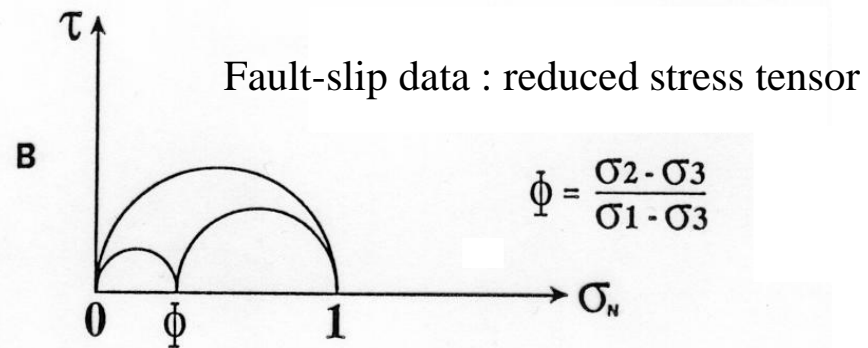
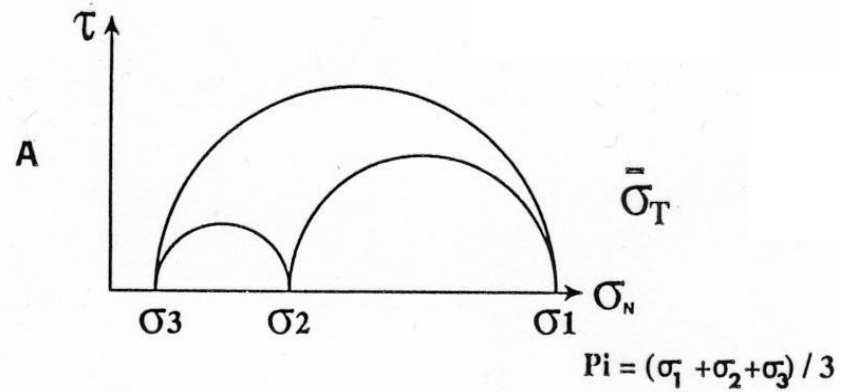
‘constant’ CRSS  
for a set of calcite grains  
of homogeneous size

**Deviatoric stress tensor (5 parameters)**

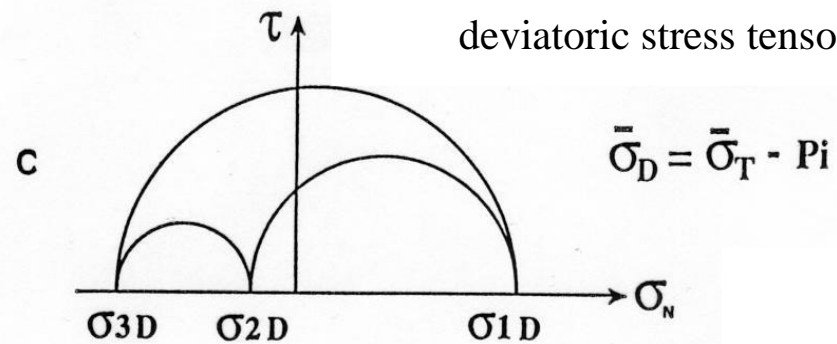
$$T_D = T - \left( \frac{\sigma_1 + \sigma_2 + \sigma_3}{3} \right) \cdot I$$

Orientation of principal stresses and differential stress magnitudes

$$(\sigma_1 - \sigma_3) \quad (\sigma_2 - \sigma_3)$$



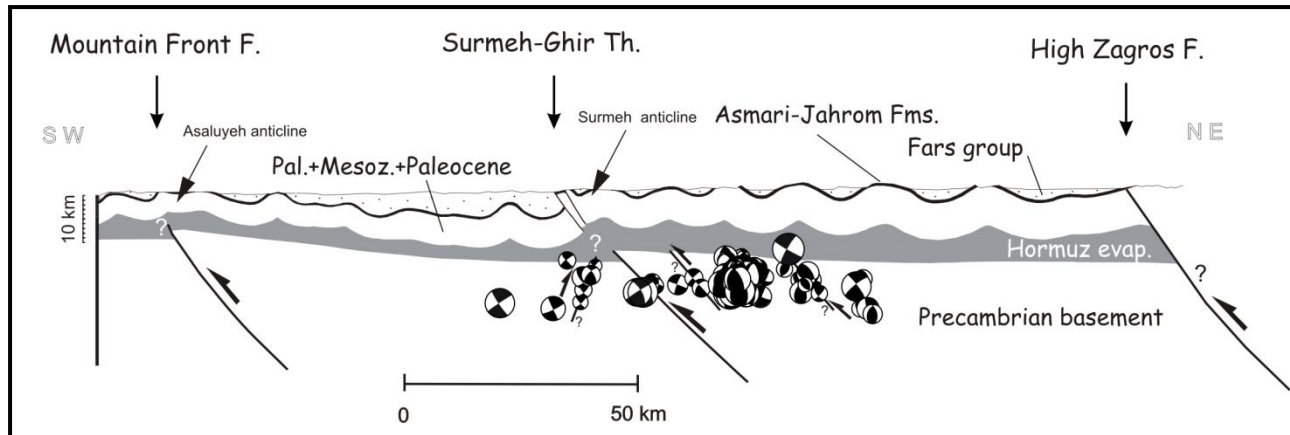
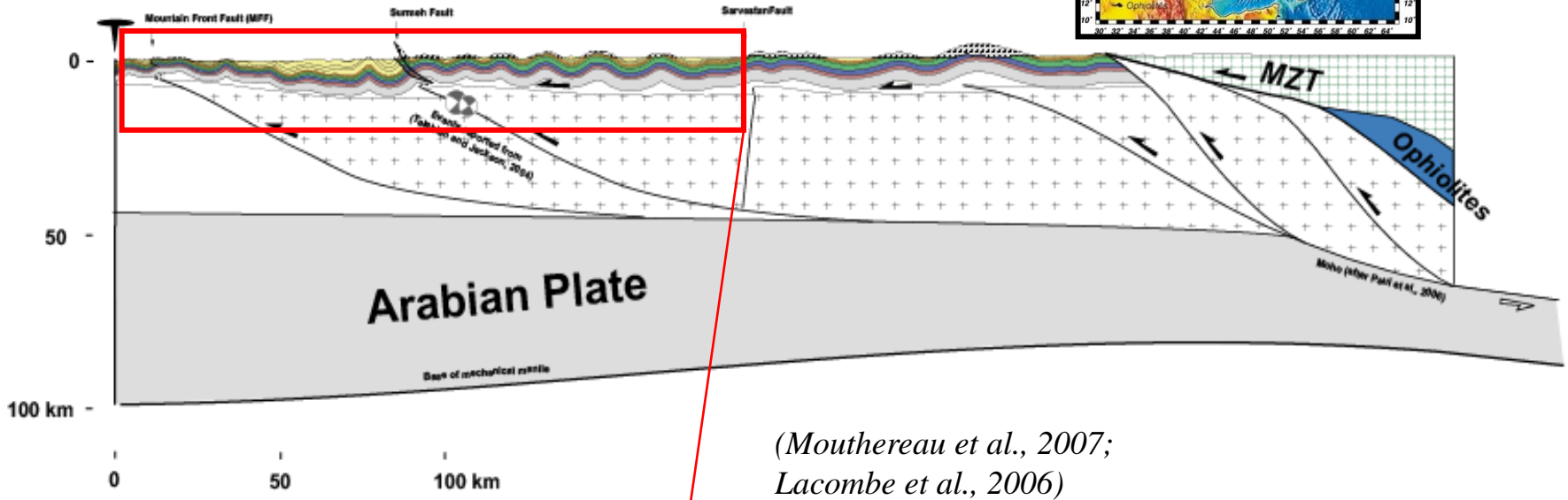
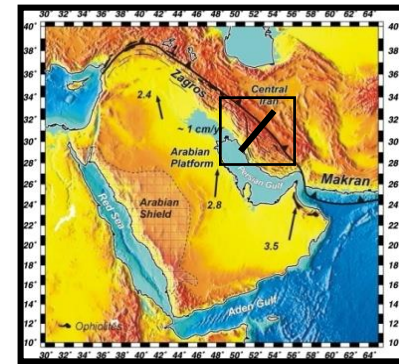
Calcite twin data :  
deviatoric stress tensor



**Differential stress magnitude across a fold-thrust belt :**  
**The Zagros case**

The Zagros belt results from the collision between Arabia and Central Iran, beginning in (Oligo ?)-Miocene times and continuing today.

About one third of the 22-25 mm/yr Arabia-Eurasia convergence is currently accommodated in the Zagros.



*Shiraz*



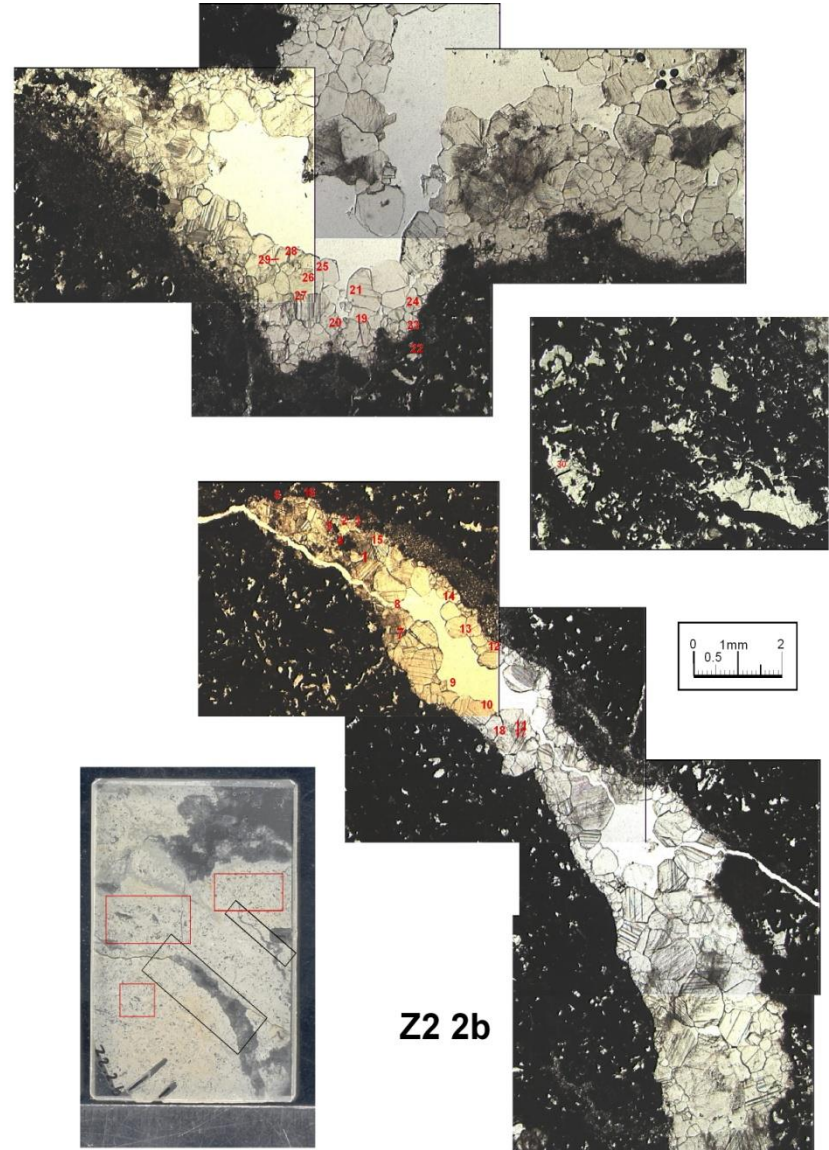
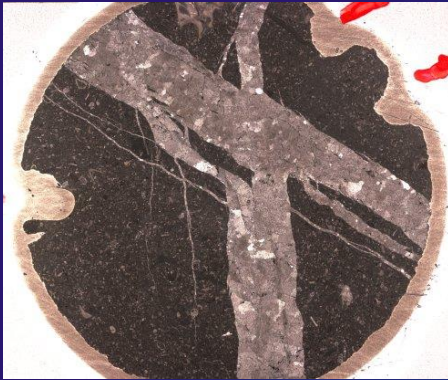
*Firuz Abad*



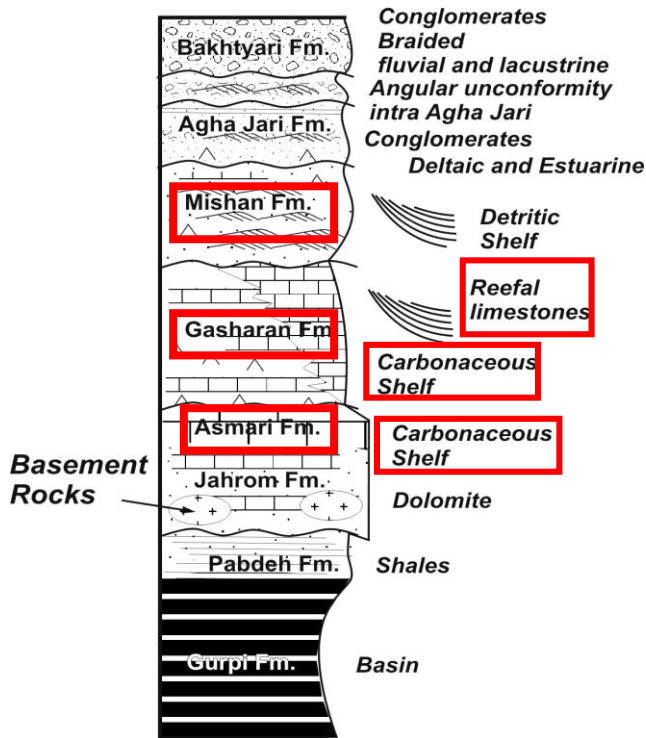
**FARS**

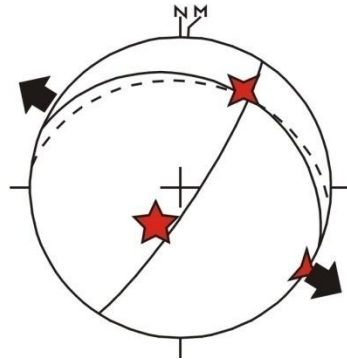
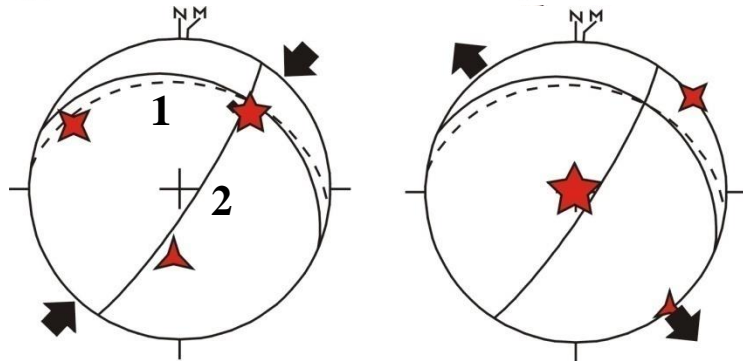
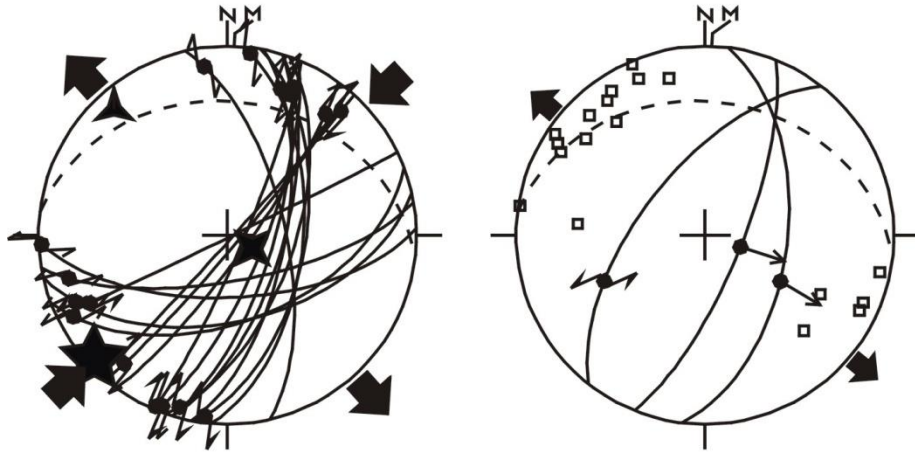


# Twins are analysed within host rocks and veins from field samples and/or drill cores



## FARS





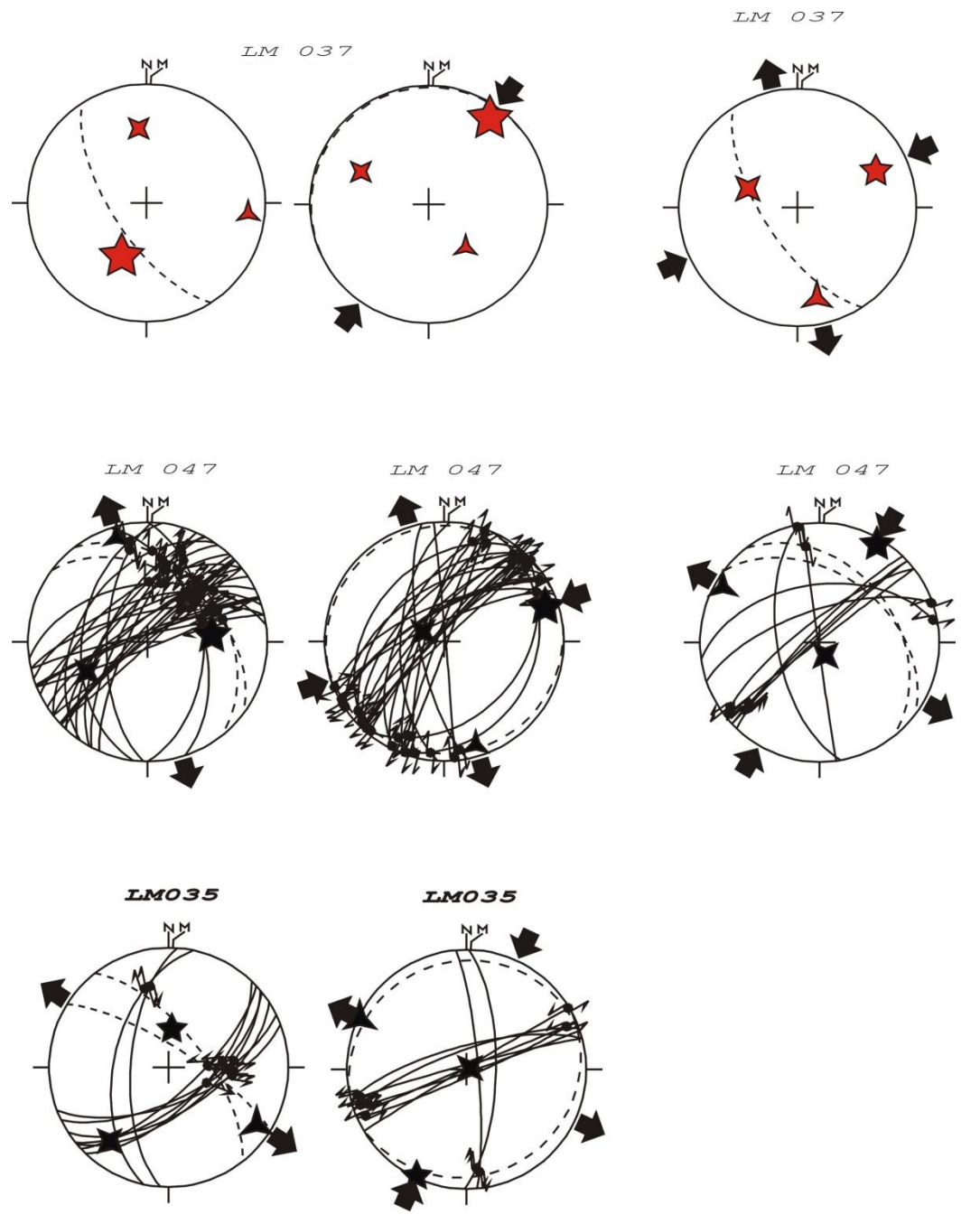
Data coming from host rocks and/or syn-folding veins are treated separately or together to check for internal consistency. Consistency with fracture and fault-slip data is also checked

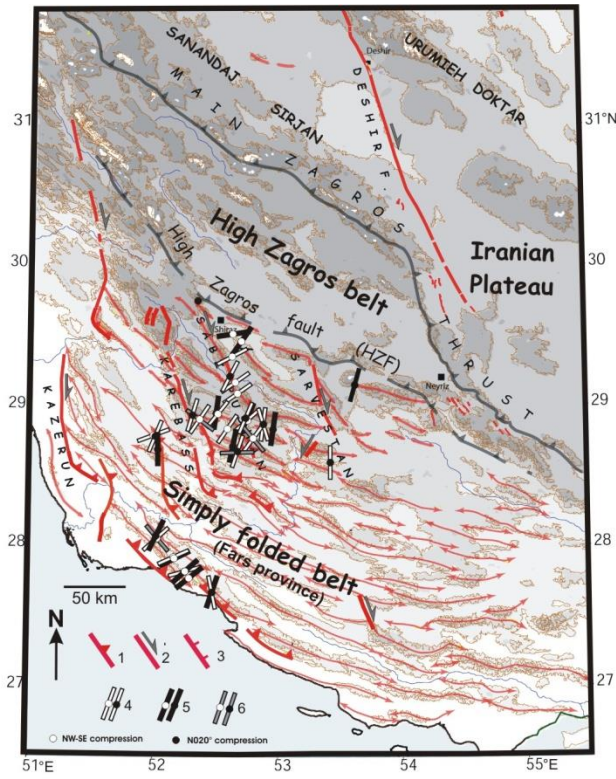
Tensors determined from vein 1

Tensor determined from vein 2

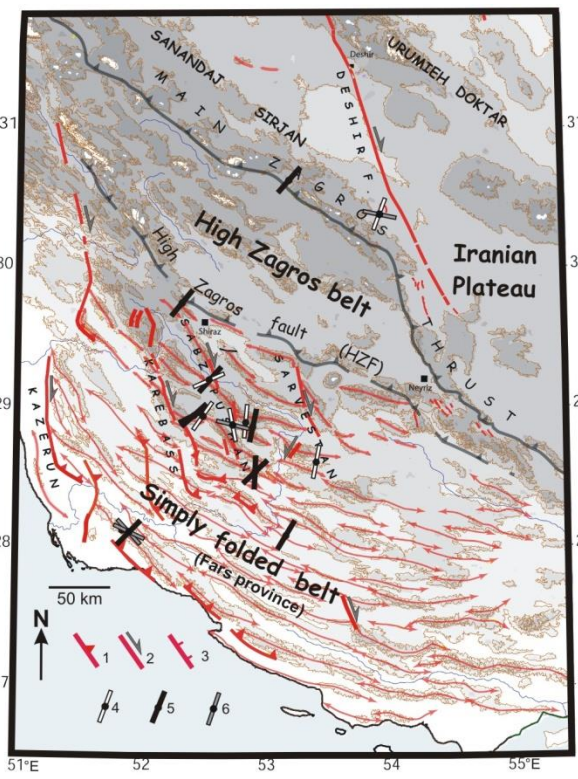
Sampling in fold limbs allows establishing a relative chronology between twinning strain and folding

Fault slip data and calcite twin data indicate that the NE-SW compression prevailed before and after folding, and therefore is responsible for folding

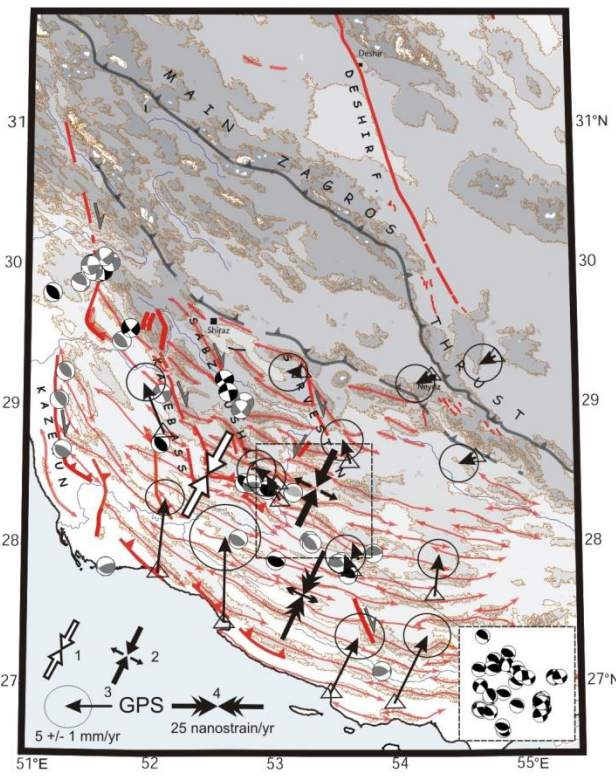




Neogene compressional trends from fault slip data in the cover (Lacombe et al., 2006)



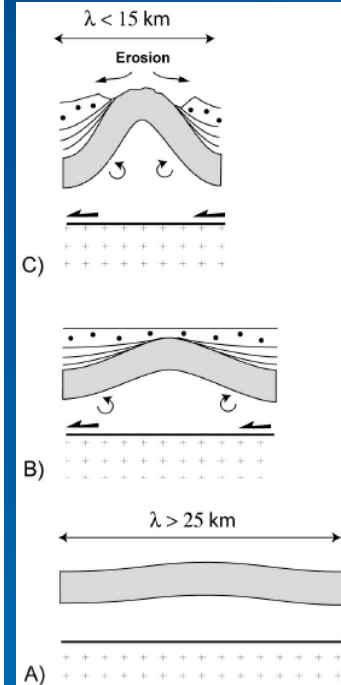
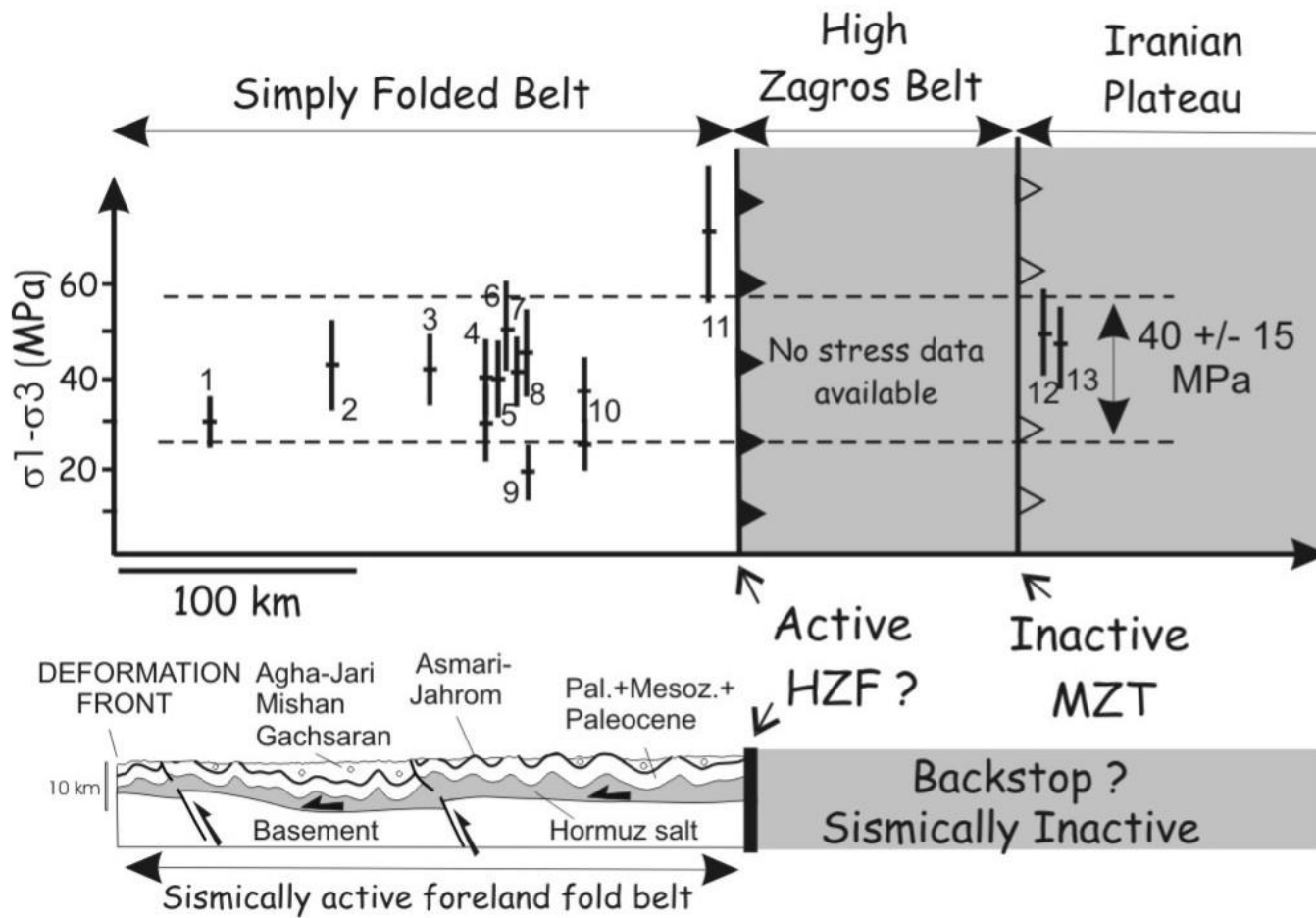
Neogene compressional trends from calcite twin data in the cover (Lacombe et al., 2007)



Current compressional trends from earthquake focal mechanisms in the basement (Lacombe et al., 2006) and GPS shortening rates (Walpersdorf et al., 2006)

→ Neogene collisional stresses consistently recorded at all scales  
 → The salt-bearing Hormuz master decollement poorly decouples basement and cover stress fields

(Lacombe et al.,  
Geology,  
2007)



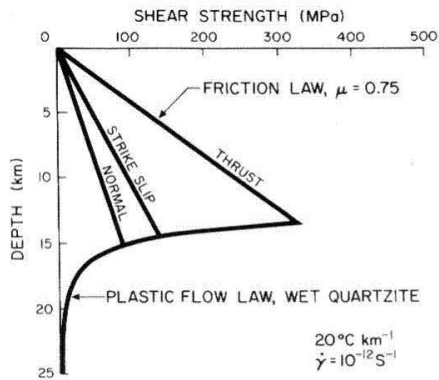
The relative homogeneity of differential stresses agrees with the homogeneously distributed shortening across the SFB, where no deformation gradient toward the backstop is observed in contrast to classical fold-thrust wedges

Both pre- and post-folding differential stresses are low --> folding likely occurred at low stresses; this favours pure-shear deformation and buckling of sedimentary rocks rather than brittle tectonic wedging.

**Differential stress magnitudes as a function of depth  
in the continental crust**

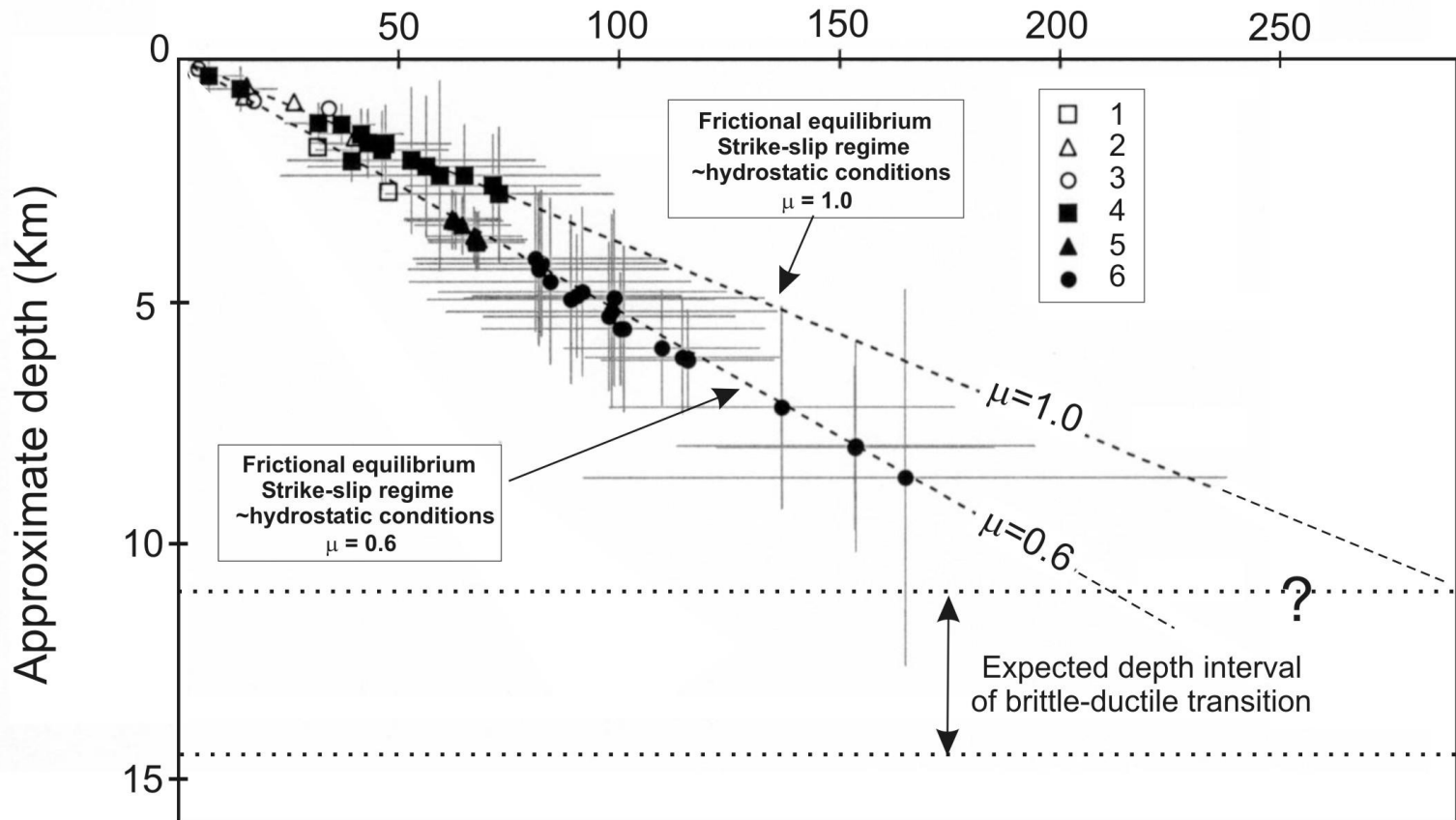
Strength of the continental crust controlled by frictional sliding on well-oriented pre-existing faults with frictional coefficients of 0.6-0.9 under hydrostatic fluid pressure (frictional stress equilibrium).

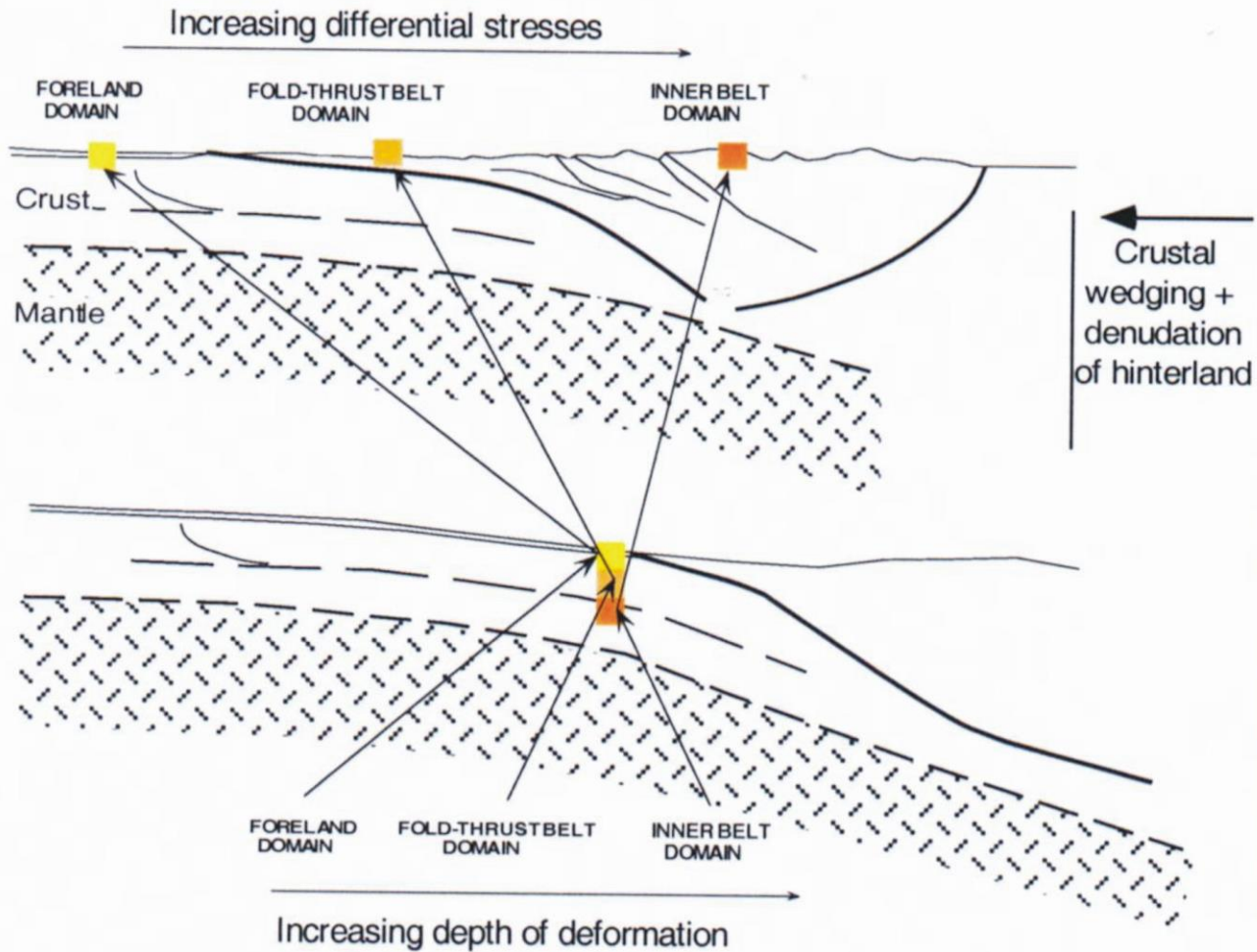
(After Townend and Zoback, 2000)



Simple model of the strength of the lithosphere. In the upper part, optimally oriented faults are assumed with Coulomb friction and constant  $\mu = 0.75$  and hydrostatic pore pressure. For the lower part, an experimentally determined flow law for wet quartzite (Jaoul, Tullis, and Kronenberg, 1984) has been extrapolated, assuming the strain rate and temperature gradient as indicated.

Differential stress ( $\sigma_1 - \sigma_3$ ) (MPa)

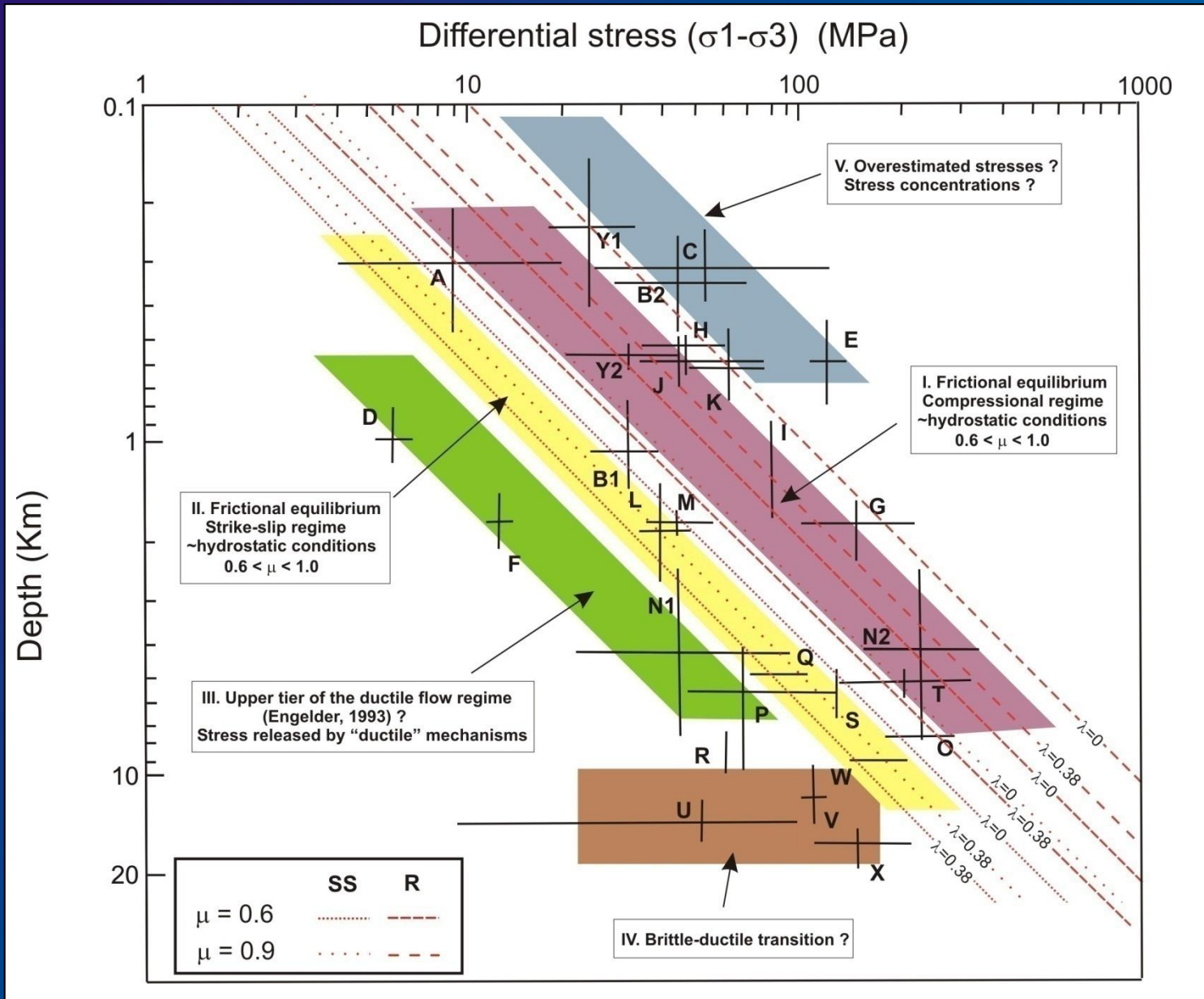




(Lacombe, *Tectonics*, 2001)



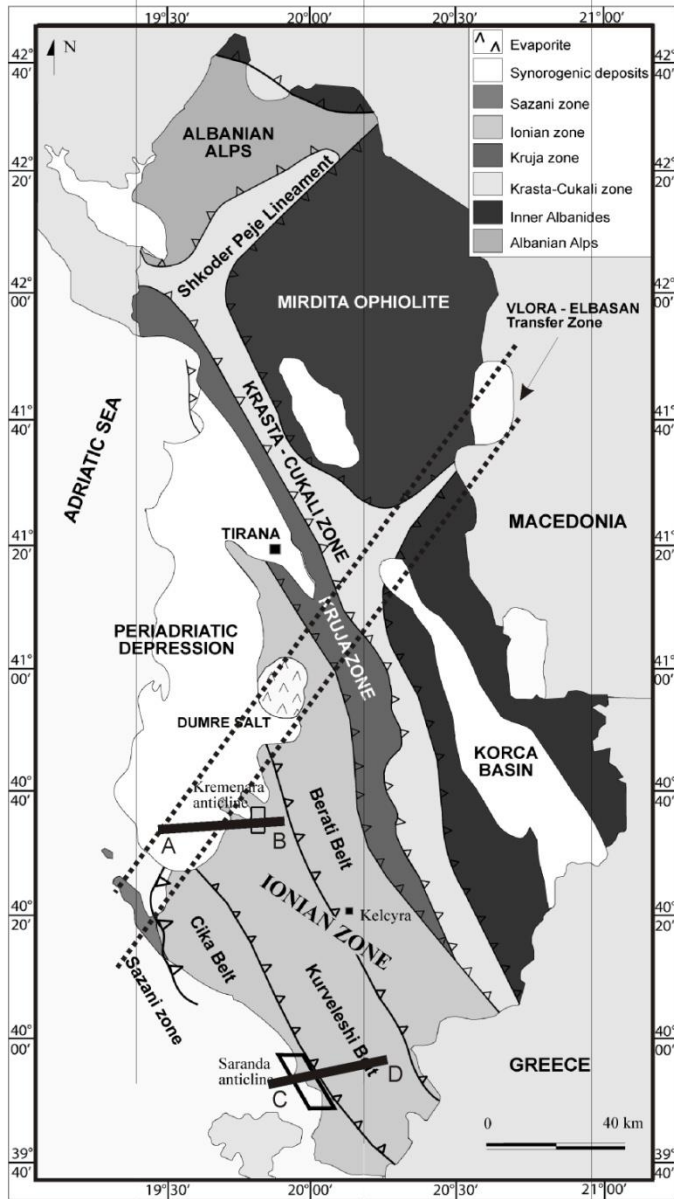
(Lacombe,  
Journal of Structural  
Geology, 2007)



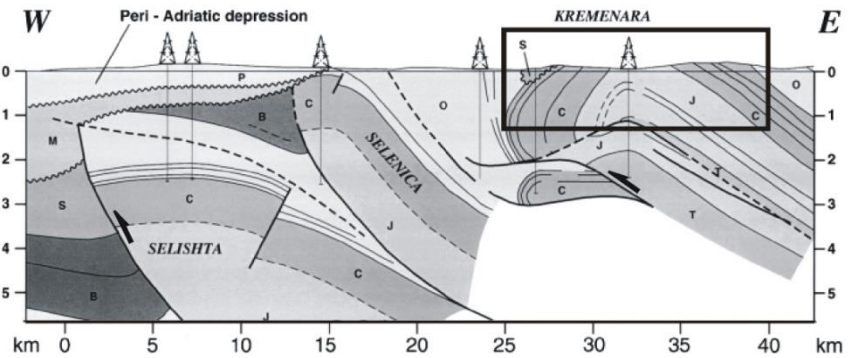
The strength of the continental crust down to the brittle-ductile transition is generally controlled by frictional sliding on well-oriented pre-existing faults with frictional coefficients of 0.6-0.9 under hydrostatic fluid pressure (frictional stress equilibrium).

Some ductile mechanisms may, however, relieve stress and keep stress level beyond the frictional yield, as for instance in the detached cover of forelands.

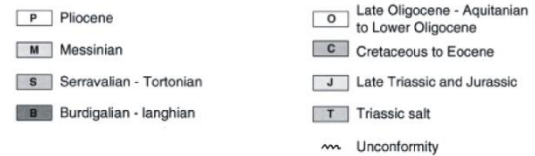
**From differential stress magnitudes to paleoburial  
and exhumation path in fold-thrust belt :  
The outer Albanides case**



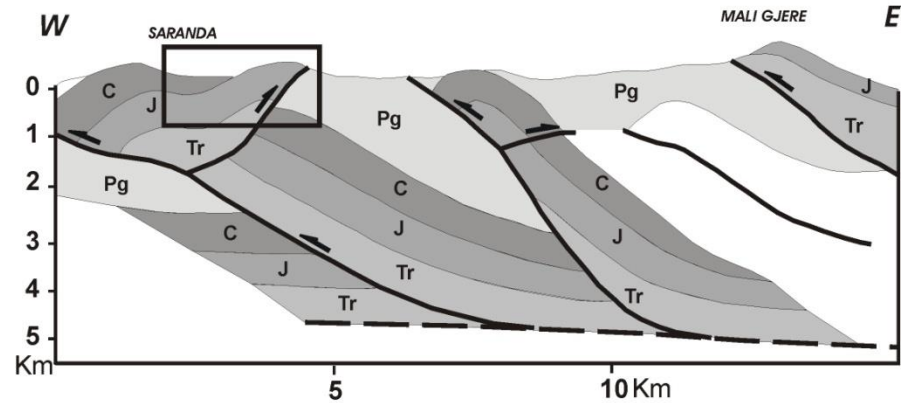
A



B



AB section

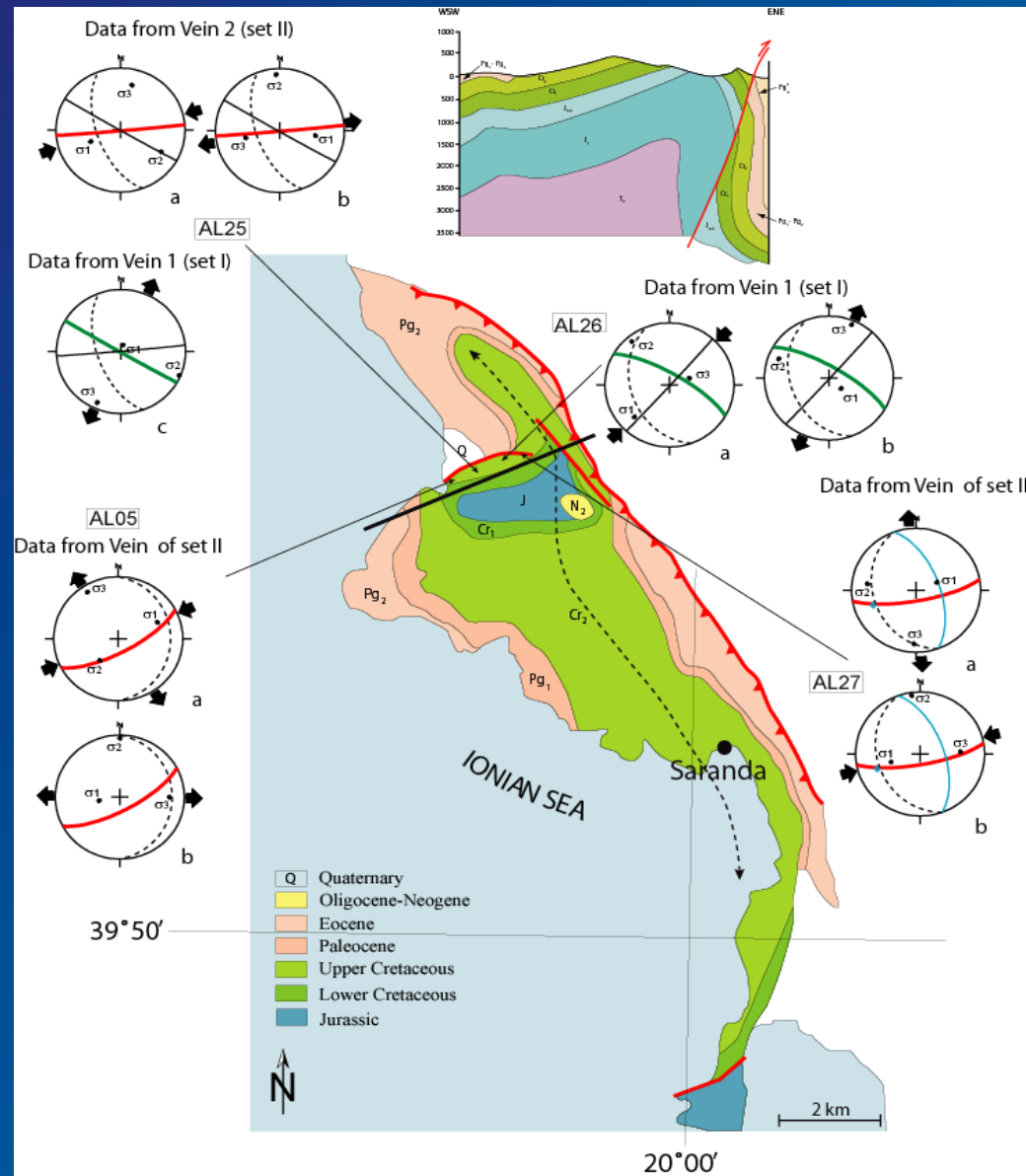
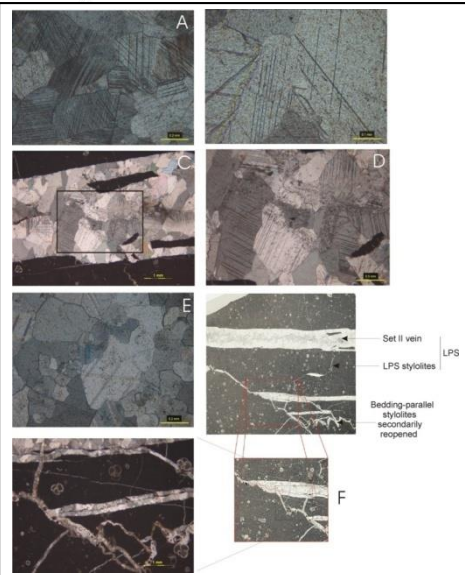
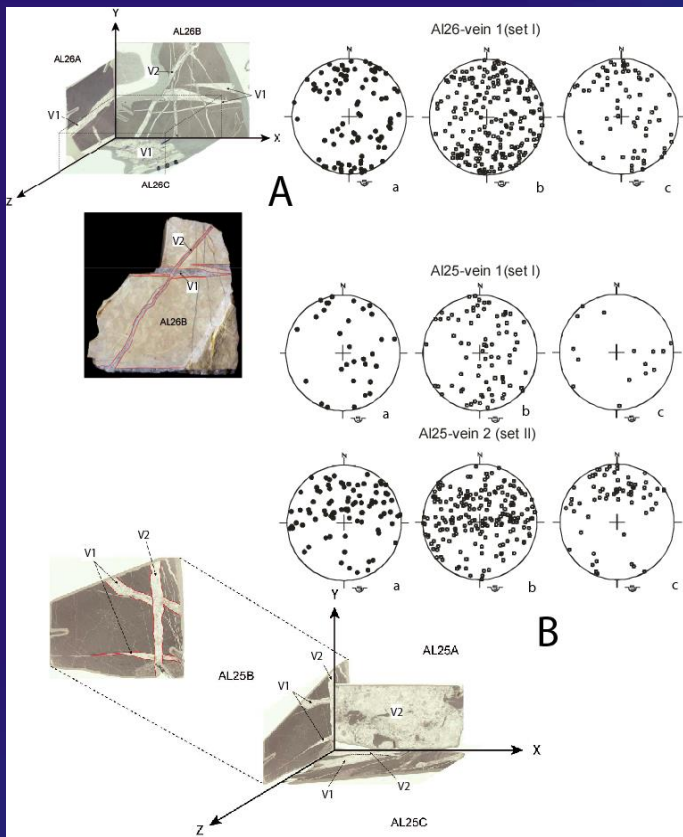


Tr, J, C : Triassic, Jurassic, Cretaceous  
Pg : Paleogene

C

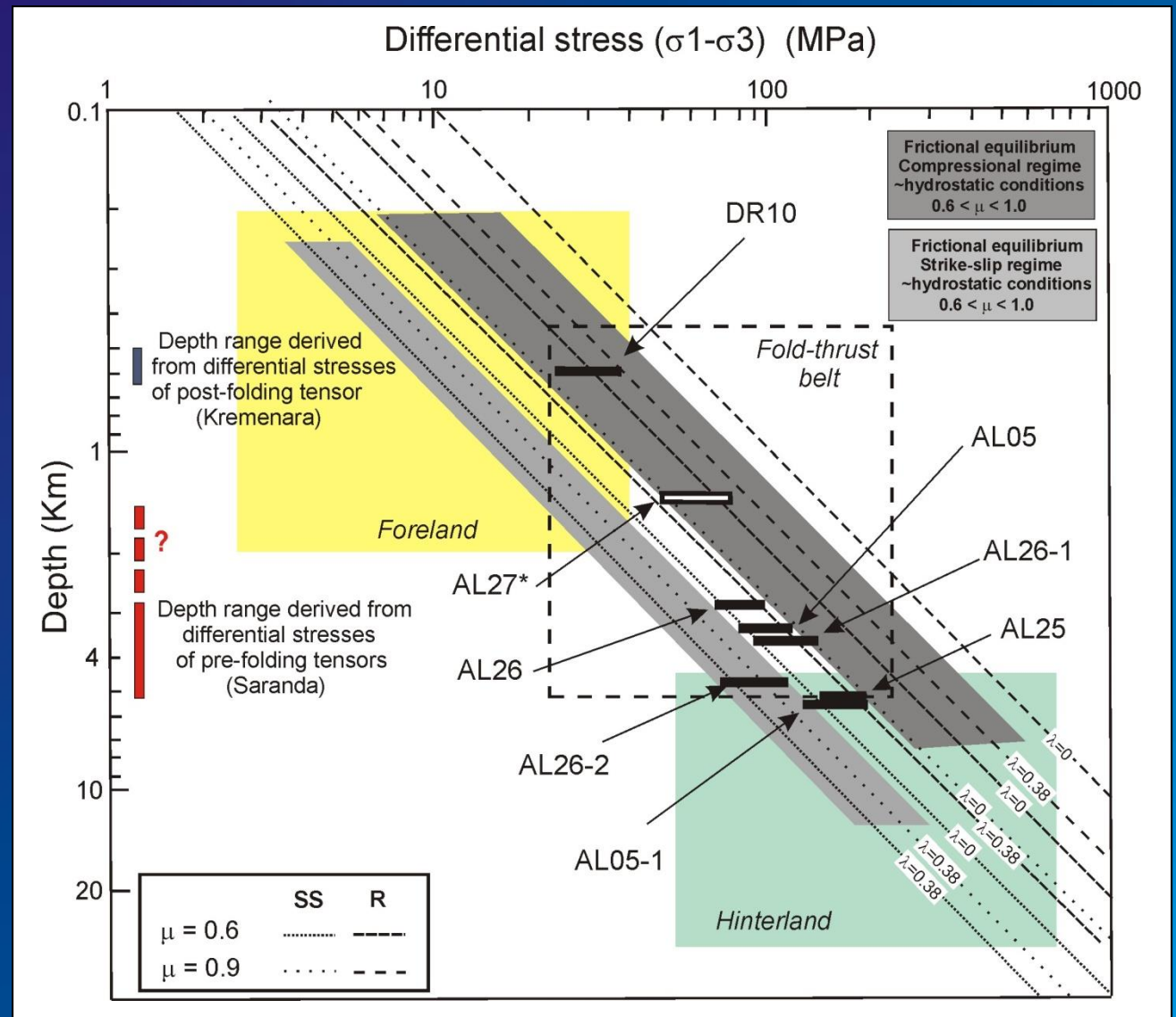
CD section

During the Alpine orogeny, the Albanian foothills formed as a consequence of the deformation of the former eastern passive margin of Apulia; the external zones were overthrust during the Neogene.

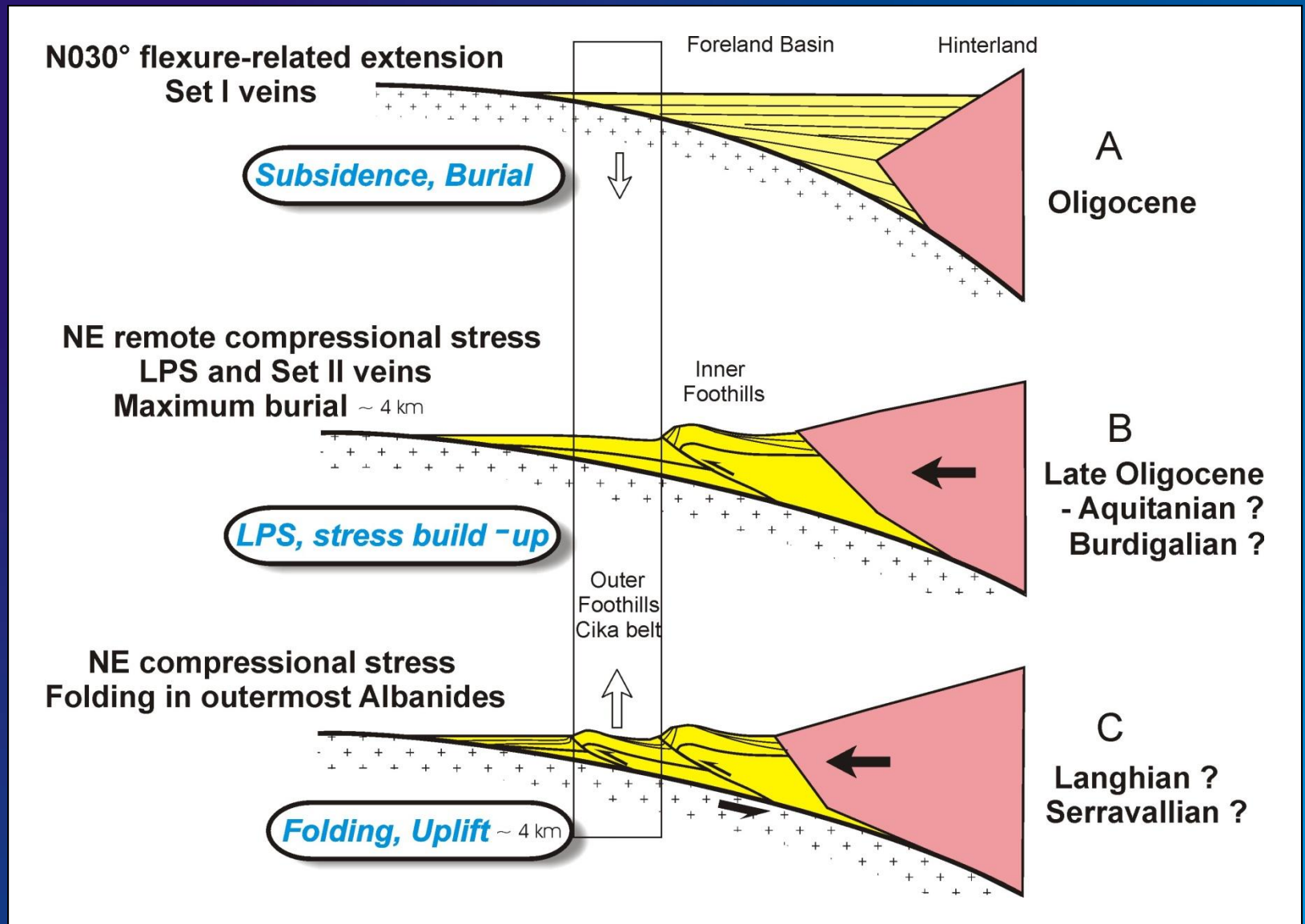


(Lacombe et al., Tectonophysics, 2009)

Calcite twins provide estimates of pre-folding paleoburial consistent with independent paleoburial estimates from micro-thermometry of fluid inclusions, maturity of organic matter and results of 1D thermal modeling.



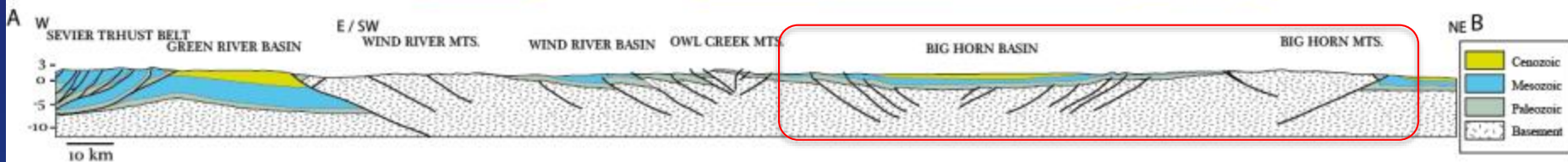
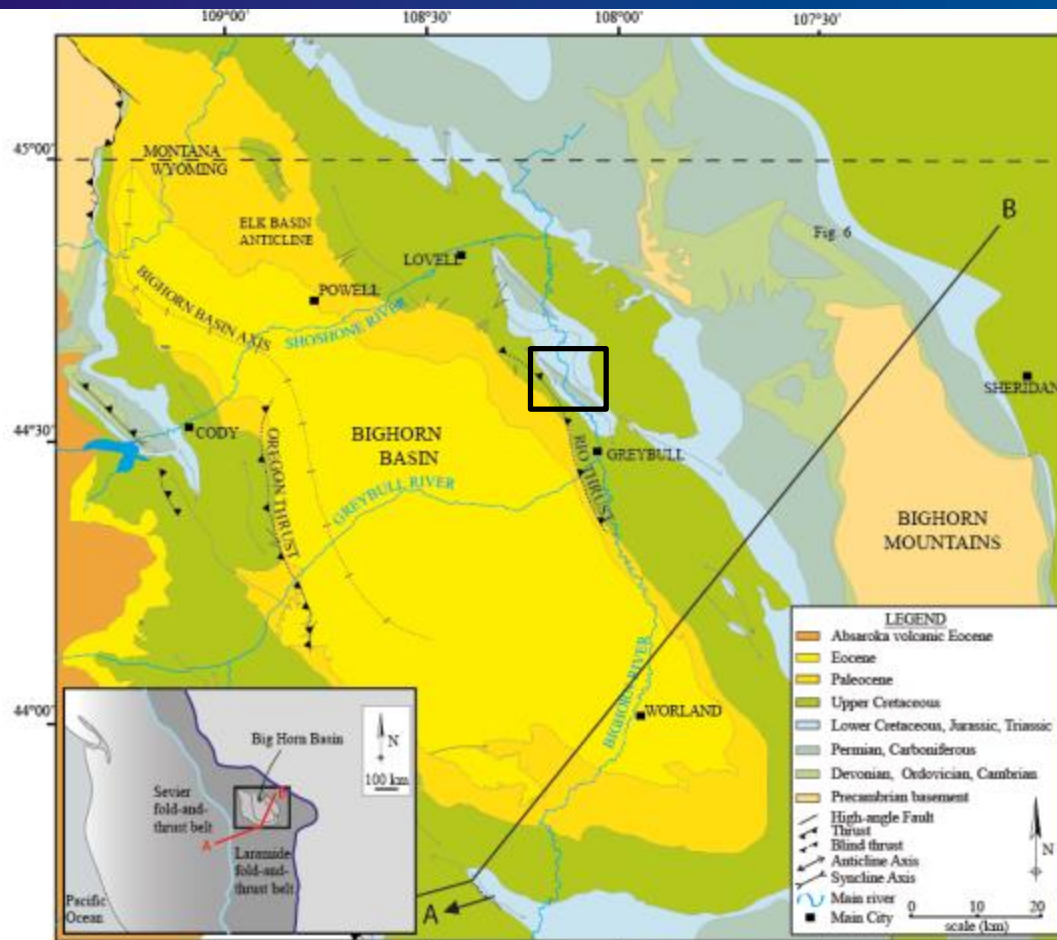
(Lacombe et al., Tectonophysics, 2009)

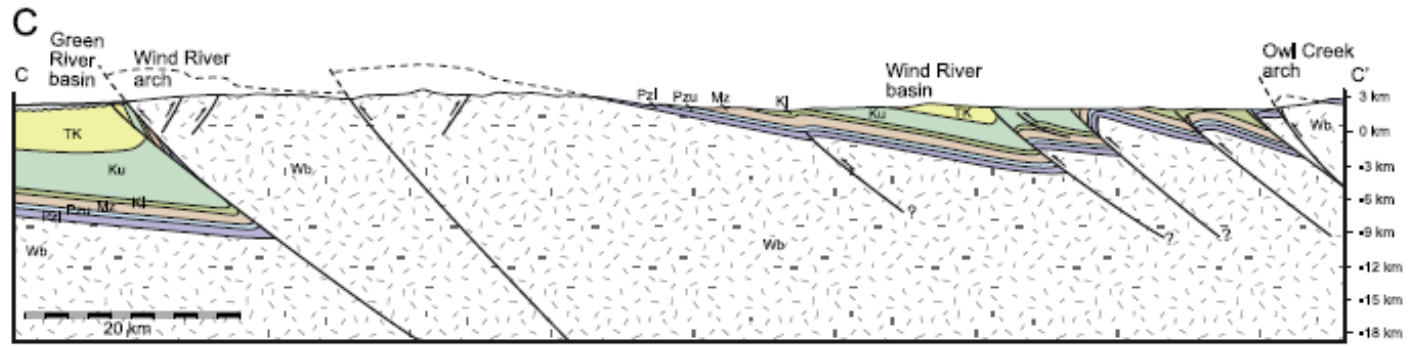
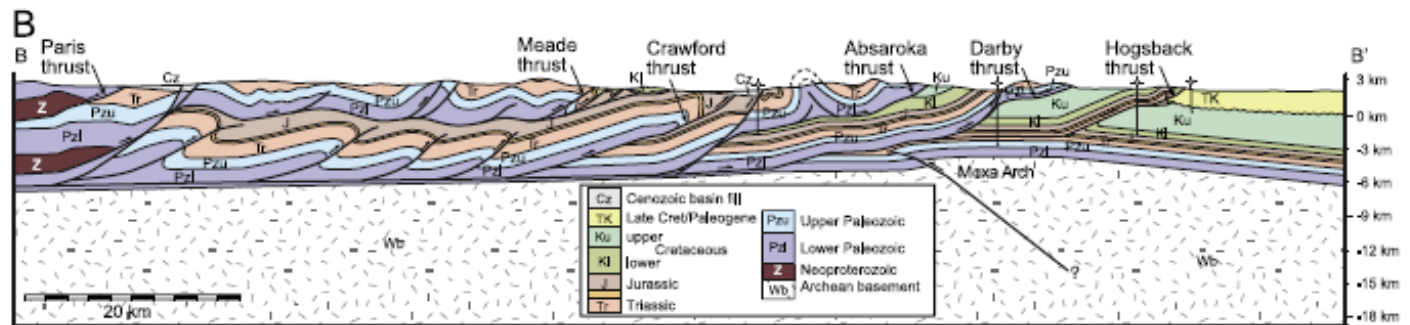
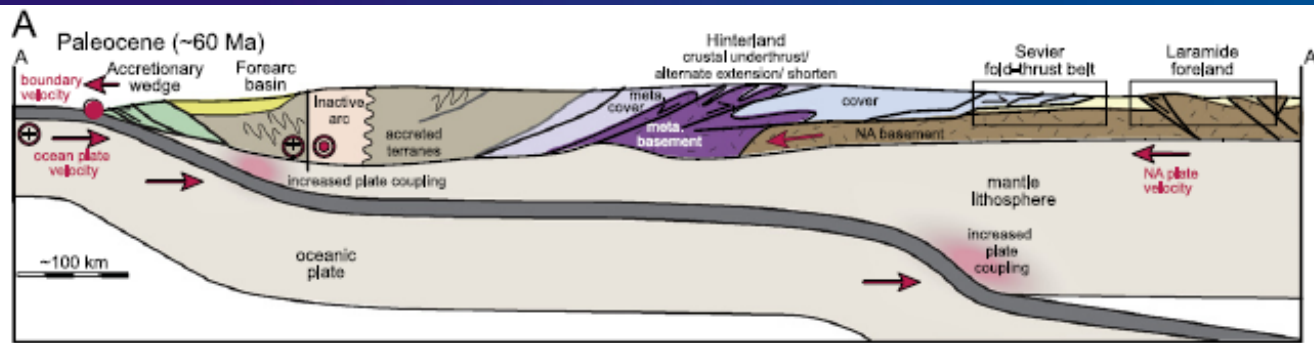


**Differential stress magnitudes, principal stress magnitudes  
and fluid (over)pressures during fold evolution :  
The Sheep Mountain Anticline case**



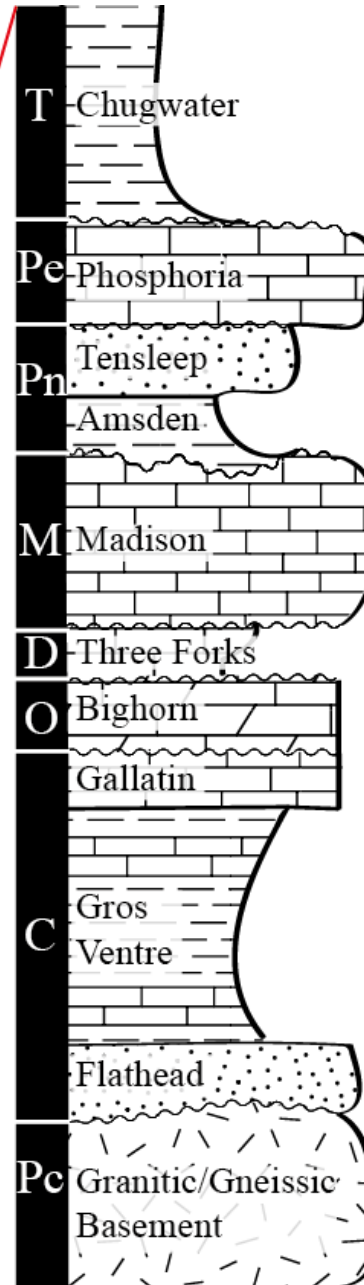
# The Bighorn Basin, and the Sevier and Laramide orogenies

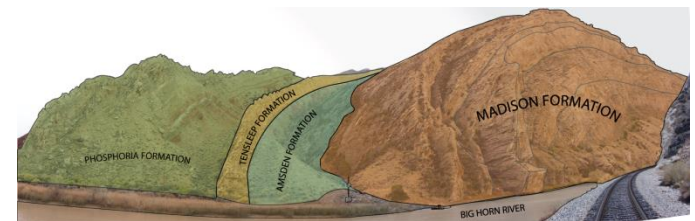
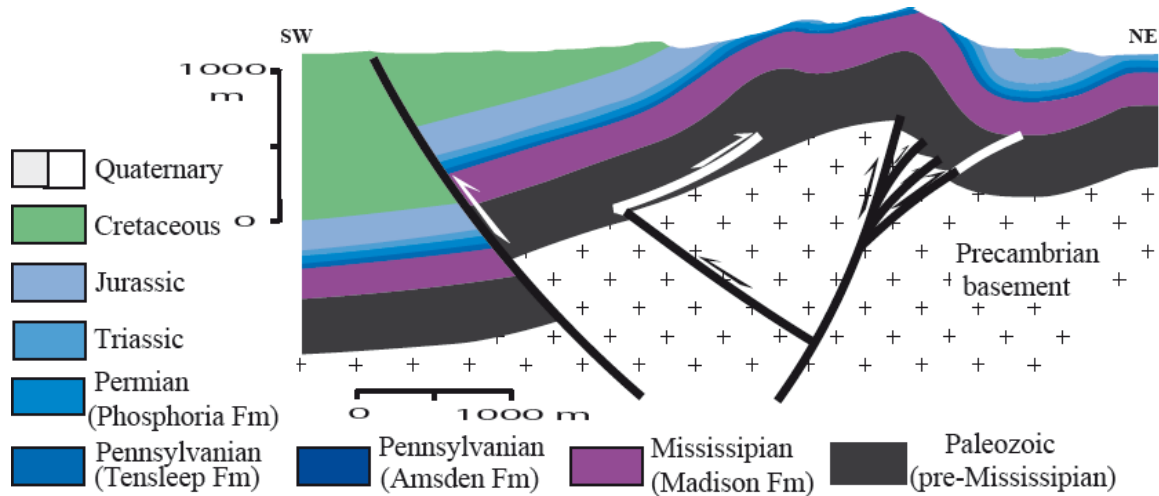
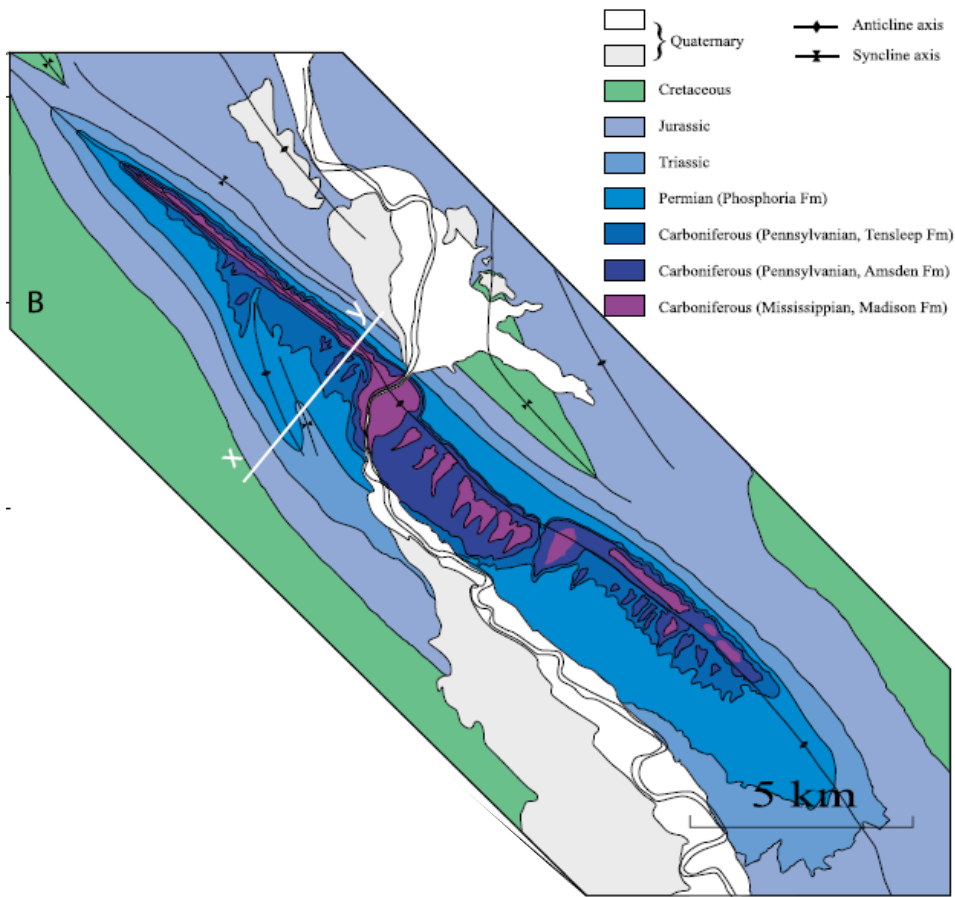


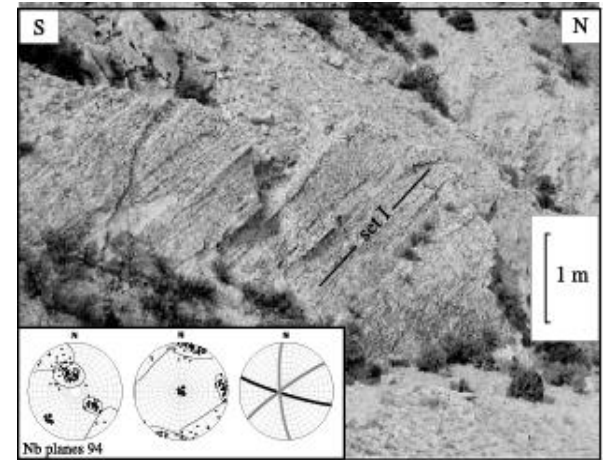
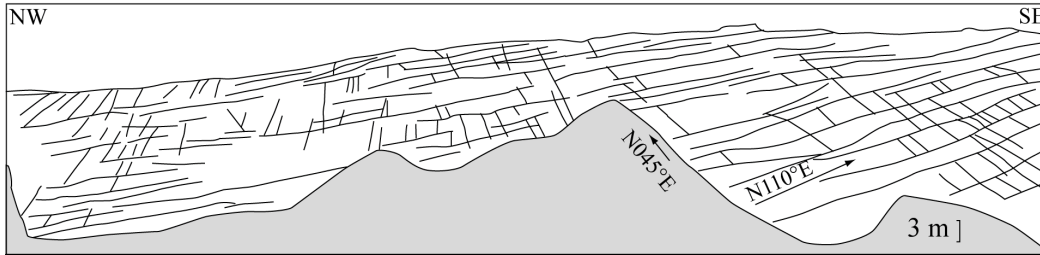


(Weil and Yonkee, 2012)

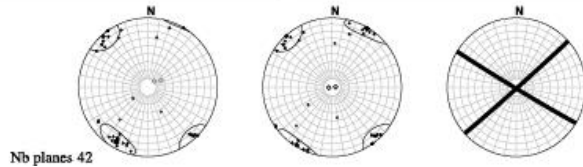
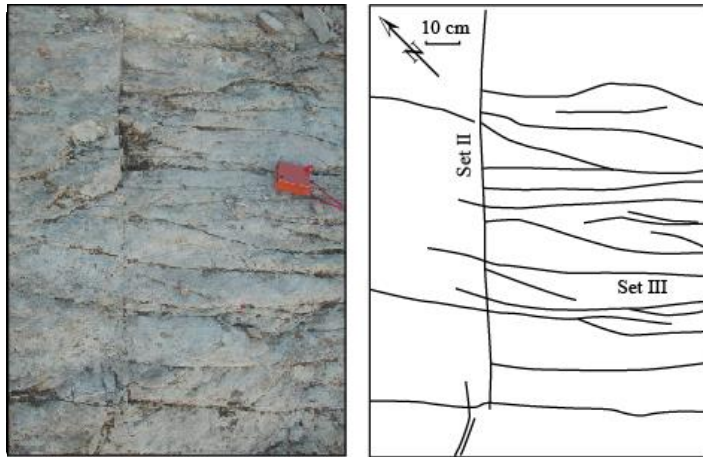
TERTIARY	Willwood	
	Fort Union	
CRETACEOUS	Lance (335 m)	
	Meeteelse (335 m)	
	Mesaverde (365 m)	
	Cody (640 - 765 m)	
	Frontier (150 - 170m)	
	Mowry (120 m)	
	Thermopolis (185 m)	
	Cloverly & Morrison (185m)	
	Sundance (120m)	
	Gypsum Spring (30m)	
JURASSIC	Chugwater (230-290 m)	
PERMIAN	Phosphoria (25-50 m)	
PENNSYLVANIAN	Tensleep (30m)	
	Amsden (90 m)	
MISSISSIPPIAN	Madison (210-250 m)	
DEVONIAN	Three Forks (60m)	
ORDOVICIAN	Bighorn (120 m)	
CAMBRIAN	Gallatin (130 m)	
	Gros Ventre (225 m)	
	Flathead (40 m)	
PRECAMBRIAN	Granite & Gneiss	



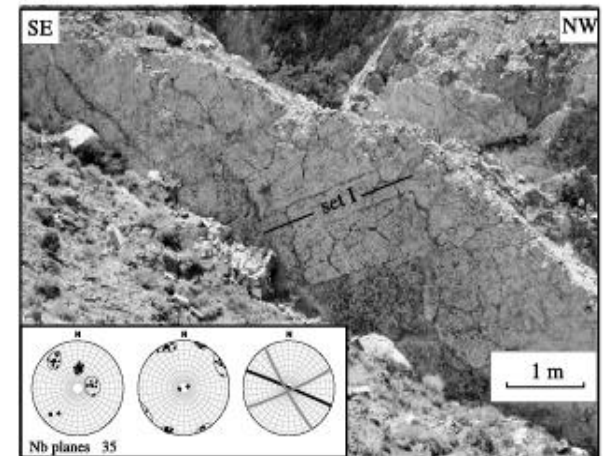




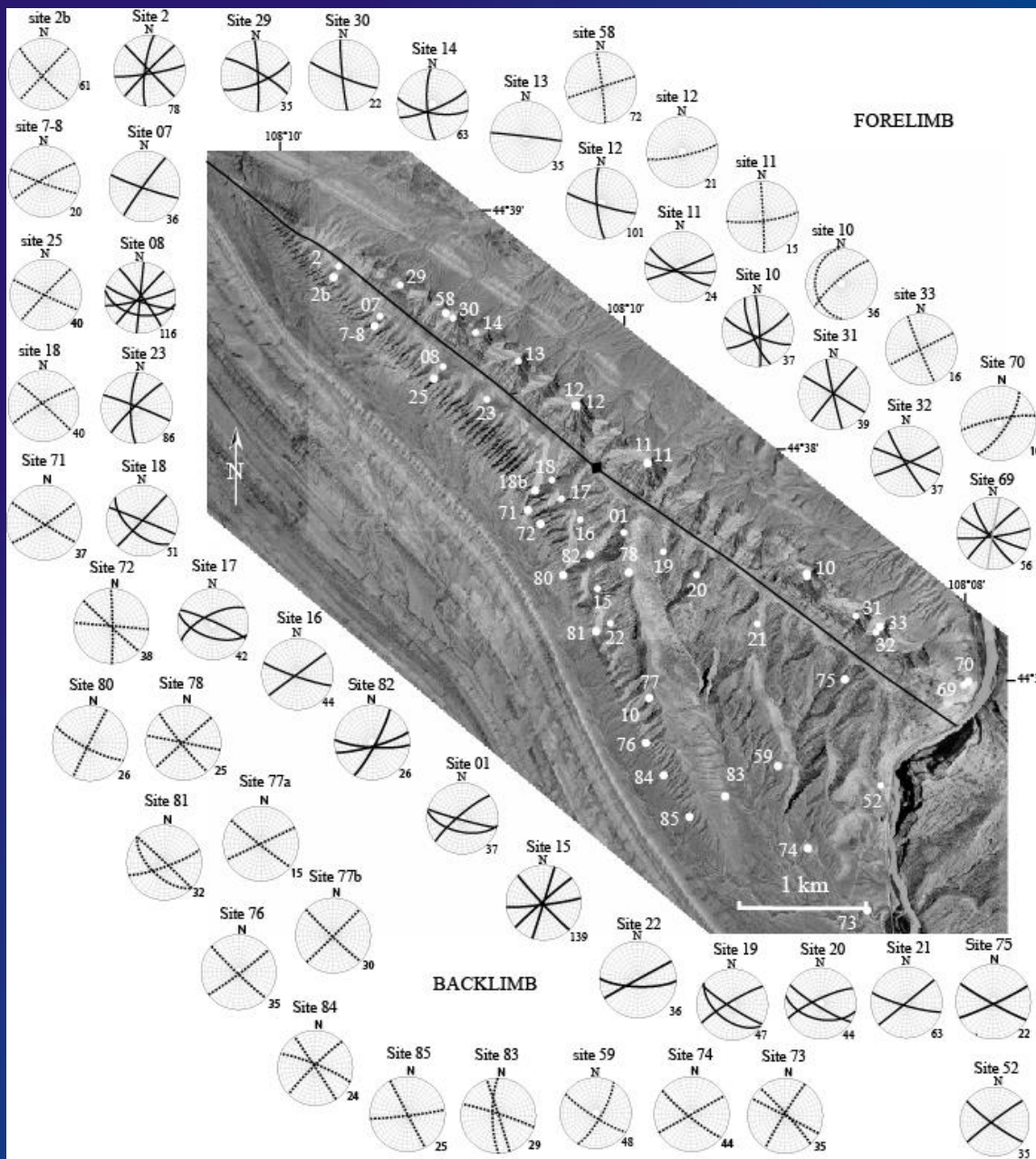
(a)



(Bellahsen et al., 2006;  
Amrouch et al., Tectonics, 2010)



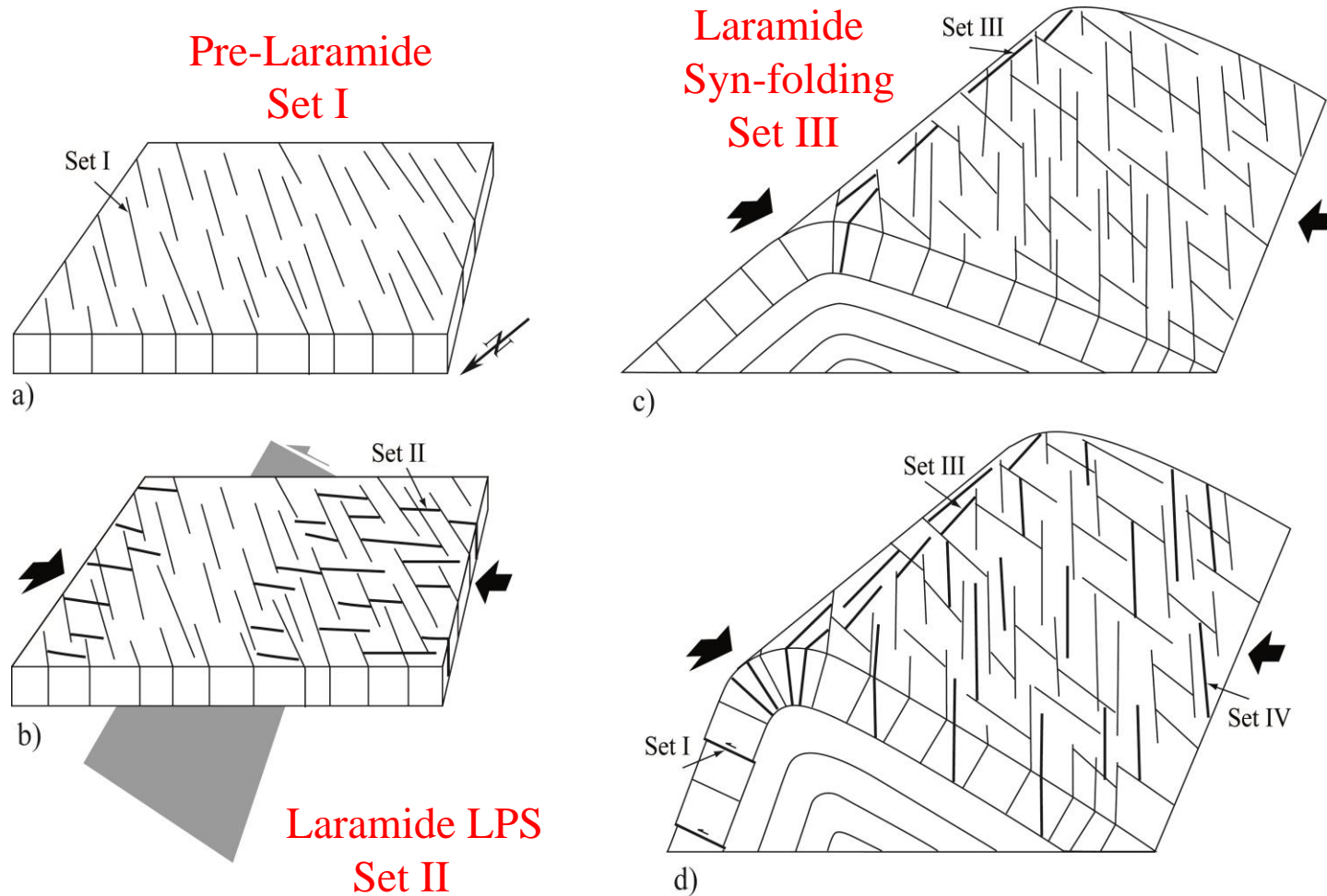
(b)



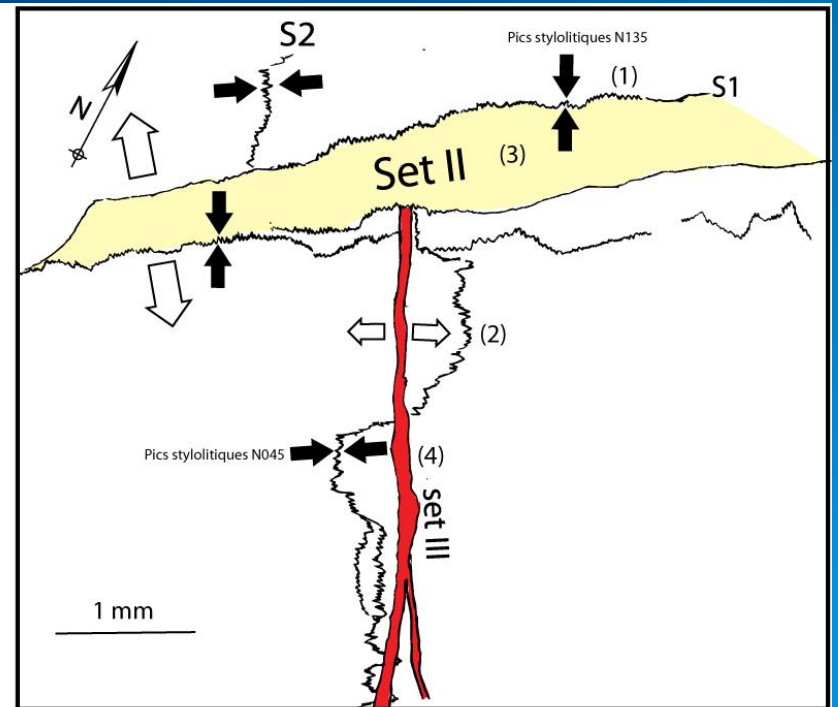
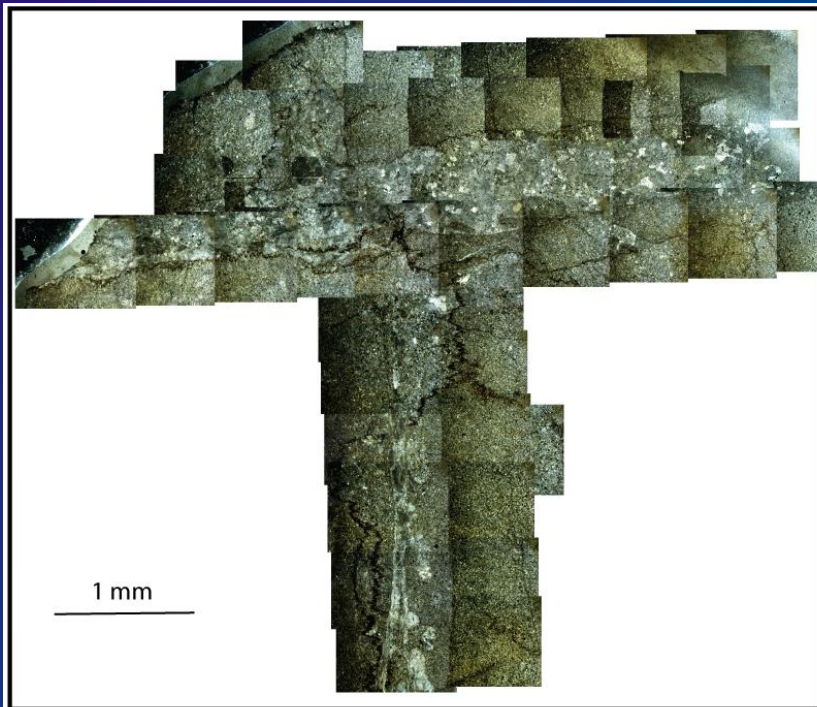
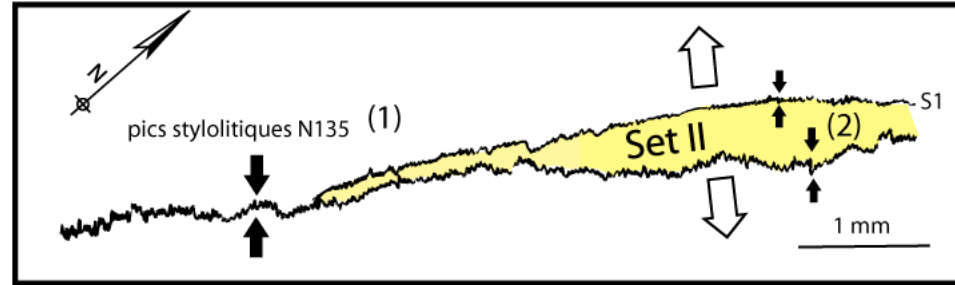
Distribution of joint/vein sets

(Bellahsen et al., 2006; Fiore, 2007; Amrouch et al., 2010)

# First-order sequence of fracture development

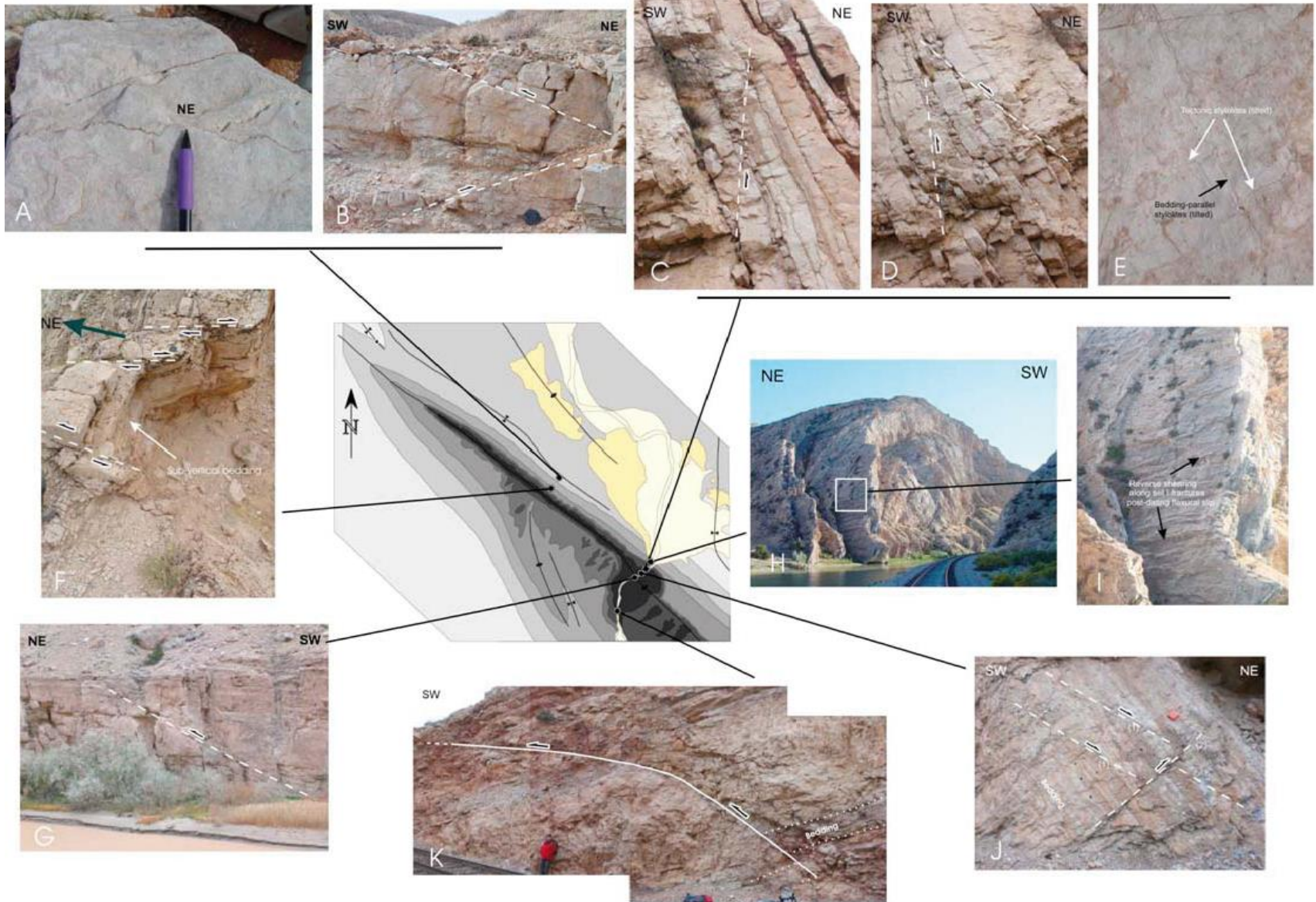


# Relationships between pressure solution seams and fractures

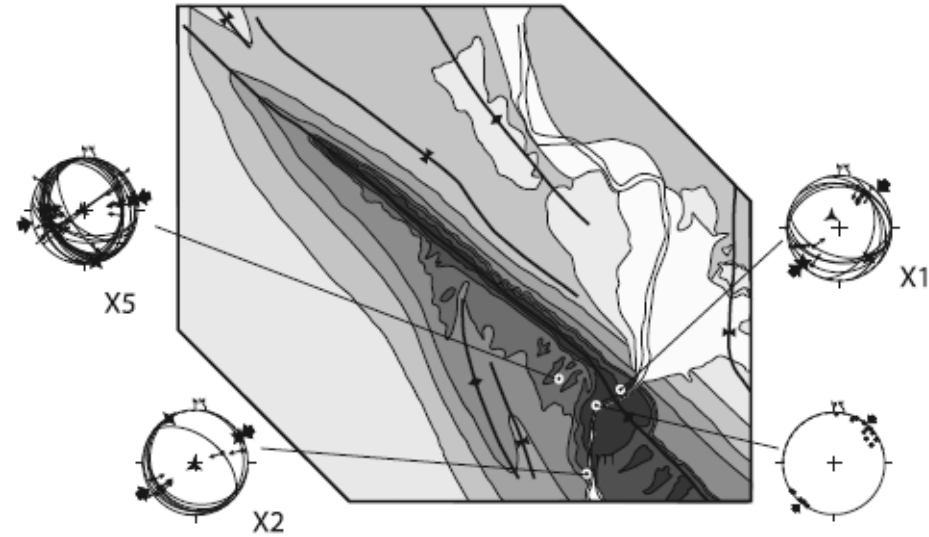
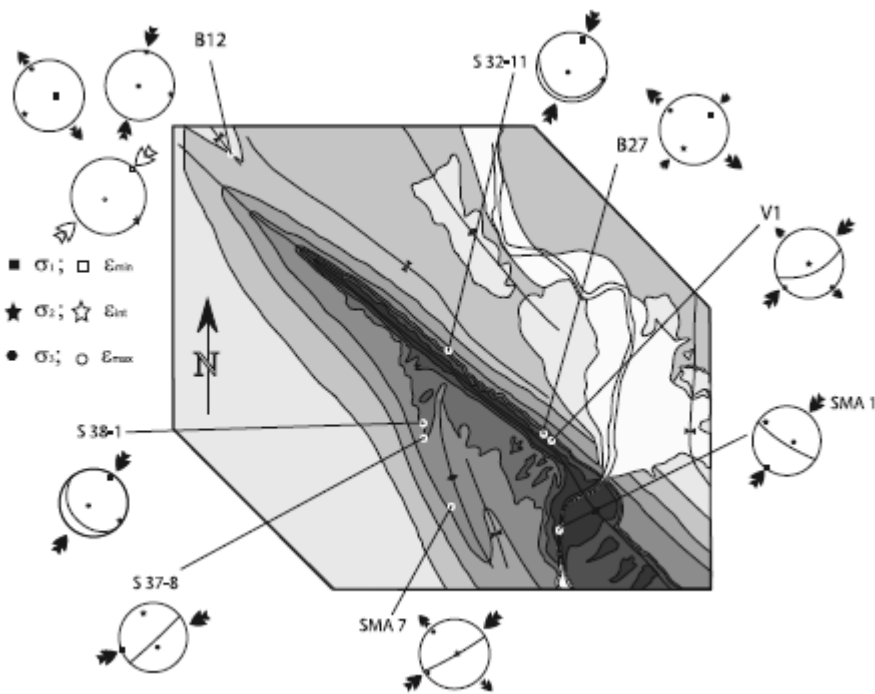




# Meso-scale faulting



# Early-folding stage: Paleostress /strain orientations related to Laramide LPS.

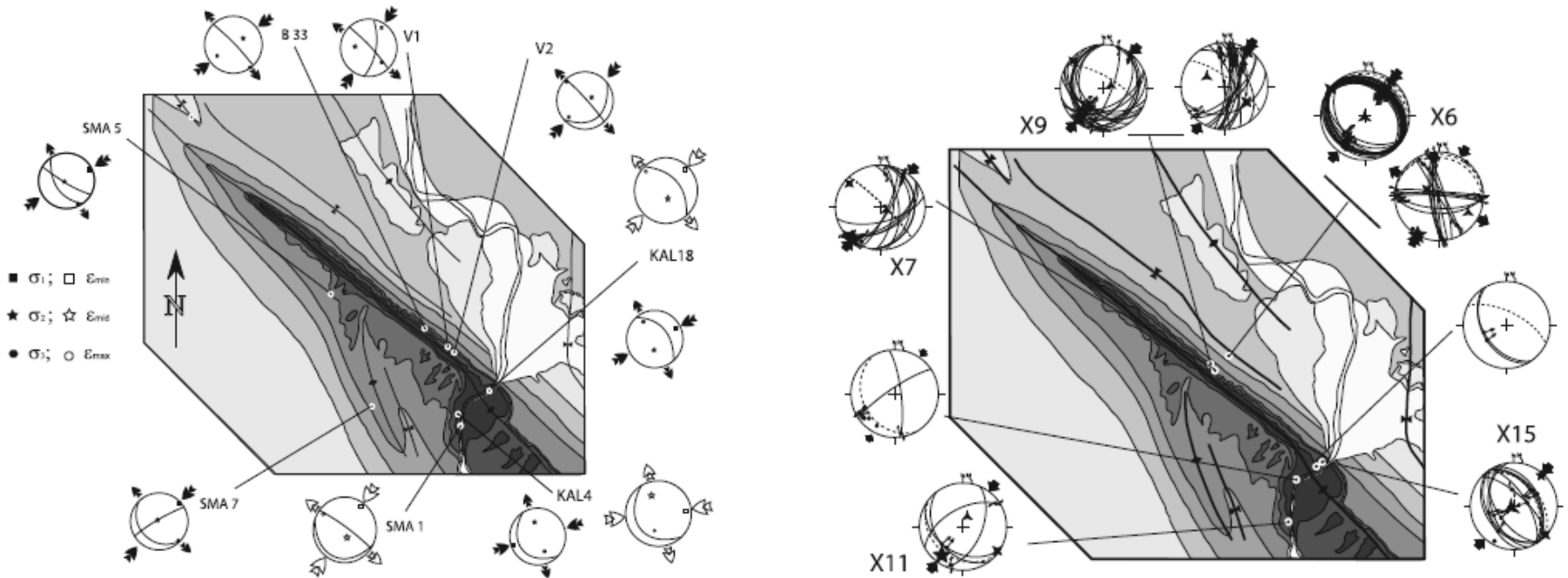


(Amrouch et al., Tectonics, 2010)

Set II joints striking  $\sim 045^\circ$  and associated stylolites are related to the Laramide Layer-Parallel Shortening (LPS). The compression was oriented NE to ENE either in a strike-slip or in a compressional regime.

# Late-folding stage: paleostress / strain orientations related to Laramide late stage fold tightening.

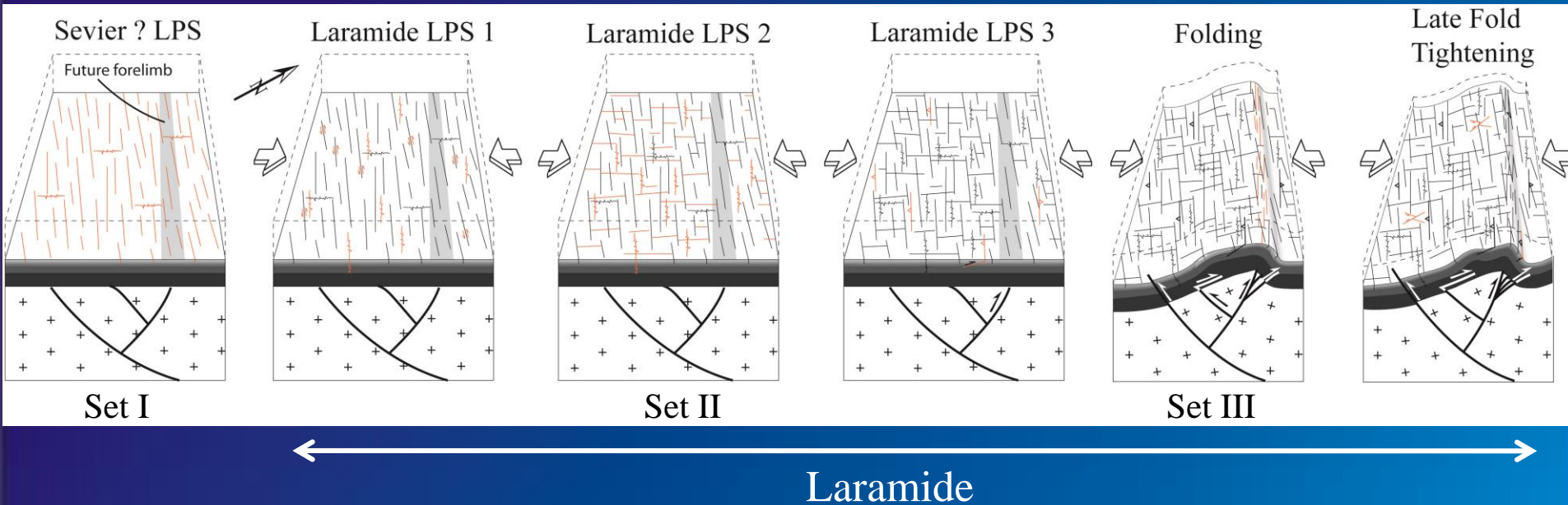
(Amrouch et al., Tectonics, 2010)



Faults and calcite twins reveal a late fold tightening stage, associated with a strike-slip stress regime and a paleo- $\sigma_1$  axis also oriented NE.

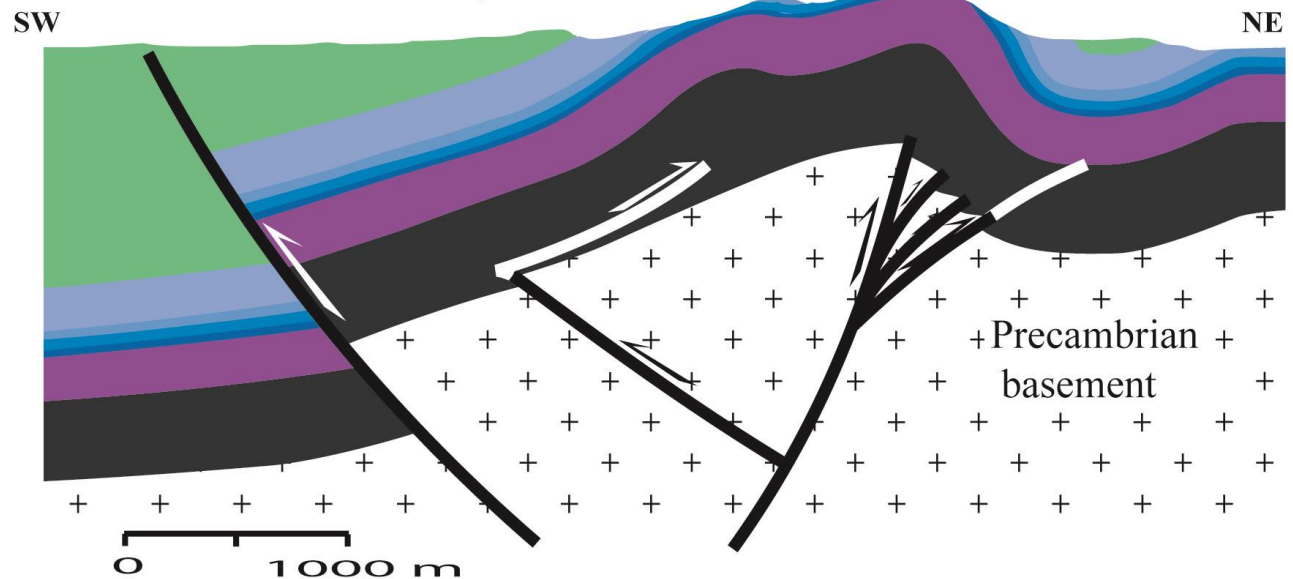
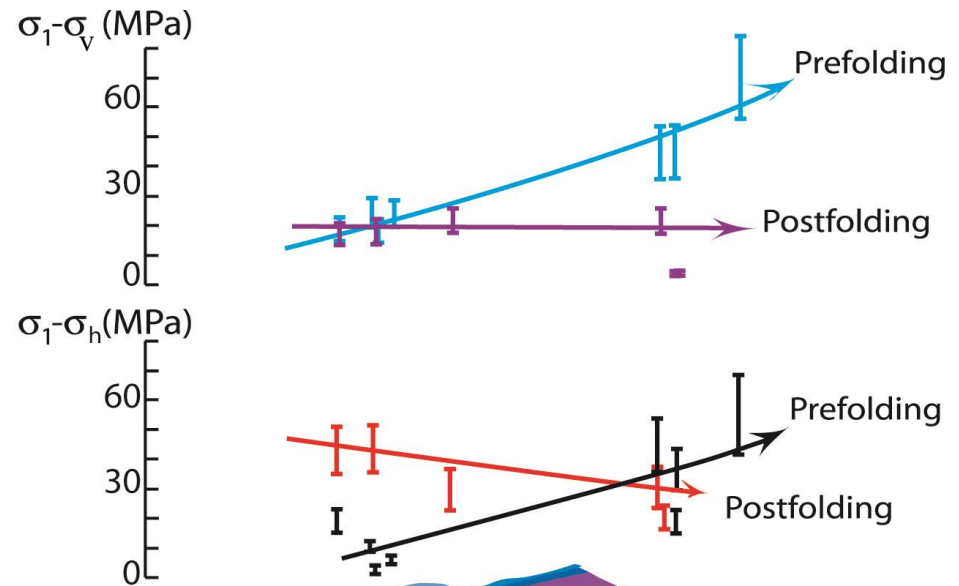
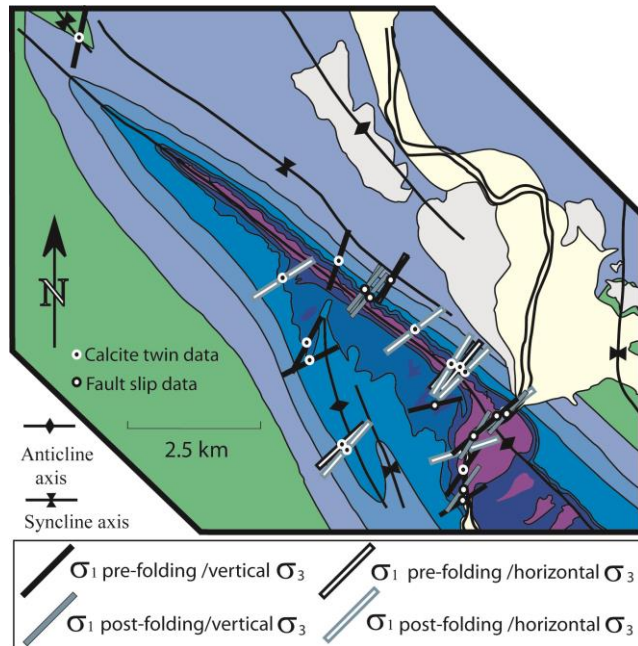
# Refined scenario of fault-fracture development in space and time

(Amrouch et al., Geophysical Research Letters, 2011)



- Mode I opening of pre-Laramide set I fractures
- Shear reactivation of pre-Laramide set I fractures (LPS 1).
- Laramide stylolites with NE-trending peaks and mode I opening of set II fractures (LPS2)
- Reverse faulting parallel to the fold axis (LPS3).
- Mode I opening of syn-folding, outer-rim extension-related set III fractures
- Late stage fold tightening (LSFT) marked by strike-slip faults and reactivation of tilted set I fractures as small reverse faults in the forelimb

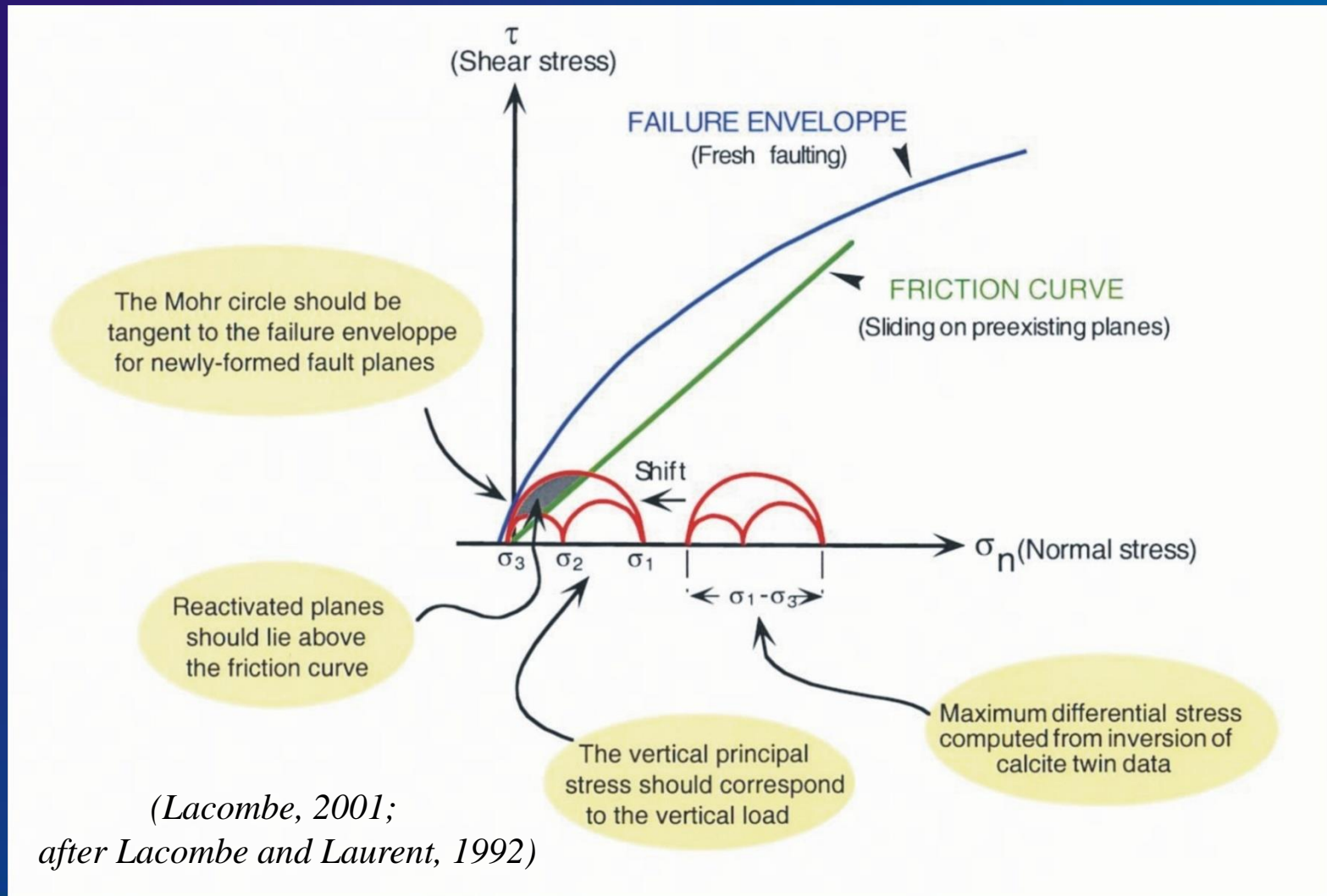
# Early-folding and late-folding Laramide paleo-differential stress magnitudes from calcite twinning paleopiezometry

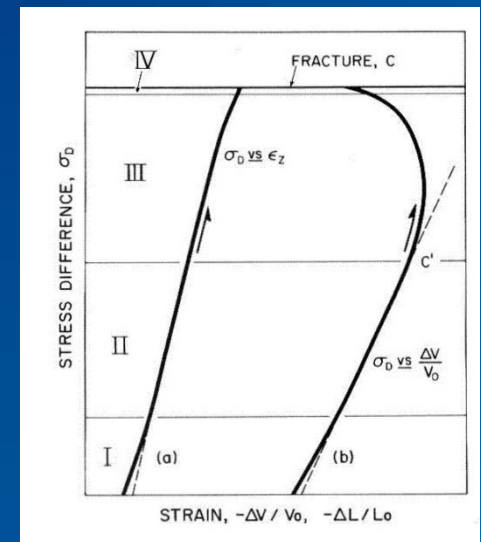
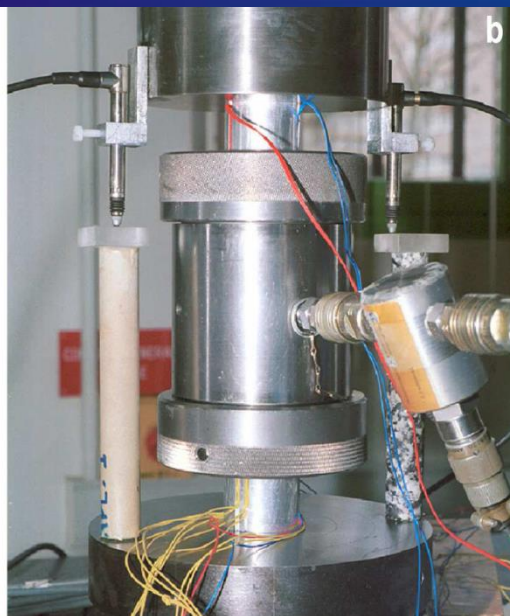
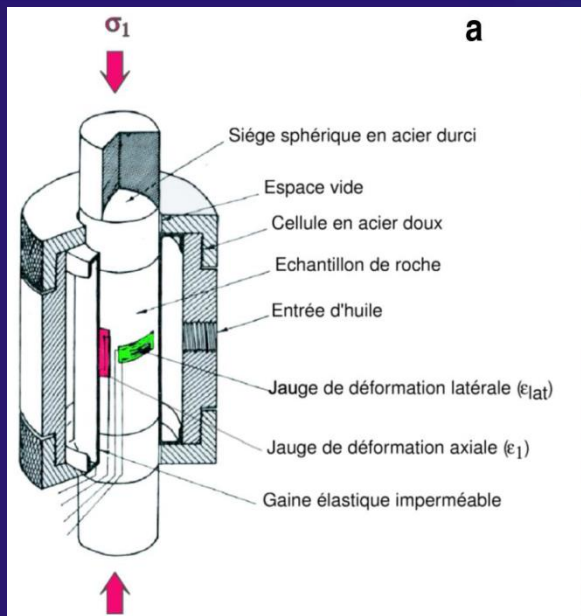


(Amrouch et al.,  
Tectonics, 2010)

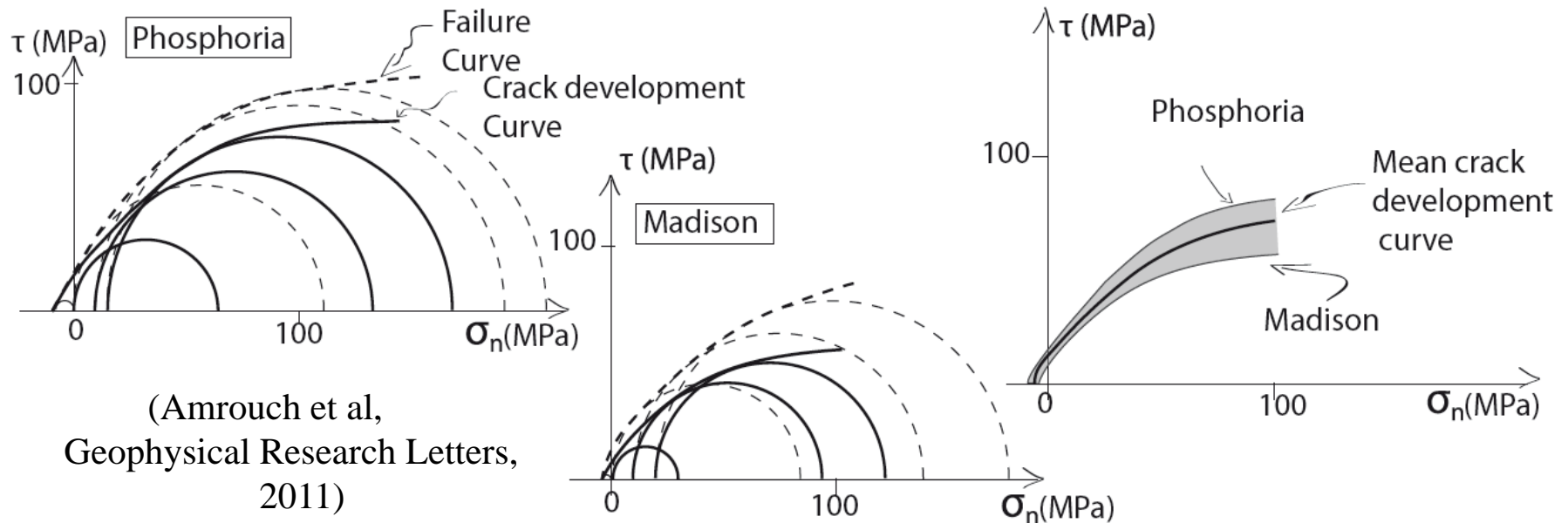
# How to constrain principal stress magnitudes :

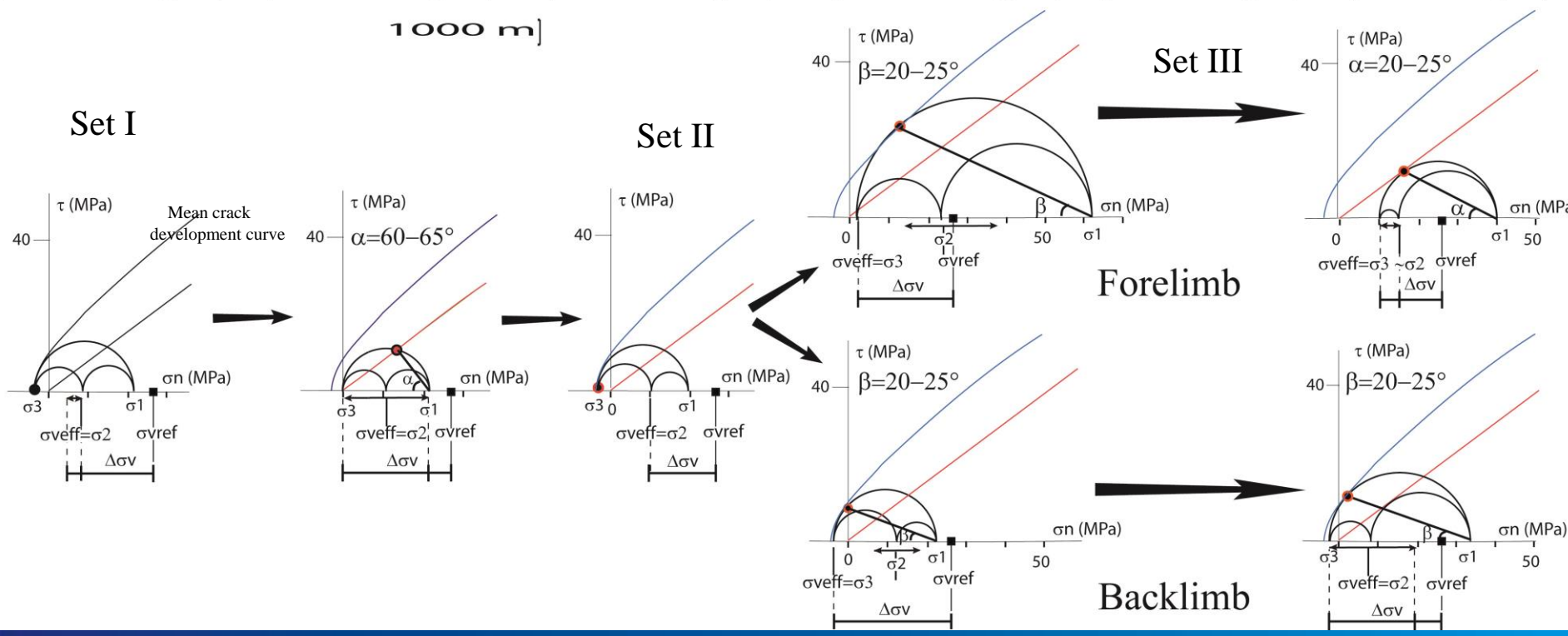
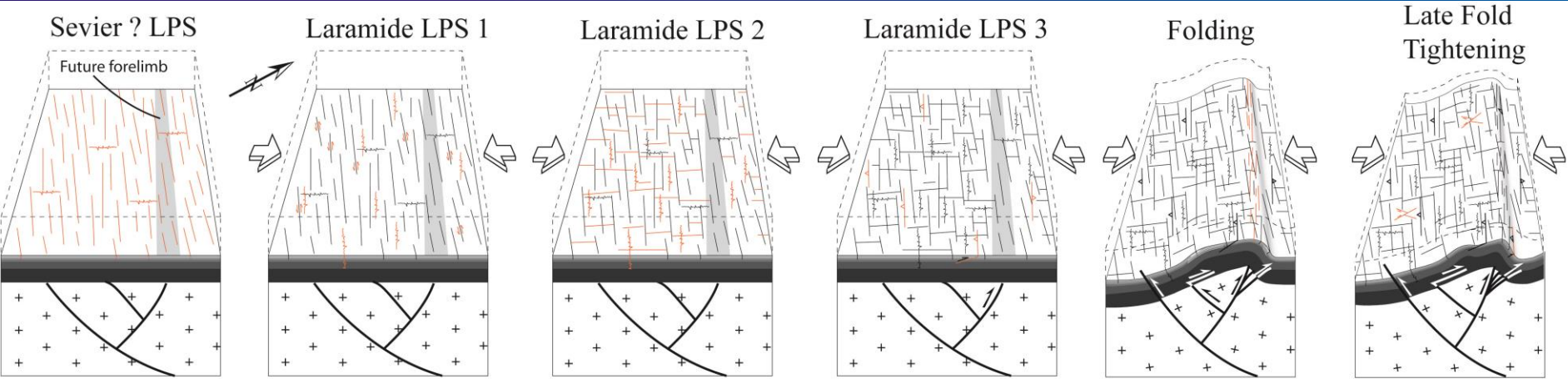
The method : finding for each deformation step the values of  $\sigma_1$ ,  $\sigma_2$  and  $\sigma_3$  required for consistency between differential stresses estimated from calcite twinning, frictional sliding along preexisting planes (i.e., Byerlee's law) and newly formed faulting/fracturing.





## Experimental determination of the intrinsic failure envelopes of the Phosphoria and Madison formations





Determination of principal stress magnitudes using simple Mohr constructions

(Amrouch et al, Geophysical Research Letters, 2011)



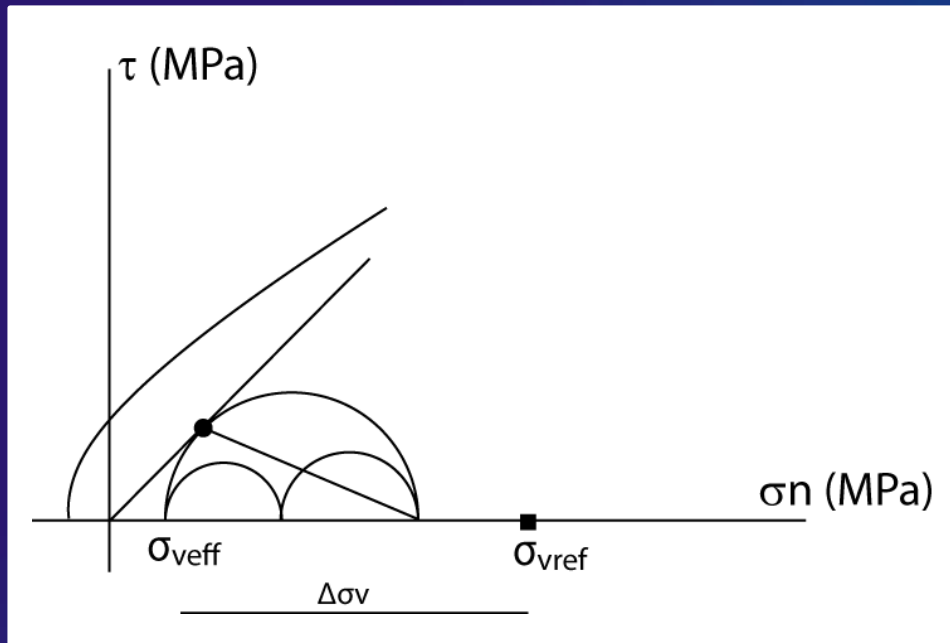
The estimated paleo- principal stress magnitudes are in the range of 20-60 MPa for  $\sigma_1$  and -3-10 MPa for  $\sigma_3$  in the limestone rocks deformed at 1000-2000m depth.

These estimates of are amongst the very few ones available for upper crustal paleo-stresses at the particular time of tectonic deformation (e.g. Taiwan, Lacombe, 2001).

Being related to ongoing deformation, and averaged over the duration of the Laramide event, they are theoretically hardly compared to modern stresses measured in situ which are rather representative of ambient instantaneous stresses.

They are nevertheless of the same order than the modern principal stress values determined in strike-slip or compressional stress regimes at various places e.g., at the SAFOD pilot hole (Hickman and Zoback, 2004)

## Calculation of the $\Delta\sigma_v$ to infer fluid overpressure



Theoretical effective vertical principal stress calculated considering lithostatic pressure corrected from hydrostatic fluid pressure:

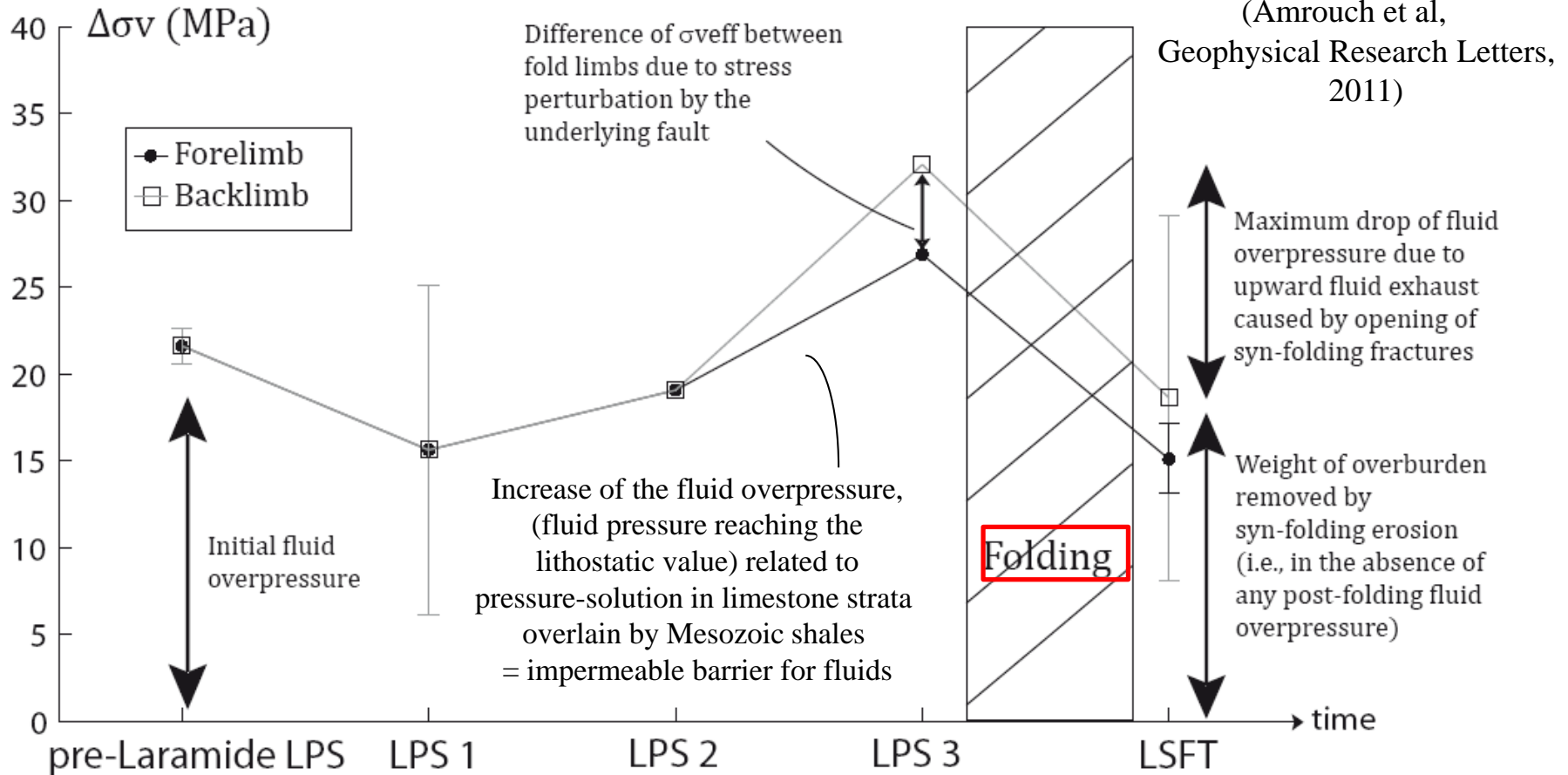
$$\sigma_{vref} = (\rho - \rho_w) \cdot g \cdot h$$

Comparison between the theoretical effective vertical principal stress  $\sigma_{veff}$  and the reconstructed effective vertical principal stress  $\sigma_{vref}$ :

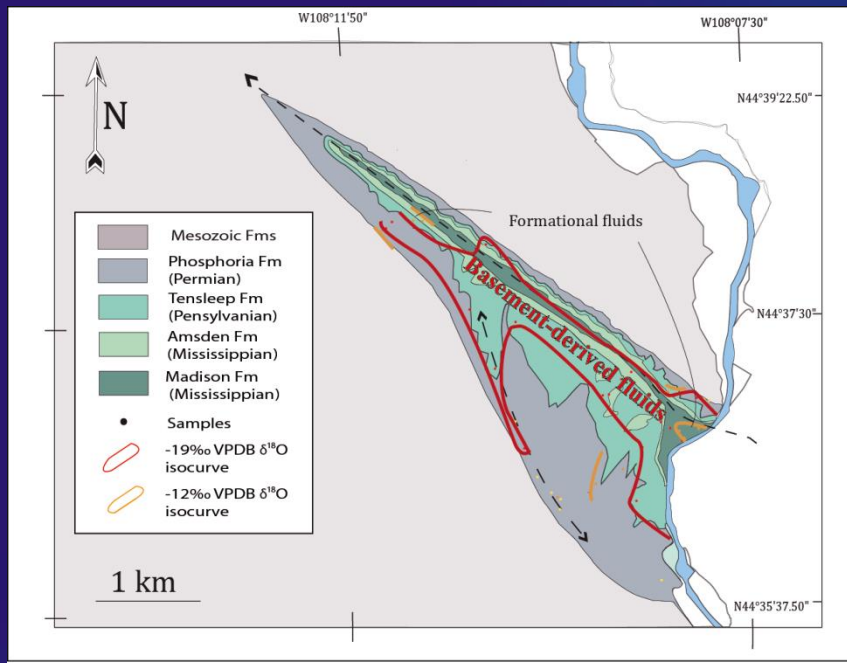
$$\Delta\sigma_v = \sigma_{vref} - \sigma_{veff}$$

No erosion or increase of burial before folding  
→  $\Delta\sigma_v$  primarily provides an estimate of the fluid overpressure.

# Inference of fluid (over)pressures

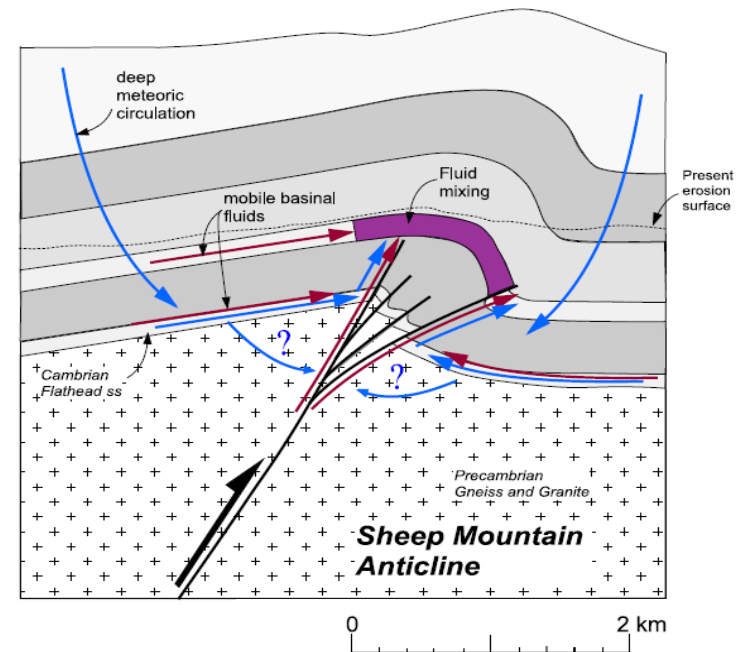
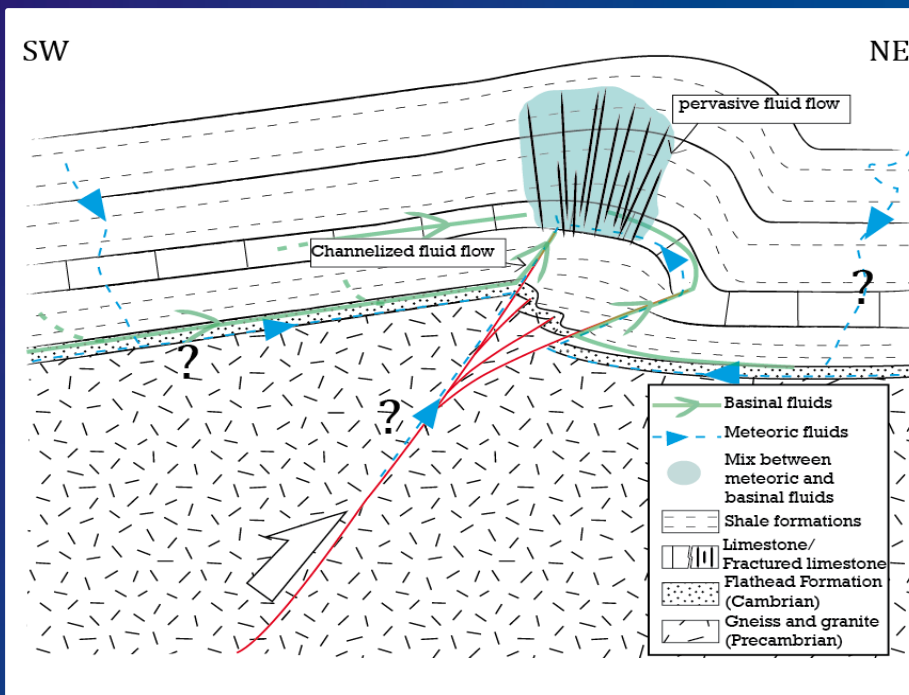


If the entire fluid overpressure was released during folding, it is possible to also derive the maximum value of syn-folding erosion (~1000m)



Basement-derived hydrothermal fluid pulse at SMA during folding as inferred from geochemical and microthermometric studies of vein cements

(Beaudoin et al, G3, 2011)



# Conclusions :

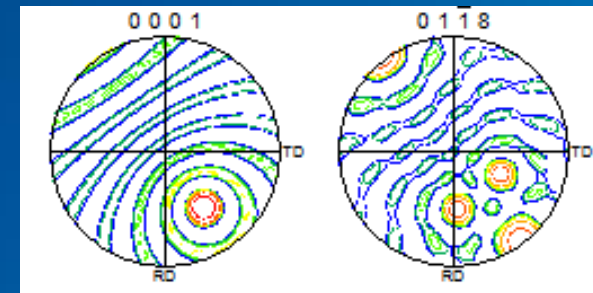
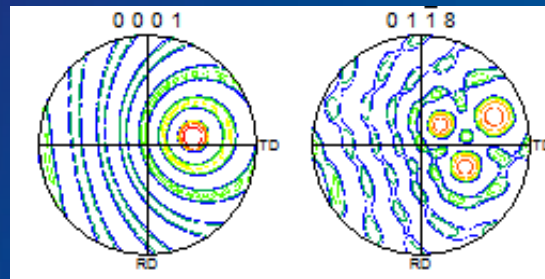
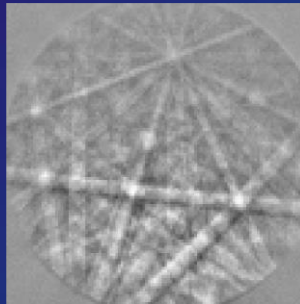
Calcite twins :  
a powerful tool which helps constrain ...

- stress orientations, regional structural/tectonic histories and geodynamic evolution;
- values of tectonic (paleo)stress magnitudes;
- upper crust mechanics;
- micro-mechanisms of internal deformation of carbonate rocks in folded/fractured reservoirs;
- basin/thrust belt modelling

... among others...

# Perspectives - forthcoming improvements

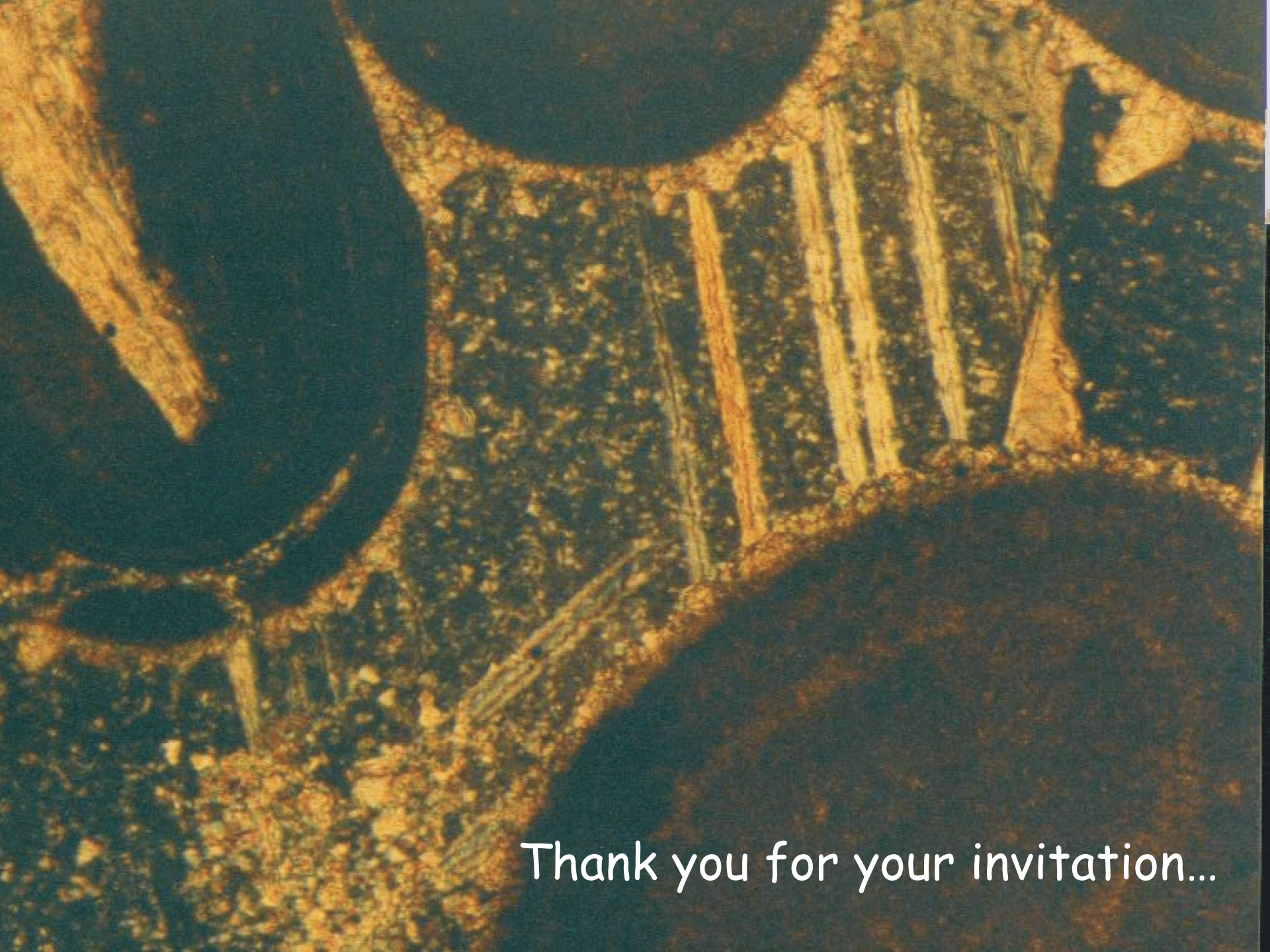
\* Automatic data acquisition using EBSD



\* New mechanical experiments to better constrain the value of the critical resolved shear stress for calcite twinning as a function of grain size and strain

... and possible cross-check  
with another paleopiezometric technique  
in carbonate rocks  
based on stylolite morphology

(Ebner et al., 2009; Koehn et al., 2007, 2012)

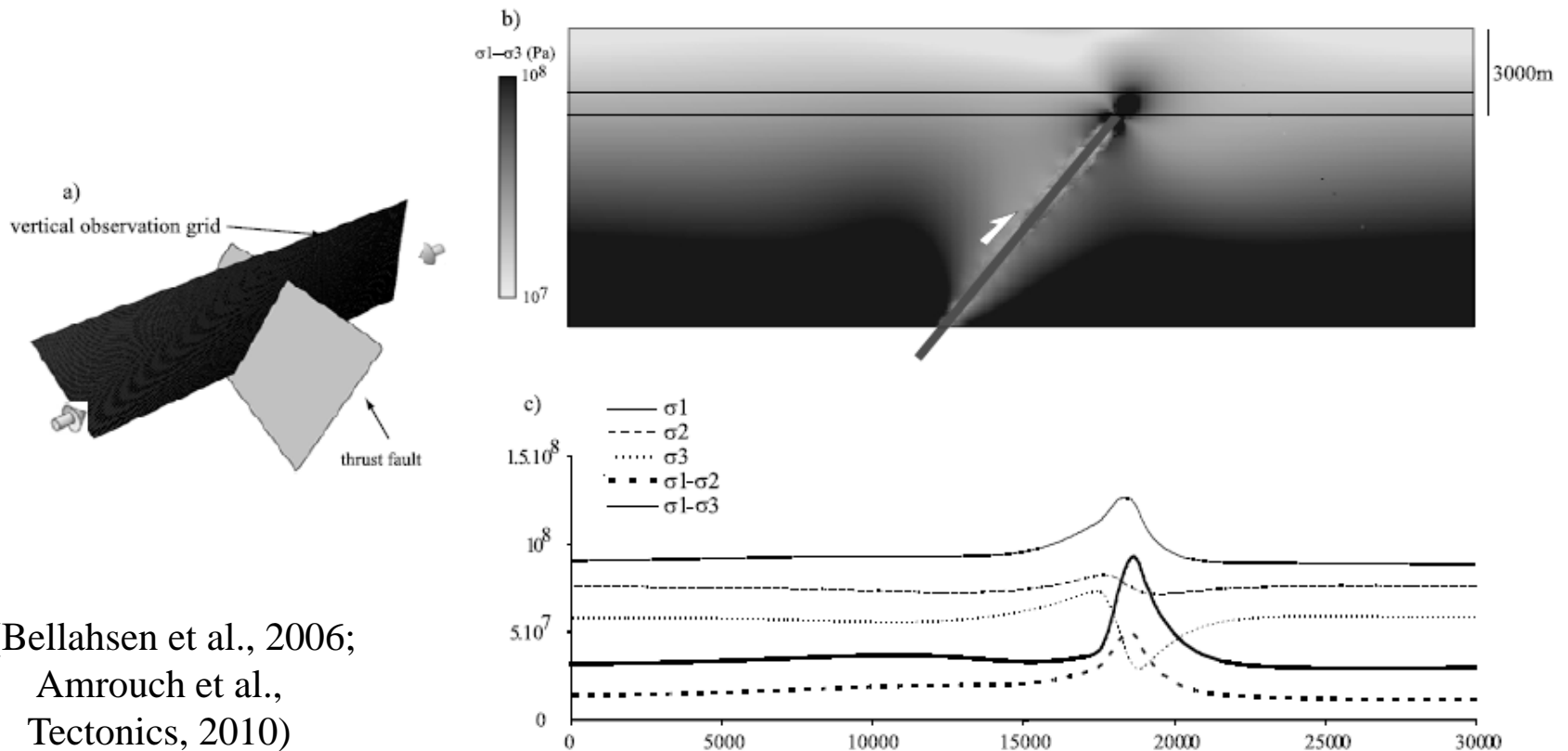
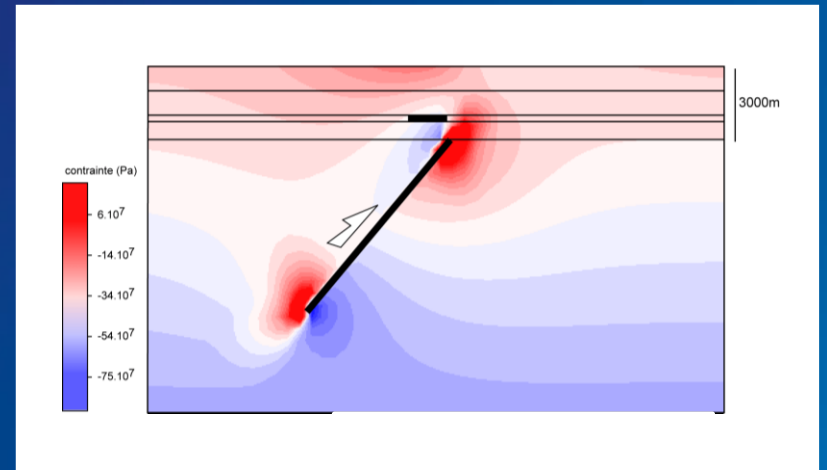


Thank you for your invitation...





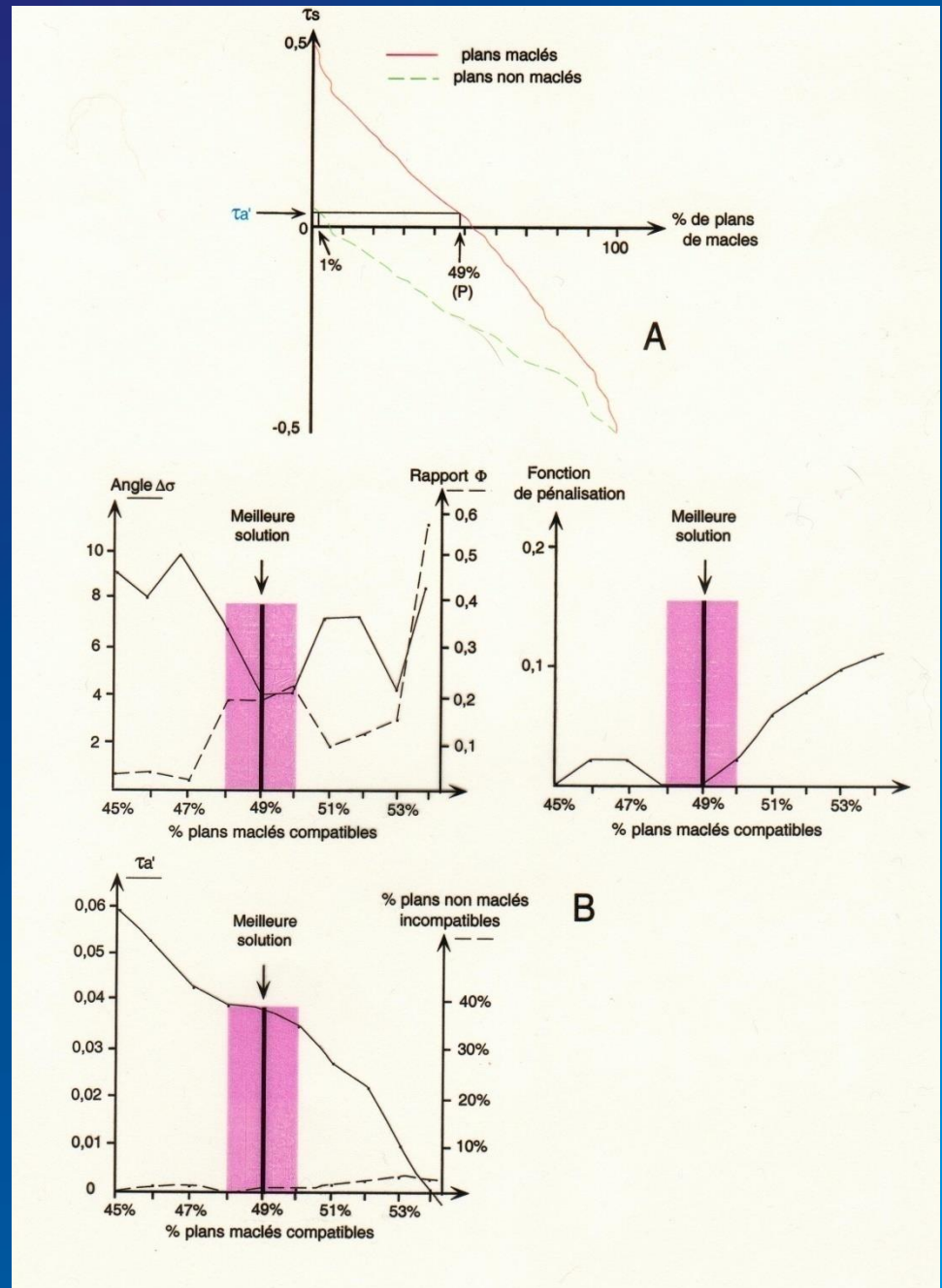
# Stress perturbations in the sedimentary cover at the tip of the underlying basement fault starting to move during Laramide stress build-up

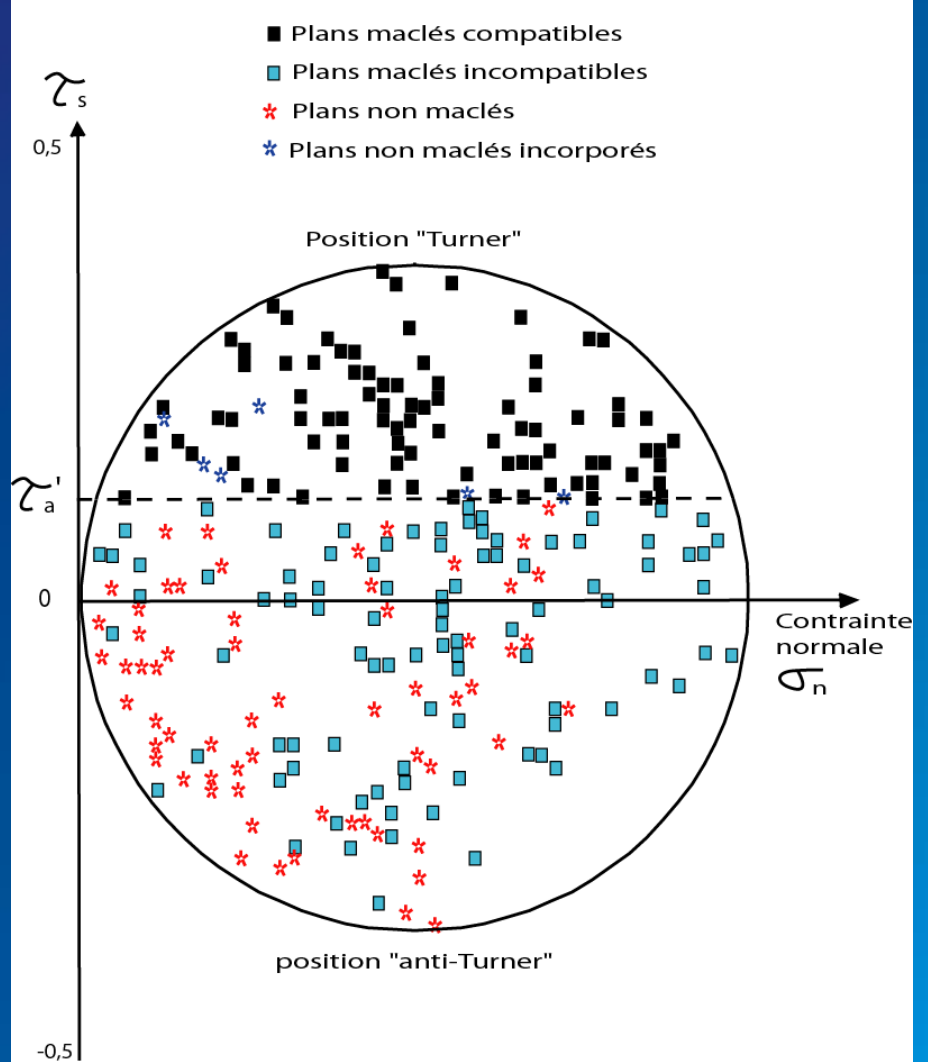
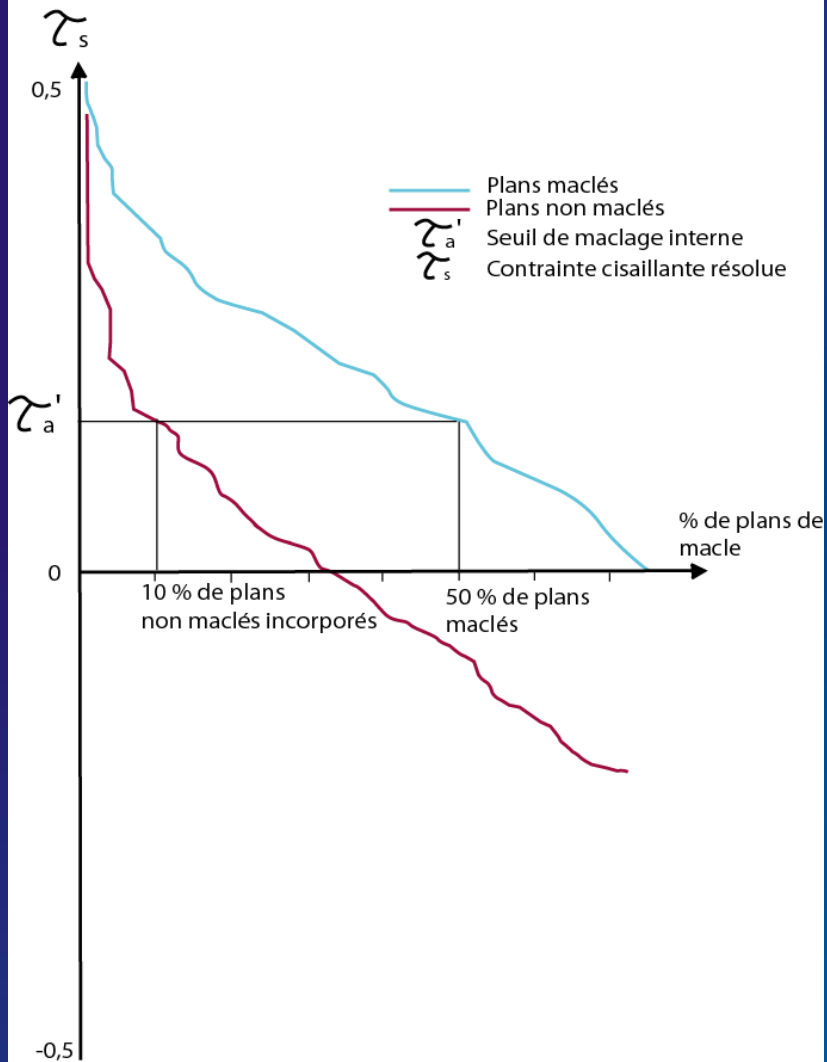


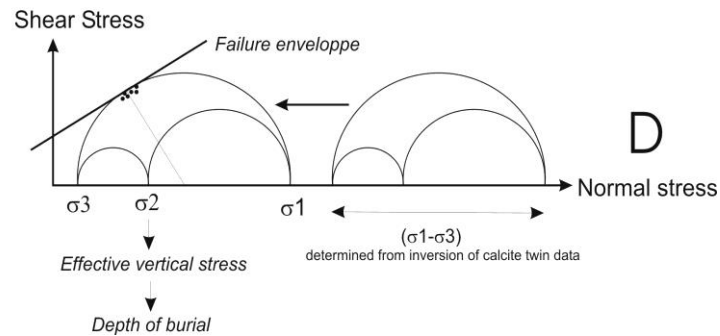
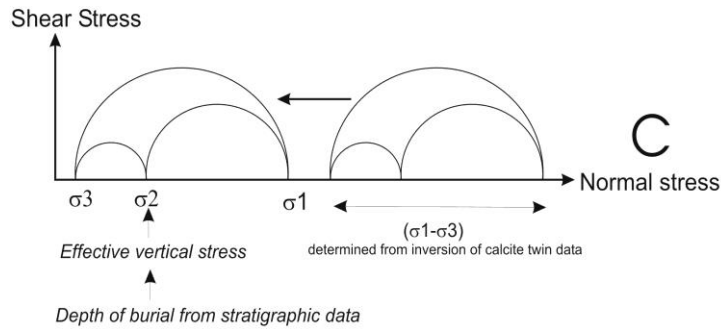
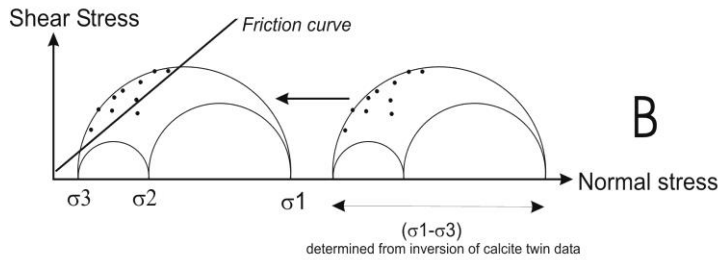
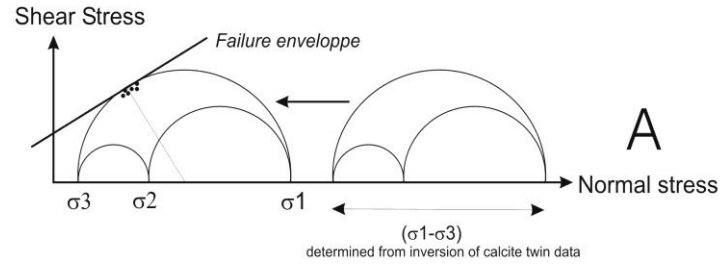
(Bellahsen et al., 2006;  
Amrouch et al.,  
Tectonics, 2010)

# Définition du tenseur -solution optimal dans l'analyse inverse

(Laurent et al., 2000;  
Lacombe, 2000)







*(Lacombe, 2007;  
Modifié d'après  
Lacombe et al., 1996)*

# Insights into mechanical behaviour of folded strata :

## \* Early folding stage - LPS :

Forelimb : stress perturbations, that partly prevented development of fractures. In turn limited fracture development + weak internal deformation (AMS and APWV) → poor stress relaxation → differential stress increase.

Backlimb : no stress perturbation + stress relaxation by widespread development of fractures and by internal strata deformation (AMS) → much lower differential stresses

## \* Late-folding stage - LSFT :

Forelimb : drop of differential stresses while limited internal deformation (poorly evolved AMS fabrics and low anisotropy of the matrix revealed by APVW → strata were tilted during folding without any additional significant internal deformation, LSFT being mainly accommodated by newly formed microfaults and reactivation of earlier fractures → stress relaxation

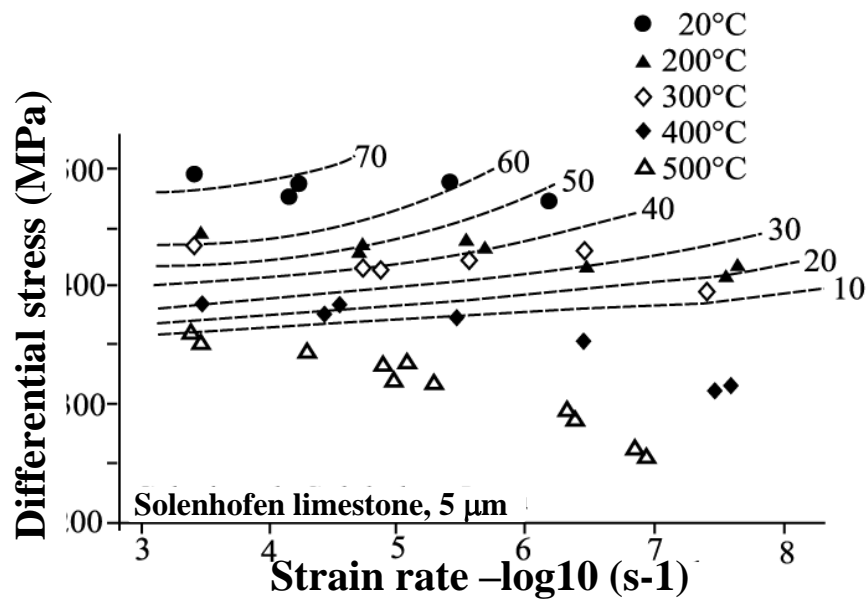
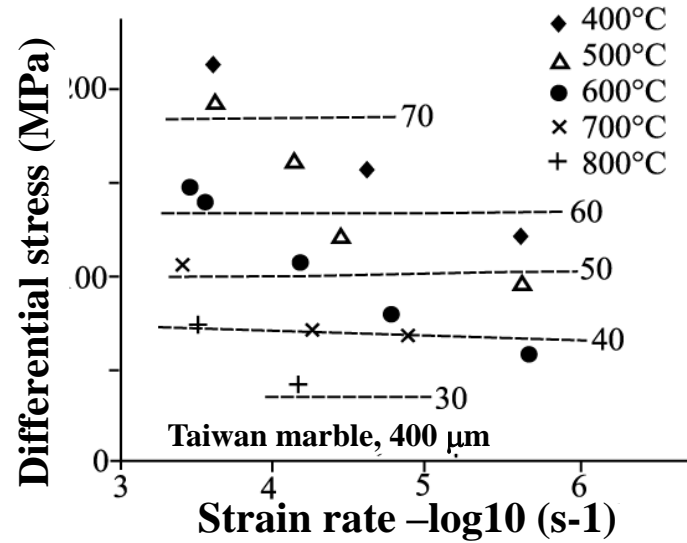
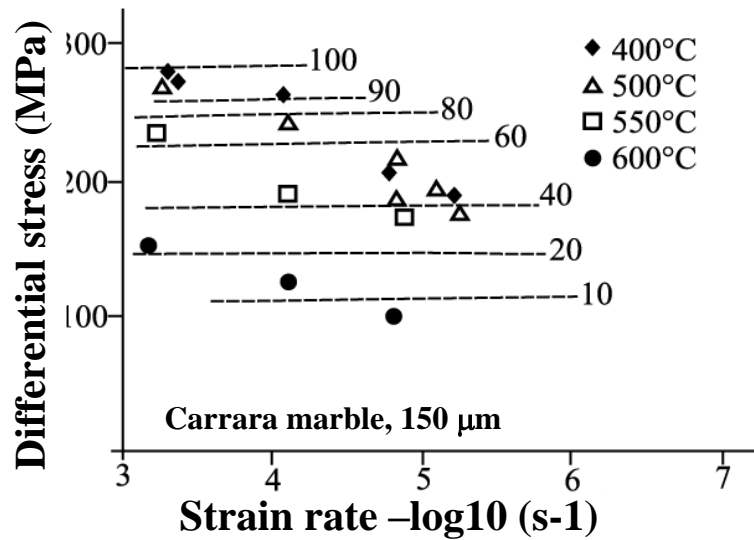
Backlimb : Strata sustained most of LSFT without developing much fractures, → increase of differential stresses and development of more evolved ASM fabrics

La résistance d'un système de glissement cristallin (maclage ou glissement ss) est exprimée conventionnellement par une **contrainte cisailante résolue critique** ou seuil  $\tau_C$ . Il s'agit de la contrainte cisailante résolue sur le plan de glissement dans la direction de glissement, qui doit être atteinte afin de produire une déformation plastique significative.  $\tau_C$  est la contrainte cisailante critique qui provoque le mouvement d'un grand nombre de dislocations, de telle sorte que le glissement devient observable, et ce indépendamment de l'orientation du cristal déformé. Un tel comportement est généralement associé au développement d'un point critique dans la courbe contrainte-déformation pour un monocristal.

La valeur de la contrainte cisailante résolue critique est obtenue par la relation :

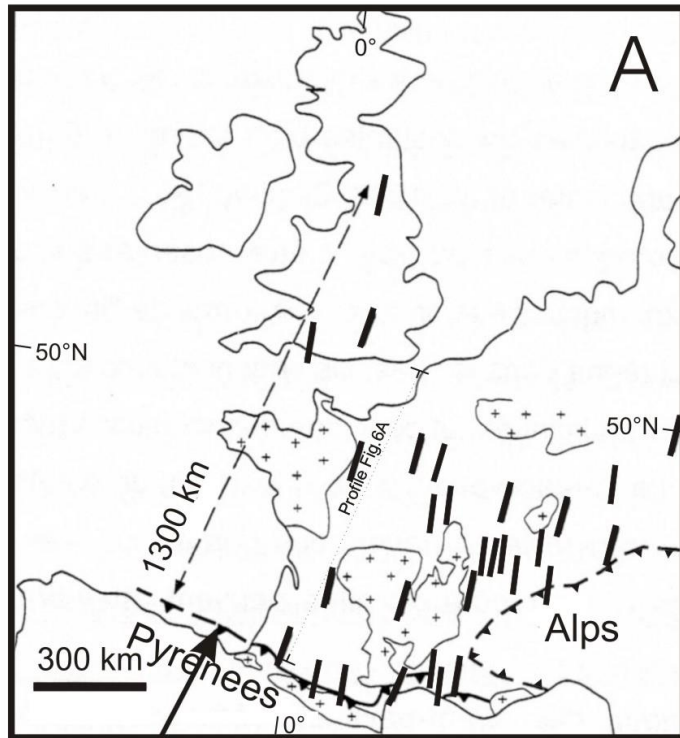
**$\tau_C = \sigma \times S$** .  $\sigma$  correspond à la valeur de la contrainte appliquée au point critique;  $S$  est le facteur de Schmid, tel que  $S = \cos \alpha \times \cos \beta$ , où  $\alpha$  est l'angle entre la direction de compression et la normale au plan de macle dans un monocristal, et  $\beta$  l'angle entre la direction de compression et le vecteur déplacement par maclage. La contrainte cisailante résolue le long du vecteur est maximale quand  $\alpha$  et  $\beta$  valent  $45^\circ$ ,  $S$  variant de 0 à 0,5 selon l'orientation du grain.

Les sources de concentrations de contraintes que sont les hétérogénéités à l'échelle du grain étant extrêmement nombreuses dans les cristaux naturels (dislocations, fractures, poinçons, macles préexistantes), **le seuil de maclage représente la contrainte nécessaire pour propager les macles plutôt que pour les nucléer.**

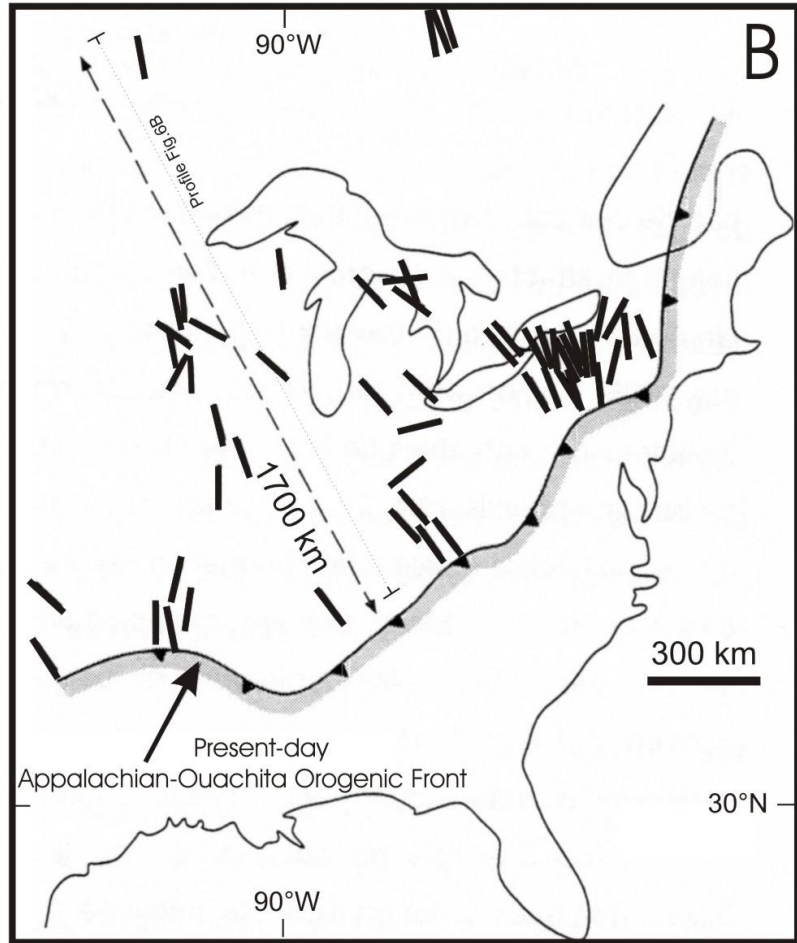


*(Rowe and Rutter, 1990)*

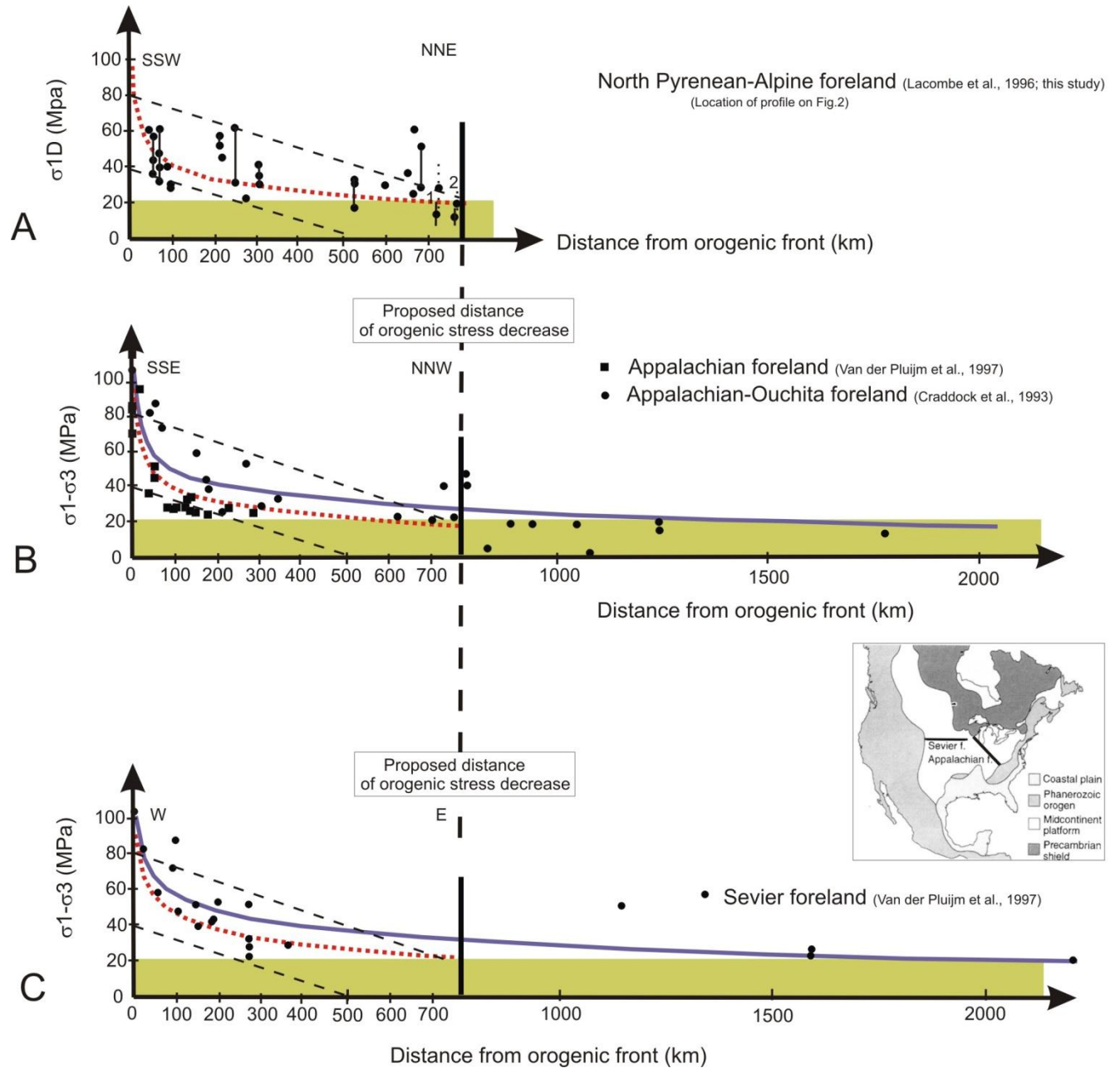




Present-day  
Pyrenean-Alpine Orogenic Front



Present-day  
Appalachian-Ouachita Orogenic Front



(Lacombe, 2010)